Inhibition of pancreatic cancer progression through EMT inhibition and induction of ER stress

By

Tao Wang
B.S., Shenyang Pharmaceutical University, China, 2015

Submitted to the graduate degree program in Pharmacology and the Graduate Faculty of the University of Kansas in partial fulfillment of the requirements for the degree of Doctor of Philosophy.

_____
Committee Chair: Qi Chen, Ph.D.

_____
Udayan Apte, Ph.D.

_____
Bruno Hagenbuch, Ph.D.

_____
Nikki Cheng, Ph.D.

_____
Wen-Xing Ding, Ph.D.

Date Defended: April 19, 2021

The dissertation committee for Tao Wang certifies that this is the approved version of the following dissertation:

Inhibition of pancreatic cancer progression through EMT inhibition and induction of ER stress

_____

Chair: Qi Chen, Ph.D.

_____

Graduate Director: Bruno Hagenbuch, Ph.D.

Date Approved: April 19, 2021

Abstract

Pancreatic cancer is a devastating disease with a current overall 5-year survival rate of only 10%, making it the deadliest cancer. The dismal treatment outcome of pancreatic cancer is largely attributed to its highly metastatic and chemo-resistant nature. Cancer cell epithelial to mesenchymal transition (EMT) contributes importantly to cell invasion, metastasis, and drug resistance in pancreatic cancer. In addition, pancreatic cancer cells exhibit an elevated basal level of unfolded protein response (UPR) signaling for survival, due to increased cellular endoplasmic reticulum (ER) stress under hypoxia. Inhibiting EMT and aggravating ER stress both pose as promising approaches to improve pancreatic cancer treatment. However, the relationship between ER stress and cancer cell EMT has not yet been fully understood. We previously reported a high throughput screening (HTS) study aiming to find small molecule inhibitors for EMT in pancreatic cancer cells. This dissertation documents our investigation on the top hit compound (namely C150) for its activities and mechanisms in inhibiting pancreatic cancer cell EMT, suppressing cell invasion, inducing ER stress, and reducing tumor growth in mice. These studies also discovered a mechanistic link between ER stress and pancreatic cancer cell EMT.

We investigated the activities of C150 in inhibiting pancreatic cancer cell invasion and the mechanism of EMT inhibition (**Chapter 4**). C150 exhibited well-separated cytotoxicity between pancreatic cancer cells and non-cancerous cells. The IC_{50} values were 1~2.5 μM in multiple pancreatic cancer cell lines and >12.5 μM in non-cancerous pancreatic epithelial cells. C150 significantly inhibited pancreatic cancer cell migration and invasion in both 3-dimensional (3D) cell invasion assays and 2-dimensional (2D) wound scratching assays and Boyden chamber trans-well migration-invasion assays. Moreover, C150 treatment decreased matrix

metallopeptidase-2 (MMP-2) and matrix metallopeptidase-9 (MMP-9) gene expressions in pancreatic cancer cells and reduced MMP-2 activity. In an orthotopic mouse model of pancreatic cancer, C150 significantly reduced tumor growth at the dose regimen of 15 mg/kg by intraperitoneal (IP) injection 3x weekly for 6 weeks. Mechanistically, C150 enhanced proteasome-mediated degradation of Snail protein, an important EMT-promoting transcription factor, and decreased the mesenchymal marker N-cadherin, while it increased the epithelial markers ZO-1 and Claudin-1. Findings from this first part of the study suggested that C150 is a novel EMT inhibitor with the potential of inhibiting pancreatic cancer growth and metastasis.

The enhanced proteasome-mediated degradation of Snail by C150 intrigued our investigation into the mechanisms by which this occurred (**Chapter 5**). Further studies found that β-catenin, Sox-2, and TP53 protein levels were also decreased by C150 treatment. Data revealed that C150 increased proteasome activity by inducing ER stress and triggering UPR. The increased proteasome activity was due to enhanced proteasome assembly but not upregulation of subunits' expressions. The increased proteasome assembly enhanced the degradation of transcription factors involved in EMT, as shown in **Chapter 4**. Moreover, as a cellular response to the ER stress, C150 treatment resulted in cell autophagy and decreased general translation in pancreatic cancer cells. The C150-induced ER stress eventually resulted in G2/M cell cycle arrest and cellular senescence. These stresses on pancreatic cancer cells greatly synergized with gemcitabine in inducing cytotoxicity in pancreatic cancer cells. In an orthotopic syngeneic mouse model, C150 treatment significantly reduced tumor growth and ascites occurrence, and improved survival of tumor-bearing mice. The elevated ER stress and senescence were confirmed in tumor tissues of C150-treated mice.

Taken together, studies in this dissertation introduced a potential drug candidate for pancreatic cancer treatment (summarized and discussed in **Chapter 6**). C150 induced ER stress in pancreatic cancer cells, causing cell cycle arrest and senescence. It significantly suppressed tumor growth and improved survival in mouse xenograft models. Furthermore, as a response to C150-induced ER stress, pancreatic cancer cells increased proteasome activity, which enhanced the protein degradation of Snail, along with other EMT or stem cell-related transcription factors, leading to EMT inhibition and reduced cell invasion. An additional consequence is that C150 greatly sensitized PANC-1 cells to gemcitabine treatment, implying the compound's value to overcome drug resistance in pancreatic cancer treatment. As C150 is the first of its class, work from this dissertation provides a preclinical basis to further explore C150 and its analogs as potential therapeutic agents for pancreatic cancer. Future studies are warranted in target identification, pharmacokinetics/pharmacodynamics, and more thorough *in vivo* mechanism examinations to eventually uncover the therapeutic value of C150 and shed more light on our understandings on inhibiting cancer cell EMT and enhancing ER stress to comprehensively inhibit pancreatic cancer.

Acknowledgments

The completion of this dissertation study would not have been possible without the help and guidance from many people.

First of all, I would like to express my deepest gratitude to my mentor, Dr. Qi Chen, who has been very supportive and encouraging throughout my graduate study. Her expertise and patience have assisted me greatly in my research work, as well as in the preparation of this dissertation document.

I would also like to thank my committee members, Dr. Udayan Apte, Dr. Bruno Hagenbuch, Dr. Nikki Cheng, and Dr. Wen-Xing Ding for their insightful inputs and advice to my research work.

I would like to thank our current and previous lab members, Ping Chen and Ruochen Dong for their support and lab discussions, and Kishore Polireddy for his pioneering work on this project.

I also wish to thank all the faculty and staff in the Department of Pharmacology, Toxicology and Therapeutics for helping me with my research and coursework.

I would like to thank all my family members, my parents, my brother, and my aunts for their emotional support.

Last but not least, I wish to thank all my friends. Their friendship and moral support have made this long journey easier and more enjoyable.

Table of Contents

List of Figures

List of Tables

List of Abbreviations

Abbreviation	Definition
ABC-transporters	ATP-binding cassette transporters
ALDH	Aldehyde dehydrogenase
AMP	Adenosine monophosphate
AMPK	AMP-activated protein kinase
APS	Ammonium persulfate
ATCC	American Type Culture Collection
ATF4	Activating transcription factor 4
ATF6	Activating transcription factor 6
ATG	Autophagy-related genes
ATP	Adenosine triphosphate
AURKA	Aurora kinase A
bHLH	Basic helix-loop-helix
BCA	Bicinchoninic acid assay
Bip	Binding immunoglobulin protein
BRG1	Brahma-related gene-1
BSA	Bovine serum albumin

CCCP	Compound-centric chemical proteomics
CDK	Cyclin dependent kinase
CDKN2A	Cyclin dependent kinase inhibitor 2A
CESTA	Cellular thermal shift assay
CHOP	C/EBP homologous protein
CI	Combination Index
CK-1	Casein kinase 1
CQ	Chloroquine
CSC	Cancer Stem Cell
CtBP	C-terminal binding protein
CXCR4	C-X-C chemokine receptor type 4
DAPI	4′,6-diamidino-2-phenylindole
DMSO	Dimethyl sulfoxide
eIF2α	Eukaryotic translation initiation factor 2A
ECM	Extracellular Matrix
EDTA	Ethylenediaminetetraacetic acid
EMT	Epithelial-Mesenchymal Transtion
ER	Endoplasmic Reticulum

ERAD	Endoplasmic Reticulum Associated Degradation
ERK	Extracellular signal-regulated kinases
FAK	Focal adhesion kinase
FOLFIRINOX	Fluorouracil + Leucovorin + Irinotecan + Oxaliplatin
GAPDH	Glyceraldehyde-3-phosphate Dehydrogenase
GDP	Guanosine diphosphate
GEMM	Genetically engineered mouse model
GSK-3β	Glycogen synthase kinase 3 beta
GTP	Guanosine triphosphate
HIF	Hypoxia-inducible factors
HRAS	Harvey rat sarcoma viral oncogene homolog
HRD1	HMG-CoA reductase degradation protein 1
HRP	Horseradish peroxidase
HTS	High Throughput Screening
IC_{50}	Half-maximal inhibitory concentration
IFNs	Interferons
IGF	Insulin-like growth factor
IKK	IκB kinase

ILs	Interleukins
IP	intraperitoneal
IRE1α	Inositol-requiring enzyme 1 α
JNK	c-Jun N-terminal kinases
KRAS	Kirsten rat sarcoma viral oncogene homolog
LATS2	Large tumor suppressor homolog 2
LC3	Microtubule-associated proteins 1A/1B light chain 3
mTOR	Mammalian target of rapamycin
MAPK	Mitogen-activated protein kinases
MDM2	Mouse double minute 2 homolog
MMPs	Matrix metallopeptidases
MTT	3-(4,5-dimethylthiazol-2-yl)-2,5-diphenyltetrazolium bromide
MUC1	Mucin-1, cell surface associated
NOXA	Phorbol-12-myristate-13-acetate-induced protein 1
ORF	Open reading frames
PAAF	Proteasomal ATPase-associated factor 1
PAC-1	Proteasome assembly chaperone 1
PanINs	Pancreatic intraepithelial neoplasia

PAK1	p21-activated kinase 1
PBS	Phosphate buffer solution
PCR	Polymerase chain reaction
PDAC	Pancreatic ductal adenocarcinoma
PDGF	Platelet-derived growth factor
PDK1	Pyruvate dehydrogenase kinase isoform 1
PE	Phosphatidylethanolamine
PEG-400	Polyethylene glycol-400
PERK	Protein kinase R (PKR)-like endoplasmic reticulum kinase
PI3K	Phosphoinositide 3-kinases
PKC	Protein kinase C
PKD1	Protein kinase D1
PNET	Pancreatic neuroendocrine tumors
POMP	Proteasome maturation protein
PRC2	Polycomb repressive complex 2
PSC	Pancreatic stellate cells
PSMC-2	26S proteasome regulatory subunit 7
PSMC-3	26S proteasome regulatory subunit 6A

PSMC-4	26S proteasome regulatory subunit 6B
PSMD-5	26S proteasome non-ATPase regulatory subunit 5
PSMD-9	26S proteasome non-ATPase regulatory subunit 9
PSMD-10	26S proteasome non-ATPase regulatory subunit 10
PUMA	p53 up-regulated modulator of apoptosis
PVDF	Polyvinylidene difluoride
REDD1	DNA damage-inducible transcript 4 protein
RIDD	IRE1α-dependent decay
RIPA	Radioimmunoprecipitation assay buffer
S1P	Site 1 protease
SAHF	Senescence- associated heterochromatin foci
SAR	Structure-activity relationship
SASP	Senescence-associated secretory phenotype
SDS-PAGE	Sodium dodecyl sulphate–polyacrylamide gel electrophoresis
SET8	SET domain-containing protein 8
SHH	Sonic Hedgehog
SIAH1	Seven in absentia homolog 1
SMAD2	SMAD family member 2

SMAD4	SMAD family member 4
SPR	Surface plasmon resonance
SREBP-1	Sterol regulatory element-binding protein 1
STAT3	Signal transducer and activator of transcription 3
TBS	Tris-buffered saline
TEMED	Tetramethylethylenediamine
TGF-β	Transforming growth factor beta
TP53	Tumor Protein P53
TRAF2	TNF (tumor necrosis factor) receptor associated factor 2
TWIST1	Twist-related protein 1
ULK1	Unc-51-like kinase 1
UPR	Unfolded protein response
UTR	Untranslated region
VCP	Transitional endoplasmic reticulum ATPase
XBP-1	X-box-binding protein 1
ZEB1	Zinc finger E-box-binding homeobox 1
ZEB-2	Zinc finger E-box-binding homeobox 2
ZO-1	Zonula occludens-1

Chapter 1. Introduction

1.1 Pancreatic cancer

1.1.1 Basics of pancreatic cancer

The pancreas is biologically made up of exocrine and endocrine components. The exocrine component mainly consists of acinar cells (digestive enzyme secreting cells) and ductal cells (epithelial cells making up the pancreatic ducts), while the endocrine component is made up of hormone-secreting cells located in the islet of Langerhans [1] (**Fig 1.1**). Tumors derived from the endocrine component are called pancreatic neuroendocrine tumors (PNET). The specific type of PNET depends on the hormone the tumor cells produce. For instance, insulinomas are tumors derived from insulin-making cells (beta-cells). PNET are relatively rare, accounting for only about 7% of all cancers in the pancreas. The majority of malignant neoplasms in the pancreas are derived from the exocrine components. These tumors, called adenocarcinomas, account for the remaining 93% of all pancreatic cancer cases. Among the exocrine tumors, pancreatic ductal adenocarcinoma (PDAC) is the most common type, making up for 95% of exocrine pancreatic cancers and 90% of all pancreatic cancers [2]. Thus, PDAC is commonly referred to as pancreatic cancer [3]. In this document, the term PDAC and pancreatic cancer will be used interchangeably.

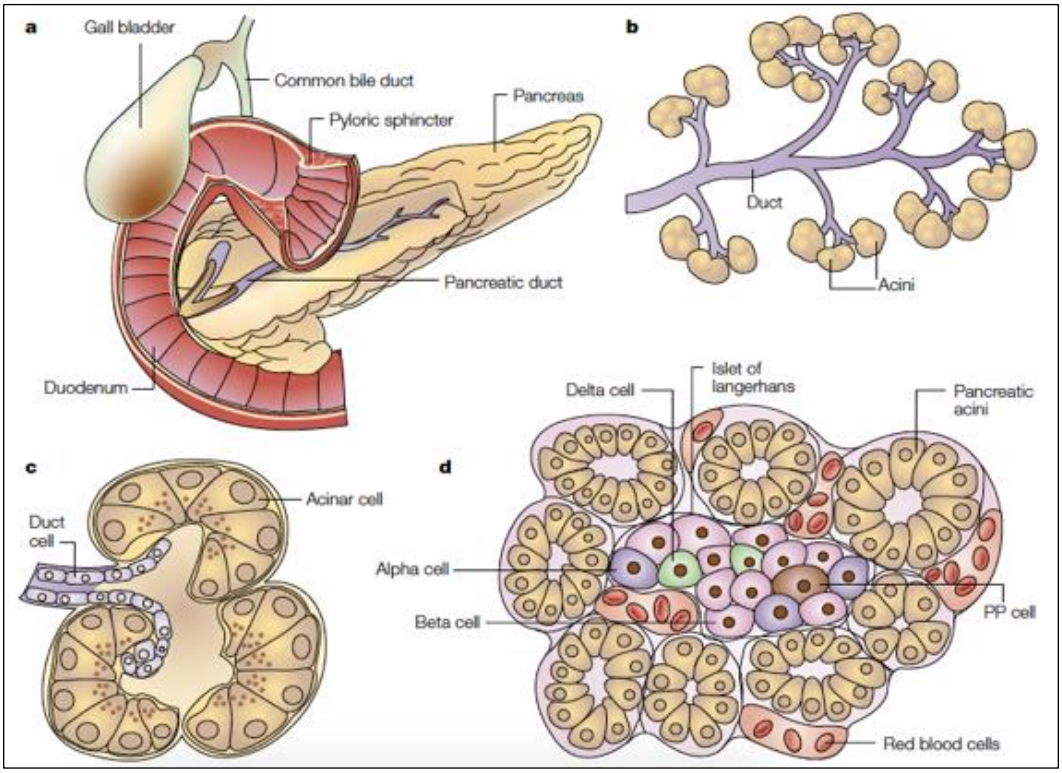

Figure 1.1 Pancreas anatomy [1]. **a.** gross anatomy of human pancreas. **b.** Pancreatic ducts and pancreatic acini of the exocrine components. **c.** Acinar cells make up a single acinus unit, which forms a small sac at the end of pancreatic ducts. **d.** Endocrine cells in the islet of Langerhans surrounded by acini. PP cells: pancreatic polypeptide secreting cells.

Pancreatic cancer is now the fourth leading cause of cancer-related deaths in the United States. It is estimated that 60,430 new cases of pancreatic cancer will be diagnosed, and more than 48,220 people will die from the disease in the year 2021 [4]. Pancreatic cancer is one of the most malignant and most lethal cancers with a current overall 5-year survival rate of 10% [4]. The high mortality rate is largely attributed to its late diagnosis because of the lack of specific symptoms during the early stages of the disease. Most pancreatic cancer patients exhibit either

locally advanced tissue invasion or distant metastases upon diagnosis, for whom the 5-year survival rate is only 3% [4]. Only 10-20% of patients present with localized and surgically removable tumors [5]. Even with removable tumors, most patients will ultimately have recurrence after the initial resection, and the 5-year survival rate for these patients is about 25% [3, 6]. The most common metastatic sites for pancreatic cancer are the liver, the lung, and the peritoneum. Because of its aggressive nature and widespread metastasis, the prognosis of pancreatic cancer remains extremely poor.

Currently, the only potentially curative treatment for pancreatic cancer is the surgical removal of the tumor [7], which is only feasible in patients without distant metastasis (less than 20%) [5]. For most patients, chemotherapy is the main option of treatment, with or without the combination of radiation. Gemcitabine has been the standard treatment since 1997 when a clinical study showed that gemcitabine offered better overall survival than fluorouracil [8]. Since then, many clinical trials have been conducted to compare other treatment regimens with gemcitabine, but success was rare. FOLFIRINOX (a cocktail of Leucovorin, Fluorouracil, Irinotecan, and Oxaliplatin) was found to improve the median overall survival in patients by a few months when compared to gemcitabine monotreatment, but with significant associated toxicity [9]. The regimen was only recommended for patients younger than 75 years with overall good performances [9]. More recently, studies found that albumin-bound paclitaxel (nab-paclitaxel) plus gemcitabine treatment showed a better treatment response and a 1.8-months improvement in median overall survival in patients with metastatic pancreatic cancer when compared to gemcitabine monotherapy [10]. Currently, FOLFIRINOX and gemcitabine plus nab-paclitaxel are both recommended as first-line choices of chemotherapies for metastatic

pancreatic cancer, but criteria for choosing FOLFIRINOX are more rigorous due to higher toxicities [11, 12].

1.1.2 Patho-histology of pancreatic cancer

Development of PDAC from pre-cancerous lesions

PDACs, as the name suggests, are tumors found in the pancreatic ductal system, although the cell origin of PDAC can stem from both ductal cells and the transformation of acinar cells [13, 14]. The location of the tumor can be found in the head, body, or tail region of the pancreas. Tumors that arise from the body or tail of the pancreas are usually associated with a worse prognosis than those that arise from the head region [15, 16]. The development of PDAC undergoes stepwise stages of progression from precursor lesions to fully invasive tumors. The most common precursor lesions of PDAC are non-cystic microscopic pancreatic intraepithelial neoplasias (PanINs) [17]. These non-invasive lesions are categorized into three grades, PanIN-1, PanIN-2, and PanIN-3, based on their histological and cytological features [18] (**Fig 1.2**). PanIN-1 lesions are low-grade dysplasia characterized by the mucinous epithelium with basally located round nuclei, while PanIN-2 lesions (moderate dysplasia) exhibit loss of mucinous epithelium with the acquisition of nuclear stratification and crowding [17, 19]. PanIN-3 lesions are associated with total loss of cell polarity, severe nuclear atypia with abnormal mitotic features, and intraluminal necrosis [19, 20]. PanIN-1 and PanIN-2 can be found in normal pancreas or chronic pancreatitis patients without signs of invasive tumors, while PanIN-3 lesions are almost exclusively found in PDACs [21], indicating that PanIN-1 and PanIN-2 have lower risks of developing into PDAC than PanIN-3. The development of PanINs is accompanied by a stepwise accumulation of genetic mutations. KRAS mutation is observed in PanIN-1 to PanIN-3 lesions with increasing

frequency (36% in PanIN-1, 44% in PanIN-2 and 87% in PanIN-3) [22]. The mutation of CDKN2A frequently occurs in PanIN-2 and PanIN-3 following KRAS mutation [23]. Finally, TP53 and SMAD4 mutations are often found in high-grade PanIN-3 lesions [24]. The stepwise accumulation of genetic mutations from PanIN-1 to PanIN-3 gradually drives the precursor lesions into fully invasive PDAC.

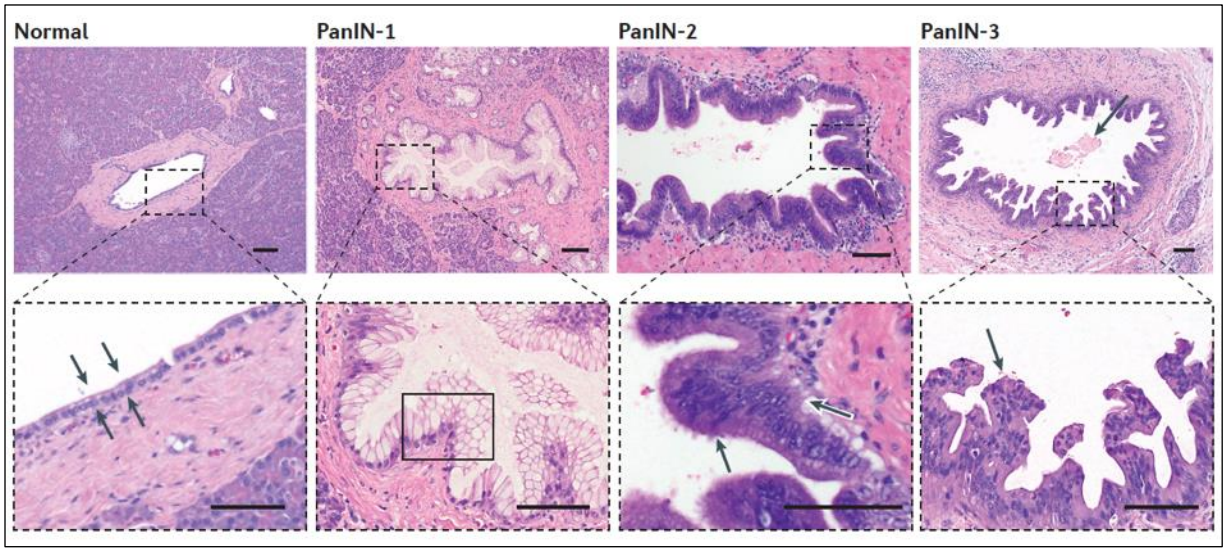

Figure 1.2 Histological features of pancreatic intraepithelial neoplasia (PanINs) and normal pancreatic duct [19]. Arrows in the "Normal" panel denote normal pancreatic ductal epithelium. Arrows in the "PanIN-2" panel denote the moderate pancreatic ductal dysplasia with nuclear stratification and crowding in the cell. The arrow in the upper "PanIN-3" panel denotes intraluminal apoptotic debris. Arrows in the lower "PanIN-3" panel denote the pseudopapillary formation. Scale bar: 100 μm.

PDAC stroma

The most typical and characteristic gross histological feature of pancreatic cancer is its rich stroma, which is called desmoplasia. The stroma, which can sometimes account for up to 80% of the total tumor mass [25], is composed of a dense fibrous extracellular matrix (ECM) network

that is made up of collagenous proteins like collagens, laminin, fibronectin, and non-collagenous proteins like glycoproteins and proteoglycans [26]. The collagen-rich ECM is predominantly produced by activated pancreatic stellate cells (PSCs) [27]. Pancreatic cancer cells reside in the stroma alongside PSCs, immune cells, macrophages, endothelial cells, and nerve cells [28]. This highly interactive microenvironment significantly facilitates pancreatic cancer progression. In the stroma, the dense ECM network not only provides a physical scaffold for cancer cells and stromal cells to proliferate and interact, but it also creates a dense barrier and high interstitial pressure within the tumor mass that restricts blood flow to the area [29]. The restricted blood flow creates a highly hypoxic environment that further accelerates genome instability and heterogeneity within cancer cells. Limited blood perfusion also impedes the delivery of therapeutic agents to the tumor, which may in part explain the poor treatment outcomes of the disease.

1.1.3 Genetic landscape of pancreatic cancer

KRAS

Like most cancers, pancreatic cancer is a genetic disease triggered by the accumulation of gene mutations in the cell. Among the genes mutated in PDAC, KRAS is the most frequently mutated gene. Mutated KRAS is found in approximately 95% of all cases [19, 30, 31]. KRAS is a small GTPase that acts as a key switch for cell growth and proliferation by cycling between the GTP-bound (active) and GDP-bound (inactive) state in the RAS/MAPK pathway [32]. The mutations of KRAS in PDAC exclusively occur at three locations in the protein, G12, G13, and Q61, with G12 being the most predominant mutated position (about 98%) [33]. These mutations render the KRAS protein in a persistent GTP-bound active state, triggering non-stoppable cell growth and

proliferation. KRAS mutations can be observed in all stages of pancreatic cancer development, from PanIN-1 to PDAC [22]. It is considered a key initiating factor for pancreatic cancer development [34]. Studies in genetically engineered mouse models of pancreatic cancer have revealed that mice with KRAS mutations in the pancreas can spontaneously develop invasive and metastatic pancreatic cancer [35]. PDAC development in KRAS mutated mice was greatly accelerated when additional mutations were introduced, such as in CDKN2A and TP53 [36, 37], suggesting the importance of other driver gene mutations in pancreatic cancer progression.

CDKN2A

CDKN2A is the next frequently mutated gene in PDAC, which occurs in 90-95% of all pancreatic cancer cases [38, 39]. The most common mutation events of CDKN2A in PDAC are homozygous deletions and hypermethylation-induced gene silencing [38, 40]. The human CDKN2A gene encodes two different tumor suppressors, $p16^{INK4A}$ and $p14^{ARF}$ ($p19^{ARF}$ in mouse) [41]. Mutation of this gene resulted in the loss of function of both proteins [42], although $p16^{INK4A}$ loss was thought to be the primary event in PDAC [43]. The two tumor suppressors work through different pathways to control cell cycle progression. $p16^{INK4A}$ functions as an inhibitor of G1 cyclin-dependent kinases (CDKs) by preventing the binding of cyclin D to CDK4/6, leading to the halt of cell cycle at G1/S phase [44, 45]. $p14^{ARF}$ functions in a CDK-independent manner. It physically interacts with MDM2 and inhibits MDM2-mediated degradation of tumor suppressor TP53, whose functions include induction of cell cycle arrest and apoptosis [46, 47]. Loss of CDKN2A function allows pancreatic cancer cells to escape from cell cycle checkpoints, cellular senescence, and apoptosis under stress conditions, leading to hyperactive cell division and proliferation.

TP53

TP53 is one of the most frequently mutated genes in all cancers. Roughly, 50%-60% of all cancers harbor mutations in this gene [48]. In PDAC, the frequency of TP53 mutation is about 85% [40]. Wildtype TP53 encodes the protein p53, a tumor suppressor, that functions as cell cycle checkpoint regulator and apoptosis inducer, thus preventing wrongful cell cycle progression under genotoxic or replicative stress [49]. Mutation of TP53 often occurs as missense mutations within its DNA binding domain, causing the protein to lose its transcriptional activity as a tumor suppressor [49]. In pancreatic cancer, up to 66% of TP53 mutations are missense mutations, although intragenic deletions and frameshift mutations were also observed [19, 40]. Importantly, it is now clear that mutated TP53 not only just loses its tumor suppressor function, it gains oncogenic properties that promote tumor development [50, 51]. Mutant TP53 acts as a co-transcription factor that modulates the expression of many oncogenic genes to promote cancer development in many cancers [50, 52]. In PDAC, the oncogenic function of mutant TP53 has been well documented. Mutant TP53 enhances proliferation and metastasis when compared to simple deletion of the protein [53-55]. The loss of tumor-suppressing function combined with the gain of oncogenic function in TP53 mutations collectively aggravates PDAC progression.

SMAD4

SMAD4 is a key downstream factor in the TGF-β signaling pathway and a tumor growth suppressor in pancreatic cancer [56, 57]. TGF-β signaling negatively controls cell growth and proliferation to maintain tissue homeostasis in normal tissues [58]. Upon TGF-β activation, SAMD4 forms a complex with SMAD2/3 and translocates to the nucleus, transcribing genes

involved in inducing cell cycle arrest and apoptosis [59]. Mutations of SMAD4 occur in approximately 55% of pancreatic cancer cases, with 30% by homozygous deletion and 25% by intragenic mutation [19], leading to the loss of its tumor-suppressing function. Clinically, PDAC patients with a SMAD4 mutation have a worse prognosis than those without the mutation [60]. Studies in genetically engineered mice have shown that SMAD4 inactivation alone could not initiate pancreatic cancer formation, but rapidly promoted tumor development and metastasis when combined with a KRAS mutation [61-63]. In agreement with these findings are the clinical observations showing that a SMAD4 mutation is often detected in invasive PanIN-3 lesions and PDAC, but not in pre-invasive PanIN-1 and PanIN-2 lesions [17, 64], suggesting that SMAD4 inactivation is a promoting factor rather than an initiating factor in PDAC development.

Many other less frequent genetic alterations are also found in PDAC. On average, pancreatic cancer contains > 60 genetic alterations, involving core signaling pathways associated with cell growth, proliferation, invasion, apoptosis, senescence, and immune evasion [65]. This represents a highly complicated signaling network that promotes pancreatic carcinogenesis. Approaches have been developed to target mutant KRAS and TP53 to control pancreatic cancer progression [66, 67]. However, loss-of-function mutations in tumor suppressors such as those in CDKN2A and SMAD4 are hard to target, and their normal functions hard to restore pharmacologically. As our understanding of the oncogenic signaling network of PDAC has grown, challenges remain because targeting only one of the mutations/pathways may not stop all the oncogenic signaling. In addition to the complexity caused by genetic alterations in tumor cells, the dynamic and immune-suppressive tumor microenvironment further complicates the treatment of the disease.

Comprehensive understanding and innovative approaches need to be developed and tested with an open mind, including but not limited to PDAC tumor microenvironment and immunology.

1.2 Epithelial-mesenchymal transition (EMT) in pancreatic cancer

1.2.1 Basics of EMT

Epithelial-mesenchymal transition (EMT) is a cellular program through which the apical-to-basal polarized epithelial cells are converted to front-to-back polarized mesenchymal cells [68]. During EMT, epithelial cells lose their cell-cell adhesions and change into fibroblast-shaped mesenchymal cells, switching their epithelial marker proteins to mesenchymal markers. The process is also accompanied by functional changes of the cell, such as increased invasiveness and mobility. Some major distinctions between epithelial and mesenchymal cells are summarized in **Table 1.1**.

Table 1.1 Major distinctions between epithelial and mesenchymal cells.

Features	Epithelial	Mesenchymal
Morphology	Cobble stone-like (Cuboidal/Columnar)	Spindle-shaped (Fibroblast-like)
Mobility	Non-mobile	Mobile
Polarity	Apical-to-basal	Front-to back
Typical cellular markers	E-Cadherin ZO-1 Claudins Cytokeratins	N-Cadherin Vimentin Zeb-1 Snail Fibronectin
Cell-Cell Contacts	Strong adhesion to adjacent epithelial cells through adhesion junctions and tight junctions, strong adhesion to basal lamina via hemidesmosomes.	Focal contacts with extracellular matrix (ECM), loss of cell-cell adhesion

The program of EMT is fundamentally required for embryonic development. For instance, during gastrulation, multiple waves of EMT are required for the formation of the mesoderm layer

of the developing embryo [69]. EMT also plays a critical role in organ repair, wound healing, and tissue fibrosis [70]. Over the past two decades, it has become more and more evident that carcinoma cells can hijack the EMT program to maintain the intrinsic plasticity between the epithelial and mesenchymal states [70-72]. The induction of EMT in cancer cells is conveyed by many different signaling pathways, such as TGF-β, WNT/β-catenin signaling, Notch signaling, and various receptor kinase signaling pathways [73-76] (**Fig 1.3**). In response to these signals, cells upregulate the expression of multiple EMT promoting factors to execute the EMT program.

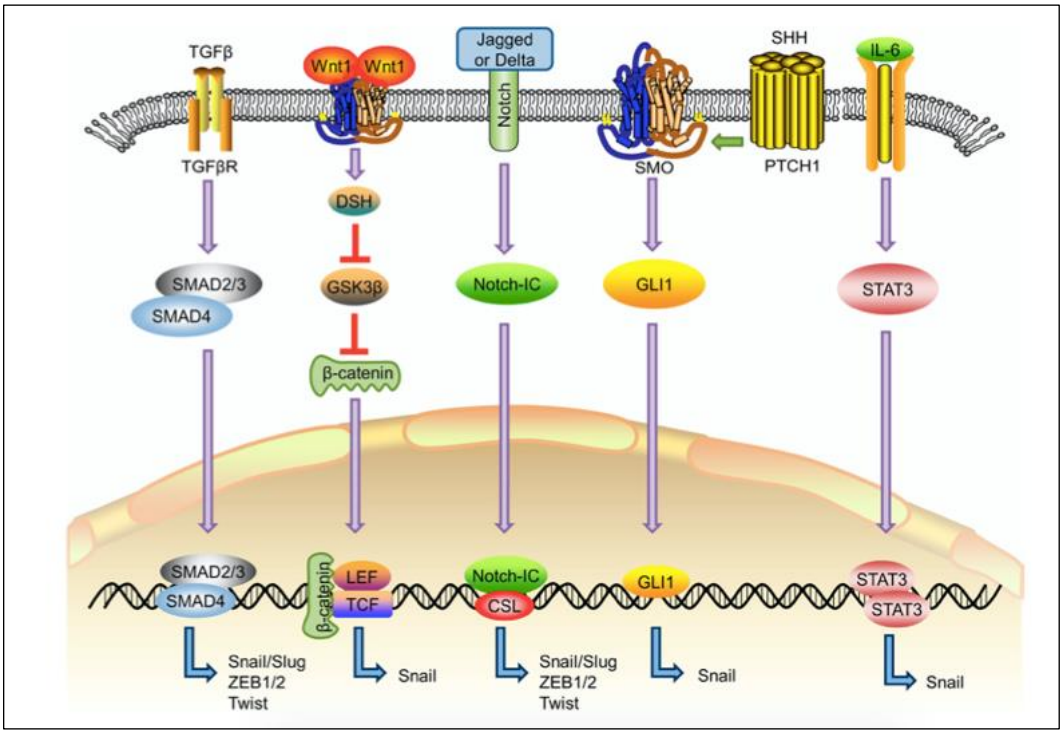

Figure 1.3 Major signaling pathways that induce EMT [76]. Activation of TGF-β, WNT/β-Catenin, Notch, Sonic Hedgehog (SHH), and STAT3 induces EMT by upregulating gene expressions of EMT promoting transcription factors (EMT-TFs), such as Snail, Slug, Zeb-1, Zeb2, and Twist.

1.2.2 EMT promoting transcription factors (EMT-TFs)

The different cellular signaling pathways stimulating EMT (**Fig1.3**) all lead to the expression of EMT-transcription factors (EMT-TFs). These EMT-TFs work independently or in combination to repress epithelial gene expressions while promoting mesenchymal gene expressions [77], and therefore control the EMT program in the cell. Different EMT-TFs are reported to induce EMT under different conditions with five of them considered the major players in cancers: Snail, Slug, Zeb1, Zeb2, and Twist1 [78].

Snail and Slug

Snail and Slug are zinc-finger transcription factors in the Snail protein family with similar structures [79, 80]. Snail and Slug bind to the E-box motif sequence through their C-terminal DNA binding domains, repressing gene expression of epithelial markers, such as E-cadherin, claudins, and occludins, while promoting expression of mesenchymal markers, such as fibronectin, MMPs, and vimentin [81]. The transcriptional activities of Snail and Slug depend on the recruitment of histone modification complexes. Upon binding to the E-box motif, Snail recruits the PRC2 complex, modifying histones around the proximal promoter region through methylation and acetylation [82].

Snail gene expression is regulated by a variety of signaling pathways, such as TGF-β, WNT, Notch, PI3K-AKT, IGF (insulin-like growth factor), and NF-κB [82-87]. Activation of these pathways leads to elevated Snail gene expression, thus promoting EMT. Aside from extracellular signaling pathways, some microRNAs (miRNAs) also control Snail gene expression. MicroRNAs are small single-stranded RNA molecules that complementarily bind to their target

regions in mRNAs and inhibit mRNA translation [88]. For instance, miR-29b and miR-30a directly target Snail mRNA to reduce its translation [89, 90], and miR-1 and miR200b directly repress Slug expression [91]. Therefore, these miRNAs are potential EMT inhibitors for silencing the family of Snail proteins. In addition to transcriptional control, Snail protein levels are also tightly controlled post-translationally through phosphorylation and the ubiquitin-proteasome degradation system (UPS) [80]. Many kinases have been reported to control Snail protein stability. Kinase GSK3β and PDK1 phosphorylate Snail to promote its nuclear exportation and subsequent ubiquitination and proteasomal degradation [92, 93], while phosphorylation by LAST2 and PAK1 increased Snail protein stability by retaining its nuclear localization [94, 95].

The correlation between Snail expression and pancreatic cancer progression has been well documented. Studies using patient tissue samples of pancreatic cancer revealed that Snail was highly expressed at the invasive front of the tumor, and its expression level was positively related to distant metastasis and lymph node invasion [96], suggesting its function in promoting pancreatic cancer tissue invasion. In addition, overexpression of Snail in pancreatic cancer cell lines resulted in more aggressive tumor development and increased metastasis in mouse xenografts [97].

Zeb1 and Zeb2

The vertebrate ZEB family of proteins are zinc-finger transcription factors that include Zeb1 (also known as TCF-8 and δEF1) and Zeb2 (also known as SIP1) [98]. Both proteins contain two zinc-finger cluster domains that bind to the regulatory region of E-box elements and repress the

expression of genes of multiple epithelial markers [98]. The transcription repression by Zeb1 often involves the recruitment of co-repressors, such as CtBP and BRG1 [99, 100]. Like Snail family proteins, ZEB proteins also promote mesenchymal gene expressions [98]. The transcription activation of mesenchymal genes by Zeb1 depends on its interaction with transcription activators p300 and P/CAF [101]. Through repressing the expression of epithelial genes while promoting the expression of mesenchymal genes, the ZEB proteins define EMT features in many different types of cancer.

The expression of ZEB family genes is regulated by many signaling pathways, such as TGF-β, WNT, STAT3, and HIF-1α signaling [102-105]. Notably, Snail expression is able to directly upregulate Zeb1 mRNA expression and enhance Zeb1 protein stability [106, 107]. Zeb1 and Zeb2 are also regulated post-transcriptionally by the miR-200 family of microRNAs and by miR-205, which repress Zeb1 and Zeb2 mRNA translation by binding to the 3'UTR regions of the mRNAs [108]. The function of ZEB proteins is also modulated by post-translation modifications. SUMOylation, which is the addition of small ubiquitin-like modifiers (SUMO) to protein lysine residues, by polycomb protein Pc2, inhibited Zeb1 and Zeb2 transcriptional activities by reducing the recruitment of co-repressor CtBP [109]. Phosphorylation of Zeb1 by PKC and ERK1/2 reduced the binding of Zeb1 to its target DNA sequence, thus attenuated its transcriptional activity [110]. Although SUMOylation and phosphorylation affected the function of ZEB proteins, the studies did not show any effects on the stability of ZEB proteins by these modifications. A more recent study showed that caspase-8-associated protein 2 (CASP8AP2 or FLASH) was able to increase Zeb1 protein stability by preventing its proteasomal degradation

[111]. Additionally, another study found that Zeb1 protein was destabilized by the ubiquitin E3 ligase SIAH1/2 and stabilized by deubiquitylase USP51 [112].

A high expression level of Zeb1 is associated with poor survival in various solid tumors, including pancreatic cancer [113]. Patient tissue samples of pancreatic cancer have high expression levels of Zeb1 and Zeb2 in cancer cells with mesenchymal phenotypes and low expression levels in cells with epithelial phenotypes, suggesting a prominent role of ZEB proteins in promoting EMT in pancreatic cancer [114]. In addition, depletion of Zeb1 largely decreased invasion and metastasis in a genetically engineered mouse model of pancreatic cancer [115].

Twist1

Twist1 is a member of the basic helix-loop-helix (bHLH) family of transcription factors. The bHLH family of proteins includes additional members, such as Twist2, E12, E47, and the inhibitor of differentiation (ID) protein. Among these members, Twist1 is the most studied in EMT [78]. Twist1 strongly promotes EMT in many cells by repressing E-cadherin while promoting N-cadherin expression [82]. Unlike Snail or ZEB that bind to a single E-box promoter region, Twist1 preferably forms a dimmer with E47 and binds to a double E-box motif region to activate gene transcription [116]. The transcriptional activity of Twist1 often requires histone modifications around its target gene region. For instance, Twist1 recruits methyltransferase SET8, which modifies histones by H4K20 methylation at the promoter regions responsible for E-cadherin repression and N-cadherin activation in breast cancer cells [117].

Twist1 gene expression is upregulated by many factors, such as STAT3, NF-κB, IFN, and HIF-1α [118]. Among these factors, HIF-1α is a direct upstream factor that promotes Twist1 gene expression [119]. HIF-1α binds to the hypoxia response element (HRE) in the Twist1 proximal promoter region and directly promotes Twist1 gene expression in different types of human cancer cells [119]. By analyzing the 3'UTR sequence of Twist1 mRNA, one study identified three microRNAs, miR-145a-5p, miR-151-5p, and miR-337-3p, that repressed Twist1 translation [120]. Subsequently, more miRNAs have been reported to inhibit Twist1 expression in human cancer cells, such as miRNA-106b, miRNA-543, and miRNA-33 [121-123]. Similar to the Snail protein, the function and stability of Twist1 are tightly regulated by phosphorylation. Phosphorylation of Twist1 on S123/T148/S184 by AURKA, on S18/S20 by CK2, and on S68 by MAPKs increases the protein stability of Twist1, and therefore enhances its transcriptional activity in promoting EMT [124-126]. Phosphorylation on S42/T121/S123 by AKT1 and on T125/S127 by IKKβ, primes Twist1 for ubiquitination and proteasomal degradation [127, 128].

A study showed that, of fifteen established human pancreatic cancer cell lines, 9 showed detectable Twist1 mRNA expressions, and the expression levels were inversely correlated with E-cadherin expressions [129]. In the non-Twist1 expressing pancreatic cell lines, Twist1 expression was strongly activated upon induction of hypoxia [96]. Additionally, Twist1 protein expression was higher in pancreatic cancer tissues than that in normal tissue by immunohistochemistry staining [130]. The higher expression of Twist1 is associated with a poorer prognosis [130]. Studies have also shown that overexpression of Twist1 or induction of hypoxia efficiently induced EMT and promoted pancreatic cancer progression in mouse

xenografts [130, 131]. These reports suggest that Twist1 is a potent EMT promoter in pancreatic cancer, especially in a hypoxic microenvironment.

1.2.3 EMT in promoting pancreatic cancer progression

EMT and pancreatic cancer metastasis

The role of EMT in promoting cancer metastasis has been extensively studied [132-134]. It is now believed that primary carcinoma cells receive EMT-promoting signals from the tumor microenvironment and are forced to initiate EMT [72]. Once the carcinoma cells undergo EMT, they shed off their epithelial properties, lose cell-cell adhesion, and acquire a more invasive mesenchymal phenotype. The mesenchymal cancer cells then disseminate from the primary tumor bulk, invade through the extracellular matrix, intravasate into the blood circulation, and eventually form new metastatic lesions at distant organs [72]. In clinical PDAC samples, cells with a mesenchymal phenotype that have lost E-cadherin are mainly found at the invasive front [96]. Furthermore, expression of EMT-TFs, such as Snail, Zeb-1, and Twist1, was upregulated in PDAC tissues [96, 114, 130]. In a genetically engineered mouse model that recapitulates the multi-step development of PDAC from PanINs, it was demonstrated that EMT happened in the very early stage of tumor formation and was associated with cancer cell dissemination and invasion before/in parallel to primary pancreatic tumor formation [135]. This study suggested that cell invasion and metastasis in pancreatic cancer could occur very early on during PDAC development, and EMT played an essential role in the early cell dissemination and invasion. In addition, depletion of Zeb-1 greatly reduced distant metastases in a similar transgenic mouse model [115]. Overexpression of Snail in human pancreatic cancer cell lines also exhibited

enhanced metastatic abilities in mouse xenografts [97]. These studies strongly supported the contributing role of EMT in pancreatic cancer metastasis.

EMT and pancreatic cancer stem cells

Cancer stem cells (CSCs) are a small fraction of stem cell-like neoplastic cells within the cancer cell population, defined by their capabilities of self-renewal, tumorigenicity, and differentiation [136]. These distinct cells bear the capacity to either divide symmetrically and generate the same daughter cells with the same stem-cell properties, or asymmetrically generate progenitor cells that differentiate into cancer cells, thus fueling tumor growth [136]. These self-renewable cells are highly tumorigenic and capable of initiating new tumors starting from very few cells [137]. In pancreatic cancer, CSCs were first identified as cells that are triple positive for surface markers CD44, CD24, and EpiCAM [138]. Subsequently, more CSC markers, such as CD133, CXCR4, and ALDH have also been reported in pancreatic cancer [139, 140]. Pancreatic CSCs can be 100-fold more potent in forming a new tumor compared to the general PDAC cell population [138]. This strong ability to form new tumors also grants them the ability to colonize at metastatic sites [141]. Depletion of $CD133^{+}CXCR4^{+}$ CSCs significantly impeded pancreatic cancer metastasis [139]. In addition, pancreatic CSCs are highly resistant to chemotherapeutic agents, which may partially explain the high relapse rate of pancreatic cancer after treatment [142].

The correlation between EMT and CSCs was first discovered by studies in breast cancer, which found that induction of EMT generated cells with stem characteristics [143]. Later, similar studies in pancreatic cancer showed that acquisition of EMT in pancreatic cancer cells was also

associated with increased stemness [144]. Murine pancreatic cancer cells that underwent EMT also exhibited strong stem-cell traits [135]. Overexpression of Zeb-1 promoted tumorigenicity while deletion of Zeb-1 reduced stemness and colonization abilities [115, 145]. A similar study showed that Snail was highly expressed in the pancreatic CSCs population, and silencing Snail resulted in reduced tumor formation in mice [146]. These findings strongly indicate that activation of EMT in pancreatic cancer cells promotes the generation of pancreatic CSCs.

EMT and chemo-resistance in pancreatic cancer

In addition to promoting cancer metastasis and the generation of cancer stem cells, studies have also demonstrated that EMT contributes significantly to cancer drug resistance [144, 147]. The exact mechanisms of EMT-induced drug resistance are not yet fully understood [76]. Two major pathways are proposed. First, cancer cells that underwent EMT may acquire resistance to drug-induced apoptosis, mediated by the up-regulation of EMT-TFs that interfere with apoptosis and DNA-damage response pathways [76]. For example, in non-small cell lung cancer (NSCLC) cells, increased expression of Slug contributed to the resistance of gefitinib-induced apoptosis by suppressing Bim expression [148]. Overexpression of Snail in breast cancer cells promoted cell resistance to genotoxic stress [149]. Another potentially important factor, perhaps the more dominant factor, of EMT-induced drug resistance is its ability to promote cancer stem cell generation [150, 151]. CSCs are well-known to be resistant to many chemotherapeutic agents, due to their quiescent status, overexpression of drug efflux transport proteins, and altered DNA damage response [150, 152]. In fact, gemcitabine-resistant pancreatic cancer cells are usually highly enriched with CSCs markers [153, 154].

1.2.4 Strategies for targeting EMT in pancreatic cancer

Given the significant roles of EMT in promoting cancer metastasis, drug resistance, and CSCs generation in pancreatic cancer, it could be of great value to target EMT for pancreatic cancer therapy. Many efforts have been made to pharmacologically intervene with the EMT process for cancer treatment. These interventions can be categorized into three groups: 1) inhibiting signaling pathways that induce EMT; 2) targeting the transcription factors of EMT, and 3) targeting the EMT mesenchymal phenotype [155].

1) Inhibition of EMT signaling receptors

EMT is initiated upon receiving extracellular signals. Typical EMT-inducing pathways are summarized in (**Fig 1.3**) [76]. The extracellular inducers are at the very upstream of the EMT process. Thus, inhibition of these pathways holds great potential to inhibit EMT at an early stage. Among these pathways, TGF-β signaling is the most studied in many different types of cancers including pancreatic cancer. The TGF-β receptor is a heteromeric complex of two type I and two type II transmembrane kinase receptors. Upon binding their ligands, type II receptors phosphorylate type I receptors, activating the signaling pathway through SMAD proteins [156]. The activated TGF-β pathway promotes EMT by upregulating the expression of many EMT-TFs, such as Snail, Twist, and ZEB-1 [83]. Developing TGF-β receptor inhibitors to prevent EMT has been carried out by many groups. The TGF-β receptor kinase inhibitor SB-431542 was reported by Halder et al. (2005) to be able to block TGF-β induced EMT in pancreatic cancer cells [157]. Since then, many other small molecule inhibitors of the TGF-β receptor have been identified in different cancer types [158, 159]. More recently, a small molecule inhibitor of the TGF-β receptor, LY2157299, was shown to improve the overall survival in pancreatic cancer

patients when combined with gemcitabine in a phase 2 clinical trial (NCT01373164) [160]. Other inhibitors of EMT-inducing signaling pathways have also been reported, such as the STAT3 inhibitor S3I-201 [161] and the WNT inhibitor LGK974 [162]. LGK974 is currently tested in a phase I clinical trial for multiple types of cancer, including pancreatic cancer (NCT01351103), while no clinical trial records have been found for the STAT3 inhibitor S3I-201.

2) Targeting EMT-TFs

Another way to pharmacologically intervene EMT is to target the transcription factors that regulate EMT process. This strategy might be, in fact, more plausible for EMT inhibition because different signaling pathways induce EMT all by increasing the expression of the EMT-TFs. In MDCK-II kidney epithelial cells that overexpressed Snail, silencing Snail expression reduced cell invasiveness and completely reverted the mesenchymal phenotype caused by Snail overexpression [163]. Similar studies also showed that Twist1 inhibition reduced invasiveness and metastasis in breast cancer and oral squamous cell carcinoma [164, 165]. Probably due to the short half-lives of EMT-TFs, small molecules directly inhibiting these TFs have not been successfully developed [155]. Alternatively, EMT inhibition has been achieved by targeting the upstream regulators of these TFs. For instance, a cyclin-dependent kinase inhibitor was identified to down-regulate Zeb-1 and Slug expression and reduced invasiveness of breast cancer cells [166]. A natural product Thymoquinone was reported to down-regulate Twist1 expression and inhibit EMT in breast cancer by increasing DNA methylation in the Twist promoter region [167]. Another study found that 2'-Hydroxycinnamaldehyde inhibited EMT by decreasing the nuclear

localization of Snail [168]. These findings indicate that pharmacological interventions of the expression of EMT-TFs could be an effective way to block EMT in cancer cells.

3) Targeting mesenchymal phenotype

Once cancer cells underwent EMT, they express characteristic mesenchymal markers, such as N-cadherin and Vimentin, which makes them molecularly different from their original epithelial cells. These characteristic markers have made the mesenchymal cells themselves a potential target for EMT inhibition. Some early efforts have been made to target these markers. An N-cadherin-blocking peptide was reported to inhibit pancreatic cancer migration and metastasis by blocking N-cadherin function [169]. A similar study also found that a monoclonal antibody against N-cadherin reduced prostate cancer metastasis in mice [170]. Another typical mesenchymal marker, Vimentin, has also been investigated as an EMT inhibition target. Withaferin-A, a natural product, was reported to inhibit cell migration and metastasis in a breast cancer mouse model by promoting depolymerization of Vimentin filaments [171]. Since mesenchymal cells usually share many similar features with cancer stem cell [143], selective inhibitors for the mesenchymal phenotype may also work as potential cancer stem cell inhibitors [172].

1.3 ER stress

1.3.1 ER stress and UPR signaling pathway

The endoplasmic reticulum (ER) is a branching tubular organelle that functions as a major protein processing factory in the cell. Virtually all cell surface proteins and most secreted

proteins need to be correctly folded and modified in the ER for proper function [173]. Proper ER processing of proteins, which is assisted by ER chaperones, glycosylation enzymes, and oxido-reductases, is essential for cell survival [174]. Therefore, the ER is working at a fine-tuned balance between protein load and folding capacity to ensure proteomic homeostasis in the cell. Disturbance of this balance results in the accumulation of misfolded/unfolded proteins in the ER, which causes a stressful cellular condition called ER Stress [173]. ER stress can be induced by a series of physiological and pathological conditions, such as hypoxia, defects in protein glycosylation, oxidative stress, cellular Ca^{2+} imbalance, protein aggregates due to mutations, and increasing demand of protein secretion [175]. In response to ER stress, cells activate the unfolded protein response (UPR) pathway in efforts to restore protein homeostasis. The UPR signaling cascades trigger the expression of hundreds of genes associated with global protein homeostasis control, which is executed in three ways: reducing ER protein load by translation attenuation, increasing protein folding capacity by increasing ER chaperons, and enhancing misfolded protein removal through ER associated degradation (ERAD) [176, 177]. The UPR pathway consists of three branches which are activated by three ER-resident proteins, inositol-requiring enzyme 1 α (IRE1α), protein kinase R (PKR)-like endoplasmic reticulum kinase (PERK), and activating transcription factor 6 (ATF-6) (**Fig 1.4**).

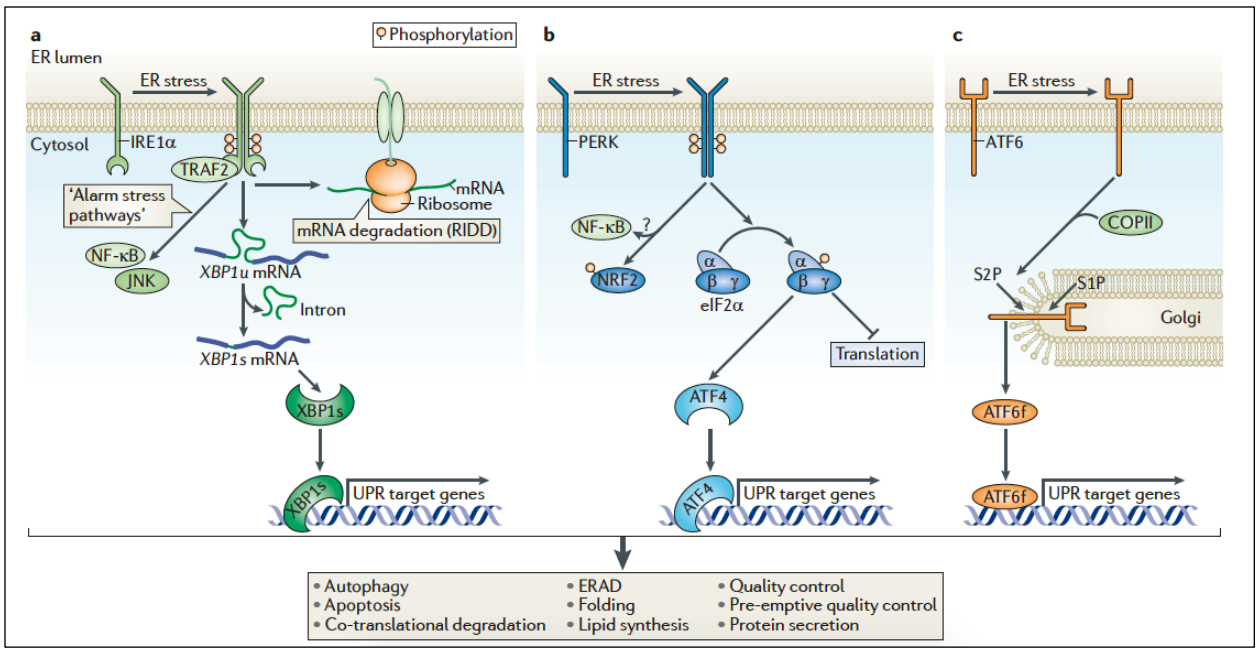

Figure 1.4 Three branches of the unfolded protein response (UPR) pathways [178].

IRE1α

IRE1α is a transmembrane protein containing an N-terminal stress sensor domain in the ER lumen and a C-terminal domain in the cytosol [179]. The C-terminal domain of IRE1α has a dual-function of kinase activity and endoribonuclease activity [179]. Under normal conditions, IRE1α is bound with ER chaperone Bip in the ER lumen to maintain it in an inactive state [180]. Under ER stress, Bip dissociates from IRE1α, leading to IRE1α dimerization and trans-autophosphorylation through the kinase domains, after which it subsequently elicits its RNase activity [181, 182]. The activated IRE1α excises a small intron from the mRNA of the unspliced X-box-binding protein 1 (XBP1u), generating an alternatively spliced form of the mRNA that

encodes the spliced form of XBP1 protein (XBP1s) [183]. XBP1s is an active transcription factor that activates the expression of a series of genes associated with protein folding chaperones, protein secretion, unfolded protein removal via ER associated degradation (ERAD), and lipid synthesis [184]. In addition, the RNase activity of the activated IRE1α cleaves a subset of cellular mRNAs and miRNAs with specific sequences and secondary structure, leading to their degradations, a process called regulated IRE1-dependent decay (RIDD) [185-187]. The degradation of mRNA by IRE1α reduces new translations, which lowers protein input to the ER.

PERK

PERK is a type-I transmembrane kinase with its N-terminal domain in the ER lumen and the C-terminal kinase domain in the cytosol [188]. It is also kept inactive by binding to the ER chaperone protein Bip through its luminal domain [180, 189]. Under ER stress, the accumulation of misfolded protein causes Bip to dissociate from PERK, leading to oligomerization and trans-phosphorylation of PERK [189, 190]. Activated PERK directly phosphorylates the eukaryotic translation initiation factor 2α (eIF2α), resulting in attenuation of global protein synthesis [188]. This limits influx of new protein load to the ER. Although PERK-mediated eIF2α phosphorylation reduced general mRNA translation, it selectively leads to the translation of mRNAs with overlapping upstream open reading frames, such as in ATF-4 [191]. Under normal conditions, these overlapping upstream open reading frames in ATF-4 mRNA prevent its translation. However, they are effectively bypassed when eIF2α is phosphorylated, leading to the successful translation of ATF-4 [192]. ATF-4 then translocates to the nucleus and transcribes genes associated with ER chaperones, redox balance, protein synthesis, and autophagy to resolve the unfolded protein stress in the ER [193]. ATF-4 also regulates gene expression in the

apoptosis pathway to initiate cell death when ER stress overwhelms the cellular rescuing capacity [194].

ATF-6

ATF-6 is a type 2 transmembrane protein with its C-terminal in the ER lumen and the N-terminal which contains a DNA binding domain in the cytosol [195]. Unlike IRE1α and PERK, which are both kinases, ATF-6 is a "pre-transcription factor" that needs proteolytic processing to its active form [195]. The full-length ATF-6 is retained in the ER membrane by binding to Bip within its luminal domain [196]. Dissociation of Bip under ER stress exposes the Golgi localization signal (GLS) sequence of ATF-6, which is then recognized by coat protein II vesicles and transported to the Golgi apparatus [196]. Once in the Golgi, the full-length ATF-6 undergoes two steps of proteolytic cleavages by Site-1 protease (S1P) and Site-2 protease (S2P), producing the active fragment of ATF-6 (ATF-6f) [197]. The active ATF-6f translocates to the nucleus, inducing the expression of genes that are involved in protein folding and ERAD [198, 199]. Interestingly, activation of the PERK pathway also activates ATF-6 by increasing ATF-6 synthesis and ATF-6 trafficking from ER to Golgi [200]. These findings suggest that the three UPR signaling branches work collectively rather than independently to restore ER homeostasis.

1.3.2 ER associated degradation (ERAD)

The fidelity of accurate protein folding in the ER is ensured by a dedicated protein quality control system. Improperly folded proteins are effectively removed from the ER through ER associated degradation (ERAD) [201]. There are two proposed types of ERAD in the cell,

proteasome-mediated ERAD (type I) and autophagy-mediated ERAD (type II) [202]. Type I ERAD removes misfolded/unfolded soluble proteins through the ubiquitin-proteasome degradation system, whereas type II ERAD clears large protein aggregates and damaged organelles via autophagy-lysosome degradation [203, 204]. Under ER stress, both types of ERAD could be triggered to enhance the clearance of misfolded/unfolded proteins to reduce ER stress.

Proteasome-mediated ERAD

Proteasomes are multi-subunit protease complexes that are crucial for maintaining intracellular protein homeostasis by degrading misfolded proteins, damaged proteins, as well as short-lived regulatory proteins [205]. Proteasomes are located both in the cytoplasm and in the nuclei of all eukaryotic cells [206]. The two major forms of proteasomes in the cell are the 20s proteasome and the 26s proteasome, both of which are large protein complexes made up of many subunits. The 20s proteasome is made up of two sets of seven different α subunits (α_{1-7}) forming a ring and two sets of seven different β subunits (β_{1-7}) forming a ring. These rings are arranged as $\alpha_{1-7}\beta_{1-7}\beta_{1-7}\alpha_{1-7}$. The 26s proteasome is composed of a 20s proteasome flanked at one or both of its ends by a 19s regulatory particle (19s RP) [207] (**Fig 1.5**). The 19s regulatory particle is also a multi-subunit complex made up of 19 different subunits. Therefore, the assembly of a full 26s proteasome requires the steps of 20s proteasome assembly, 19s RP assembly, and the docking of 19s RP to the 20s proteasome [208]. The 26s proteasome serves as a major harbor for intracellular protein degradation in a ubiquitin-dependent manner [209]. Substrate proteins destined for 26s proteasome destruction are first polyubiquitinated through the addition of ubiquitin molecules to the lysine residues of the protein, a process assisted by three ubiquitin

linking enzymes, ubiquitin-activating enzyme (E1), ubiquitin-conjugating enzyme (E2), and ubiquitin ligase (E3) [210]. The polyubiquitinated substrates are then recognized by the 19s RP and degraded by the 20s core of the 26s proteasome in an ATP-dependent manner [209, 210]. Although the majority of proteasome-mediated protein degradation is carried out by 26s proteasomes, up to 20% of cellular protein can be degraded by 20s proteasomes [211]. Proteins degraded by 20s proteasomes are not ubiquitinated, rather they enter the catalytic chamber of the 20s proteasome through their partially unfolded regions [212]. Together, the 26s and 20s proteasome form a fine-tuned network for intracellular protein degradation.

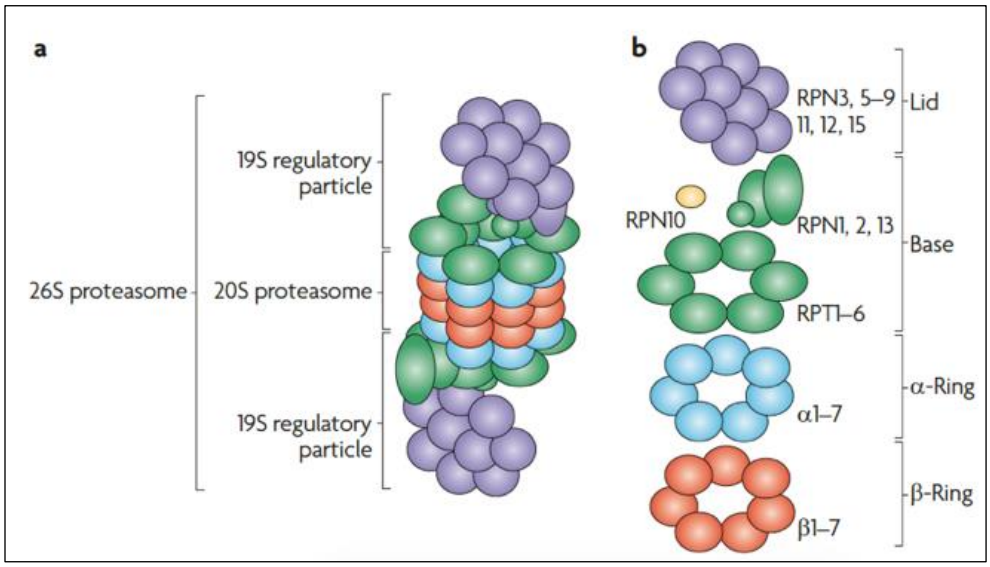

Figure 1.5 Diagram of the 26s proteasome [208]. **a**, the 26s proteasome consists of a catalytic 20s core proteasome and two 19s regulatory particles (19s RP) on both ends of the 20s proteasome. **b**, subunit composition of the 20s and 26s proteasome.

The ubiquitin-proteasome system serves as a major protein quality control machinery to remove misfolded/unfolded proteins from ER under both physiological and pathological conditions [201,

213]. Proteomics studies revealed that up to 64% of protein degradation under tunicamycin- or thapsigargin-induced ER stress is carried out through the proteasome system [214]. The destruction of ER misfolded proteins by proteasomes is a highly dynamic process that involves substrate recognition, transportation of substrate out of ER, and final proteasomal degradation [215]. Misfolded protein substrates in the ER are recognized and delivered to the ER membrane-embedded protein HRD1 by ER chaperones and lectins, such as Bip and EDEM [216, 217]. The transmembrane domain of the HRD1 protein functions as a channel through which substrate proteins are exported out of the ER, while the cytosolic domain of HRD1 functions as an E3 ligase that polyubiquitinates the substrate proteins [215, 218, 219]. The ubiquitinated substrates are then extracted from the channel and transferred to the proteasome by VCP (also known as p97 and CDC48) for degradation [220].

Because of the critical role of the proteasome in ERAD, proteasome levels often increase under ER stress. Studies have shown that ER stress often activates the Nrf2 pathway, which is known to induce gene expressions of multiple proteosome subunits, therefore increasing proteasome levels [221-223]. Additionally, inducing ER stress also enhances the rate of proteasome assembly by increasing and stabilizing proteasome assembly chaperones [224, 225]. These collective efforts to increase proteasome abundance are a rescue response under ER stress to enhanced misfolded protein removal.

Autophagy-mediated ERAD

Although the ubiquitin-proteasome system is very efficient in removing misfolded proteins from the ER, large protein aggregates, long-lived proteins, as well as some parts of ER sheets are

cleared through autophagy [204, 226]. Macro-autophagy (sometimes simply referred to as autophagy) is a general term for the delivery of cytoplasmic materials to lysosomes for degradation through the fusion of autophagosomes and lysosomes [227]. Autophagy is highly conserved in eukaryotes as a pro-survival mechanism under cellular stress by degrading damaged proteins and organelles for recycling [226]. The process of autophagy involves the nucleation of the phagophore membrane, membrane expansion and cargo packaging, formation of the autophagosome, autophagosome fusion with the lysosome, and cargo degradation by lysosomal hydrolases. The nucleation of the phagophore is initiated by the activation of the ULK1 complex and the recruitment of the PI3KC3 complex at the phagophore assembly site (PAS) on the ER membrane [228]. Subsequently, the phagophore membrane expands, sequesters cargo molecules, and seals to form autophagosomes [228]. During autophagosome expansion, the nascent LC-3 protein (LC-3I) is conjugated with PE (LC-3II) and anchored to the phagophore membrane, a process that is essential for autophagosome maturation and cargo recruitment [229, 230]. The mature autophagosome then fuses with lysosomes for degradation of its contents.

Autophagy was previously considered as a secondary response for misfolded protein removal under ER stress, only needed when the proteasome pathway is overwhelmed [226]. However, more studies have shown that autophagy is induced by all three branches of UPR singling for clearance of large protein aggregates and damaged ER membranes that could not be removed by proteasomes [204]. The program of autophagy is tightly controlled by a series of autophagy-related genes (ATGs). To sustain the autophagy flux under ER stress, ATGs are usually upregulated by UPR signaling. Activation of UPR signaling induces dozens of ATGs, such as Map1lc3b, Becn1, ATG3, ATG12, ATG5, ATG10, and ATG7 [231]. Induction of autophagy is

mainly regulated by mTORC1 activity [232]. Inhibition of mTORC1 leads to the activation of autophagy induction complex UKL1, thus promoting autophagy [233]. Activation of the PERK and ATF-6 pathways under ER stress could result in mTORC1 inhibition. For example, the PERK/ATF-4 pathway induced the expression of REDD1 that inhibits mTORC1 activity [234]. Activation of ATF-6 leads to downregulation of AKT1, which in turn inhibits mTORC1 activity [235]. ER stress also induces autophagy through activation of AMPK signaling. Activation of AMPK induces autophagy either by inhibiting mTORC1 or by direct activation of autophagy induction complex ULK1 [236, 237]. AMPK is a cellular energy sensor that is often activated by reduced cellular ATP levels. ER stress was reported to reduce the cellular ATP level via PERK/ATF-4, which in turn activated AMPK and induced autophagy [238].

1.3.3 ER stress and cell survival

Under initial and mild ER stress, the cells activate UPR signaling pathways to restore ER balance as a pro-survival mechanism. However, if ER stress persists to a level that goes beyond rescue, UPR signaling will ultimately induce cell death [239]. Although the detailed mechanisms by which the cell transits from adaptation to cell death remains elusive, many studies have demonstrated that prolonged or severe ER stress leads to apoptosis mainly through PERK and IRE1α pathways [240, 241]. Hyperactivation of PERK leads to increased expression of the transcription factor CHOP [242]. CHOP downregulates expression of the anti-apoptotic factor Bcl-2 [243], but upregulates expression of pro-apoptotic BH-3 only proteins, such as Bim, Puma, and Noxa [244-246]. In addition, increased CHOP expression also enhances reactive oxygen species that further promotes apoptosis [243]. Activation of IRE1α also induces apoptosis if ER homeostasis cannot be restored [247]. The process of RIDD under sustained ER stress degrades

miRNAs that target Caspase-2 mRNA, leading to an increased level of Caspase-2 and subsequent apoptosis [187]. Furthermore, activated IRE1α interacts with adaptor proteinTRAF2 to activate JNK and NF-κB pathways for apoptosis induction [248, 249]. Collectively, pro-apoptotic signaling induced by PERK and IRE1α ultimately converges onto the intrinsic apoptotic pathway that triggers the release of cytochrome C from mitochondria, which eventually initiates apoptosis in a caspase-dependent manner [176].

Although unresolved ER stress often leads to apoptosis, it should be noted that in some cases, sustained ER stress could lead to cellular senescence [250]. Senescence is a cellular state characterized by irreversible and durable cell-cycle arrest [251]. The onset and maintenance of cellular senescence are mainly controlled by the cell cycle regulating factors, p53/$p21^{CIP1}$ and $p16^{INK4A}$/Rb [252]. Activation of p53 upon cellular insults leads to upregulation of $p21^{CIP1}$, which blocks cell cycle progression by inhibiting CDK2 [253], and $p16^{INK4A}$ activation blocks cell cycle by inhibiting CDK4/6 [254]. While $p21^{CIP1}$ expression is involved in senescence onset, the maintenance of senescence heavily relies on $p16^{INK4A}$ expression and CDK4/6 inactivation [255]. Upon entering senescence, cells are nonresponsive to mitotic signals, leading to halted cell proliferation and growth. Of note, despite being trapped in permanent cell cycle arrest, senescent cells are alive with active metabolic activities [252]. These cells are actively secreting protein factors, such as cytokines, chemokines, and proteases, a process called senescence-associated secretive phenotype, which plays a significant role in maintaining the senescent phenotype through autocrine feedback [252]. The common features of senescent cells are increased cell size, enlarged cell nuclei with specific chromatin organization called senescence-associated heterochromatin foci [256], and increased senescence-associated β–galactosidase (SA-β-gal)

activity [257]. The enzymatic activity of β-galactosidase in non-senescent cells requires an optimum pH 4.0 - 4.5. However, due to its accumulation in lysosomes under senescence conditions, the enzyme activity could be detected at pH 6.0 [258, 259]. Therefore, histochemical detection of SA-β-gal activity at pH 6.0 has been widely used to identify cellular senescence [260].

Initially, senescence was considered as an intrinsic pathway to exit cell cycle after limited cell divisions. More evidence now indicates that it is a cellular response to stressful conditions, such as ER stress [252, 261]. Many studies have shown that ER stress and activation of the UPR pathways effectively induced cellular senescence. For example, known ER stress inducers, like tunicamycin and thapsigargin, increased the senescent phenotype in various types of cells [262, 263]. Chemical-induced ER stress through PERK/ATF-4 activation increased senescence in human fibrosarcoma and mouse melanoma cells [264]. Activation of ATF-6 induced senescence in multiple human breast cancer cell lines [265]. Senescence in human fibroblasts relied on the ATF-6 pathway [266]. Silencing ATF-4, ATF-6 and XBP-1 drastically reduced the senescent cell population in HRAS mutated melanocytes [267]. These studies suggest that activation of UPR signaling under ER stress could be a major mechanism behind stress-induced senescence, and the specific UPR signaling responsible for senescence induction may be cell type dependent [261]. Overall, mild and short-term ER stress activates UPR signaling as an adaptation mechanism for survival. Under severe and sustained ER stress, where the rescue capacity is overwhelmed, cells initiate apoptosis or senescence as the terminal response. Whether the cell progresses to apoptosis or senescence under such conditions may depend on the nature of the stressful insult and the cell type.

1.3.4 ER stress in pancreatic cancer

Higher ER stress level is perhaps a common feature in most solid cancers, due to higher proliferation demand and the highly hypoxic microenvironment [268, 269]. Elevated ER stress has been observed in various types of cancers. For instance, overexpression of XBP1, ATF-6, or ER chaperones has been observed in breast cancer, hepatocellular carcinoma, gastric cancer, colorectal cancer, and lung cancer [270-274]. In pancreatic cancer, the ER stress marker Bip and the UPR signaling regulator ATF-6 were highly expressed, and their expression was associated with a poor prognosis [275, 276]. To respond and to cope with the elevated basal level of ER stress, cancer cells activate UPR signaling to survive [277]. However, hyperactivation of UPR under severe or prolonged ER stress causes cell death, which could lead to cancer regression [278]. Thus, UPR signaling seemingly plays a dual role in cancer development depending on the extend of ER stress [279], and the elevated basal activation of UPR keeps cancer cells on a delicate balance between survival and death [240]. Therefore, either inhibiting UPR or further activating UPR has been proposed as effective approaches for tumor growth inhibition [280]. On the one hand, inhibiting UPR signaling impairs cancer cell's capacity to relieve ER stress, leading to cell death. Allying with this theory, pharmacological inhibition of IRE1α induced apoptosis and reduced tumor growth in pancreatic cancer [281]. A specific PERK kinase inhibitor, GSK2656157, also inhibited pancreatic tumor growth [282]. On the other hand, further increasing ER stress leads to hyperactivation of UPR, which in turn initiates cell death. The natural product Tanshinone (Tan)-IIA induced apoptosis in pancreatic cancer by increased ER stress [283]. Similarly, the compound Triptolide induced ER stress and promoted apoptosis or autophagy-related death in multiple pancreatic cancer cell lines [284, 285]. Taken together, these

studies suggest that pancreatic cancer survival relies on a balanced UPR activation to cope with ER stress. Inhibiting UPR signaling or exacerbating ER stress would both impede pancreatic cancer cell survival.

Chapter 2. Statement of purpose

The program of EMT contributes significantly to pancreatic cancer metastasis, cancer stem cell generation, and chemoresistance. Therefore, pharmacological inhibition of EMT holds a great promise to comprehensively inhibit pancreatic cancer progression. To discover potential EMT inhibitors, we previously performed a high throughput screening (HTS) study identifying small molecule compounds that upregulate the epithelial marker E-cadherin in pancreatic cancer cells [286]. In this study, we utilized the top hit compound, namely C150, to investigate the inhibition of EMT as an approach for inhibiting pancreatic cancer cell invasion and proliferation. Also investigated were the mechanisms of actions of C150, which include ER stress induction and enhanced proteasome activity with subsequent degradation of EMT-TFs. Our hypothesis is that induction of ER stress in pancreatic cancer cells triggers cellular responses leading to EMT suppression and comprehensive inhibition of pancreatic cancer progression. To test our hypothesis, we performed studies with the following two specific aims:

2.1 Specific aim 1: To investigate the inhibition of EMT by C150 in suppressing pancreatic cancer cell invasion and tumor growth (Chapter 4). We investigated the mechanisms underlying C150-induced EMT inhibition in pancreatic cancer cells and evaluated its effects on inhibiting cell migration and invasion using multiple 2D and 3D cellular assays. The *in vivo* activity of C150 in reducing pancreatic cancer growth was examined in an orthotopic mouse xenograft model.

2.2 Specific aim 2: To investigate the cellular responses caused by C150-induced ER stress in pancreatic cancer (Chapter 5). The mechanism of action for C150 was further explored in this aim. Multiple ER stress markers were examined by western blotting upon C150 treatment in

pancreatic cancer cells. Proteasome activity, proteasome abundance, as well as autophagy, were also examined as downstream responses to the ER stress. Cell cycle and senescence were investigated to determine the cell fate under C150 treatment. The *in vivo* effects of C150 were further evaluated in a syngeneic pancreatic cancer mouse model.

Chapter 3. Materials and methods

3.1 Cell culture

Human pancreatic cancer cells PANC-1, MIA PaCA-2, HPAF-II, and BxPC-3 were obtained from American Type Culture Collection (ATCC). Immortalized human pancreatic duct epithelial cells (hTERT-HPNE) and the murine pancreatic cancer cell line Pan02 were donated by Dr. Shrikant Anant from the University of Kansas Medical Center. L3.6 pl pancreatic cancer cells were donated by Dr. Liang Xu from the University of Kansas. All cancer cells were cultured in the recommended media with 10% FBS (Sigma-Aldrich, cat. no. F0926) and 100 units/ml penicillin/streptomycin (Corning Life Sciences, cat. no. 30-001-CI) and were used within 20 passages in our lab. The hTERT-HPNE cells were cultured with DMEM medium (Corning Life Science, cat. no. 10-013 CV) supplemented with 5% FBS, 1x N2 supplement (Invitrogen, cat. no. 17502-048), 10 ng/mL bFGF (Invitrogen, cat. no. PHG0024) and 50 μg/ml Gentamicin (Gibco, cat. no. 15710-064) and were used within 10 passages in our lab. All cells were cultured at 37°C in a cell culture incubator with humidified 5% CO_2. Compound C150 was purchased from ChemBridge (San Diego, CA) and stocked in dimethyl sulfoxide (DMSO). All C150 treatments were diluted in cell culture medium with a final DMSO concentration lower than 0.1% (v/v%). All control groups were treated with the same volume of medium containing DMSO (< 0.1% v/v%).

3.2 MTT cell viability assay

Cells were seeded in 96-well plates at 5,000 cells/well and incubated in a cell culture incubator overnight. The next day, the old medium was replaced with 200 μl fresh medium containing different concentrations of C150. After treatment for 48 hours, 20 μl of 5 mg/mL 3-(4,5-Dimethylthiazol-2-yl)-2,5-Diphenyltetrazolium Bromide (MTT) were added into each well and

the plates were incubated in the cell culture incubator for 4 hours. The medium was then removed and 150 µl DMSO was added into each well. Absorbance was measured at 570 nm using a microplate reader (BioTek, Winooski, Vermont).

3.3 Trans-well migration and invasion assay

Cells were seeded (5x 10^4 cells/insert) into trans-well cell culture inserts (Corning Life Science, cat. no. 353097) coated or non-coated with 1 mg/ml (0.1%) of Matrigel (Corning Life Sciences, cat. no. 356237) in medium without FBS. Inserts were then placed into 24-well tissue culture plates with culture medium supplemented with 10% FBS as nutrient attractor. Drugs were present in the medium in inserts and in wells. After 24 or 48 hours of treatment, inserts were removed from the wells, and cells inside the inserts were removed by cotton swabs. Cells on the outside bottom of the insert membrane were fixed in 4% formaldehyde for 10 minutes and then stained for 10 minutes with 0.5% crystal violet solution. Inserts were then washed in water and let dry before being photographed. Pictures of the whole inserts were taken using light microscopy and the total number of cells on each insert membrane were counted using ImageJ software.

3.4 Scratch / Wound-healing assay

Cells were seeded in 24-well plates at 2 x 10^5 cells/well and cultured to a confluent monolayer. A scratch was made using a 200-µl pipette tip on the monolayer. Cell debris was washed away with 1xPBS. Fresh medium with drugs was then added, and cells were treated for 24 hours. Pictures at 5 different areas in each well were taken at 0, 12, and 24-hour time points under 100x magnification. Wound distance was measured using ImageJ software, and migration was

quantified as wound recovery % = (0-hour wound distance – 24-hour wound distance) / 0-hour wound distance.

3.5 Three-dimensional (3D) cell invasion assay

PANC-1 cells were seeded at 8,000 cells/well in an ultra-low attachment, round-bottomed 96-well plate (Corning Life Science, cat. no. 7007) in complete growth medium and cultured for 4 days to form compact spheroids (one spheroid/well). Type I rat tail collagen (Corning Life Science, cat. no. 354236) was adjusted to neutral pH with setting solution (100 ml 10x EBSS, 2.45 g $NaHCO_3$, 7.5 ml 1 M NaOH, and 42.5 ml H_2O) and kept on ice. The medium was completely removed from each well and then 100 μl neutral-pH collagen was added. The plate was then placed into the 37 °C cell culture incubator for 30 minutes for collagen to solidify. Then, 100 μl complete growth medium was added to each well, and pictures were taken as 0-hour. Drugs were present in both collagen and medium. Spheroids were treated for 72 hours. Pictures were taken using a phase-contrast light microscopy. Cell invasion was analyzed using ImageJ by drawing an enclosed line tracing the invasion edge to obtain the total area. Then an enclosed line was drawn along the core spheroid to get the core spheroid area. The invaded area was calculated by subtracting the core spheroid area from the total area. Invasion score = invaded area / core spheroid area.

3.6 Western blotting

Total cell lysates and tumor tissue lysates were obtained using the Pierce RIPA buffer (Thermo Scientific, cat. no. 89901) in the presence of protease and phosphatase inhibitor cocktails (Sigma-Aldrich, cat. no. P8340, P5726, P0044). Lysis of the nuclear and cytoplasmic fractions

was performed according to the protocol of the Pierce NE-PER Nuclear and Cytoplasmic Extraction kit (Thermo Scientific, cat. no. 78833). The protein concentration of the lysates was determined using the Pierce BCA protein assay (Thermo Scientific, cat. no. 23225). Lysates were mixed with 2x Laemmli buffer (Bio-Rad, cat. no. 161-0737), separated in 8% or 10% SDS-PAGE gels, and transferred onto 0.2 μm PVDF membranes (MilliporeSigma, cat. no. ISEQ00010). The membranes were blocked in 5% blocking grade milk (Bio-Rad, cat. no. 1706404XTU) in 0.1% TBST solution (0.1% Tween-20 in 1xTBS) for 2 hours in room temperature, then incubated with primary antibodies at 4 °C overnight in 5% BSA / 0.1 %TBST solution. Following primary antibody incubation, membranes were washed 3 times with 0.1% TBST solution and then incubated with HRP-linked anti-rabbit (7074S) or anti-mouse (7076S) secondary antibodies (Cell Signaling Technology, Danvers, MA) with 1: 5000 dilution in 5% milk in 0.1% TBST for 2 hours in room temperature. Protein bands were then detected using Pierce ECL plus reagents (Thermo Scientific, cat. no. 32132). Primary antibody information was listed in **Table 3.1**.

Table 3.1 Primary antibodies used for western blotting.

Antibodies	Dilutions	Source	Catalog NO.	Manufacturer
PARP	1:1000	Rabbit	9542S	Cell Signaling Technology
Caspase-3	1:1000	Rabbit	9662S	Cell Signaling Technology
Vinculin	1:1000	Rabbit	4650S	Cell Signaling Technology
PCNA	1:2000	Mouse	sc-25280	Santa Cruz Biotechnology
Snail	1: 500	Rabbit	3879S	Cell Signaling Technology
ZO-1	1:500	Rabbit	13663S	Cell Signaling Technology

Claudin-1	1:500	Rabbit	13995S	Cell Signaling Technology
N-cadherin	1:1000	Rabbit	13116S	Cell Signaling Technology
Histone-3	1:2000	Rabbit	4499S	Cell Signaling Technology
α-Tubulin	1:2000	Rabbit	2144S	Cell Signaling Technology
β-Actin	1:3000	Mouse	3700S	Cell Signaling Technology
Cofilin	1:4000	Rabbit	5175T	Cell Signaling Technology
p-Cofilin (Ser3)	1:1000	Rabbit	3313T	Cell Signaling Technology
MMP-2	1: 250	Mouse	sc-53630	Santa Cruz Biotechnology
20s proteasome β-1 subunit	1: 1500	Mouse	sc-374405	Santa Cruz Biotechnology
20s proteasome β-2 subunit	1:1000	Mouse	sc-58410	Santa Cruz Biotechnology
20s proteasome β-5 subunit	1:1000	Mouse	sc-393931	Santa Cruz Biotechnology
20s proteasome α-5 subunit	1:1000	Mouse	sc-137240	Santa Cruz Biotechnology
20s proteasome α-6 subunit	1:1000	Mouse	sc-271187	Santa Cruz Biotechnology
19s proteasome PSMC-2 subunit	1:500	Mouse	sc-166972	Santa Cruz Biotechnology
19s proteasome PSMC-3 subunit	1:1000	Mouse	sc-100462	Santa Cruz Biotechnology

19s proteasome PSMC-4 subunit	1:1000	Mouse	sc-166115	Santa Cruz Biotechnology
anti-puromycin	1:500	Mouse	PMY-2A4	Developmental Studies Hybridoma Banks
eIF2α	1:500	Mouse	PCRP-EIF2S1-1E2	Developmental Studies Hybridoma Banks
Bip	1:1000	Rabbit	3177T	Cell Signaling Technology
ATF-4	1:1000	Rabbit	11815S	Cell Signaling Technology
ATF-6	1:1000	Rabbit	65880T	Cell Signaling Technology
XBP-1s	1:500	Rabbit	40435S	Cell Signaling Technology
LC-3	1:1000	Rabbit	3868S	Cell Signaling Technology
p-eIF2α (Ser51)	1:1000	Rabbit	3398T	Cell Signaling Technology
Lamin-B1	1:1000	Rabbit	12586S	Cell Signaling Technology
GAPDH	1:3000	Rabbit	2118S	Cell Signaling Technology
Sox-2	1:250	Mouse	sc-365823	Santa Cruz Biotechnology
β-Catenin	1:1000	Rabbit	8480s	Cell Signaling Technology
TP-53	1:1000	Mouse	sc-126	Santa Cruz Biotechnology
GSK-3β	1:1000	Rabbit	9315P	Cell Signaling Technology
p-GSK-3β (Ser9)	1:1000	Rabbit	5558P	Cell Signaling Technology

Table 3.2 Gene primer sequences for RT-qPCR.

Gene name	Primer	Sequence from 5' to 3'
PSMG-1 (PAC-1)	Forward	TCC TTT CCT GAG AGC CCT AAA A
	Reverse	TGT TCT AGC AAT GGA CAA CAC G
PSMG-2 (PAC-2)	Forward	ACC GAT TGT CTT GTG CCA ATG
	Reverse	AGG CAA TGA ATA CAC TTC AGC AT
PSMG-3 (PAC-3)	Forward	GAA GAC ACG CCG TTG GTG ATA
	Reverse	GAA GGA CTT TTG TGG TGA GCA
PSMG-4 (PAC-4)	Forward	GTC CAC TTC CAC GTC ATG C
	Reverse	GGG AGG TAG ACA CGG GGA T
POMP	Forward	ACT TGG ATC TGA GCT AAA GGA CA
	Reverse	GGG GAT GAC TAG GCA AAA GTT C
PAAF-1	Forward	GGA GGT CTT GGT GTG TCT TCT
	Reverse	CAA CGA TGG CTG TAT CCA GGA
PSMD-10	Forward	GGG TGT GTG TCT AAC CTA ATG G
	Reverse	GGC CAG AAT ACT CTC CTT CAA CT
PSMD-5	Forward	GCG CTG CTG AGA GAG GTA G
	Reverse	AGT CTT TTC CCT ATG GTT CTC GT
PSMD-9	Forward	AGG AGG AGA TAG AAG CGC AGA
	Reverse	GTG CGG ACT TGG TAC AGG T
GAPDH	Forward	CCA GGT GGT CTC CTC TGA CTT CAA CA
	Reverse	AGG GTC TCT CTC TTC CTC TTG TGC TC
Snail	Forward	TCG GAA GCC TAA CTA CAG CGA

	Reverse	AGA TGA GCA TTG GCA GCG AG
MMP-2	Forward	TAG CTG CTG GCT CAC TGT GT
	Reverse	CTT CAG CAC AAA CAG GTT GC
MMP-9	Forward	GAA CCA ATC TCA CCG ACA GG
	Reverse	GCC ACC CGA GTG TAA CCA TA

3.7 Reverse transcription-quantitative polymerase chain reaction (RT-qPCR)

Total RNA was extracted from the cells using TRIZOL reagent (Invitrogen, cat. no. AM9738) according to the manufacture's protocol. cDNA synthesis was carried out with 1 μg total RNA using the OneScript cDNA Synthesis Kit (cat. no. G234, Applied Biological Materials, Richmond, BC, Canada). cDNA was then diluted 1:5 in nuclease-free H_2O. RT-qPCR was performed using the BioRad iQ iCycler detection system with One-Step BrightGreen reagents (cat. no. MasterMix-S, Applied Biological Materials, Richmond, BC, Canada) according to the protocol provided in the kit. Each reaction was carried out in 10 μl volume with 5 μl 2x BrightGreen qPCR MasterMix, 0.6 μl forward and reverse primer mix (10 μM), 2 μl diluted cDNA, and 2.4 μl nuclease-free H_2O. All qPCR reactions were run under the following cycling condition: enzyme activation at 95 °C for 10 mins, 40 cycles of denaturation (95 °C for 15 secs), and annealing/extension (60 °C for 60 secs). The melting curve was detected at 55°C-95 °C with 0.5 °C increments. Three independent experiments were performed, and reactions were carried out in triplicates for each experiment. Gene expression was quantified using the $2^{-\Delta\Delta Ct}$ method with GAPDH as the internal control. Primer sequences for specific genes are listed in **Table 3.2**.

3.8 MMP gelatin zymography

PANC-1 cells were seeded in 6-well plates at 5x 10^4 cells/well and incubated in a cell culture incubator overnight. The next day, the medium was removed, and cells were washed twice with 1x PBS. After washing, 1ml fresh FBS-free medium containing drugs was added to each well, and the cells were treated for 24 hours. The supernatants were collected, and protein concentration was determined with the Pierce BCA protein assay (Thermo Scientific, cat. no. 23225). Ten micrograms of total protein in the supernatant were then mixed with 5x non-reducing loading buffer (Thermo Scientific, cat. no. 3900) and samples were separated in 10% SDS-PAGE gels containing 0.2% gelatin (SigmaAldrich, St. Louis, MO). The gels were re-natured in renaturing/washing buffer (1 M Tris pH 8.0, 1 M $CaCl_2$, 2.5% Triton X-100) for 1 hour, followed by equilibrating in incubation buffer (1 M Tris pH 8.0, 1 M $CaCl_2$) for 10 minutes in room temperature. The gels were then incubated in the incubation buffer at 37°C for 24 hours. The gels were then stained with Coomassie Brilliant Blue R-250 (Bio-Rad, cat. no. 1610436) followed by de-staining in de-staining solution (40% methanol, 10% acetic acid, 50% H_2O) until clear bands were visible. Clear bands representing the MMP enzyme activity were analyzed and quantified using ImageJ.

3.9 Snail overexpression in PANC-1 cells

PANC-1 cells were transfected with the pCMV-Flag-Snail plasmid (Addgene, Cambridge, MA) or empty vector plasmid (Addgene, Cambridge, MA) using Lipofectamine™ 3000 (Invitrogen, cat. no. L3000015) according to the manufacture's protocol. Briefly, PANC-1 cells were seeded in 6-well plates at 2 x 10^5 cells / well and incubated for 24 hours. The medium was removed, and 500 μl fresh medium was added per well. A total of 125 ng Snail-plasmid DNA or empty-vector plasmid DNA were mixed with 0.5 μl Liopfectamine-3000 and 0.6 μl P-3000 reagents in 62.5 μl

OPTI-MEM medium (cat. no. 31985-062, Gibco Life Technologies), and the mixture was then added to the well. Forty-eight hours after transfection, cells were collected by trypsinization and seeded for wound healing (scratch) assays as described earlier. Snail overexpression was confirmed by western blotting.

3.10 Immunohistochemistry

Paraffin-embedded tissue slides (5 μm thickness) were deparaffinized and hydrolyzed with a sequential change of Xylene, 100% ethanol, 95% ethanol, 75% ethanol, and H_2O. Antigen retrieval was carried out by submerging the slides in pH 6.0 citrate buffer for 30 mins at 95 °C. Immunohistochemistry staining was performed according to the protocol of the Abcam IHC detection kit (cat. no. ab64264, Abcam, Cambridge, MA). Briefly, after antigen retrieval, slides were blocked in the protein blocking solution for 1 hour at room temperature and then incubated with primary PCNA antibody (dilution 1:100, cat. no. sc-25280, Santa Cruz Biotechnology, Dallas, TX) in 0.1% TBST (1x TBS with 0.1% Tween-20) overnight at 4 °C. After washing in 0.1% TBST solution, slides were incubated in H_2O_2 blocking solution for 15 mins, then incubated with biotinylated secondary antibody for 1 hour followed by 30 mins incubation with streptavidin-peroxidase solution at room temperature. AB chromogen was then applied to the slides for staining. After immunostaining, the slides were counterstained in Mayer's hematoxylin solution for 30 seconds. The slides were observed under a light microscope at 200x magnification. Pictures of at least 5 different areas per sample were taken. Data were analyzed using ImageJ (Fiji Version) by subtracting the hematoxylin staining color to reveal only DAB staining color. Then DAB positively stained cells were counted on each picture.

3.11 Cell cycle analysis

Cells were seeded at 5 x 10^5 cells in 60-mm petri dishes and incubated in the cell culture incubator. The next day, the medium was removed, and fresh medium with drugs was added. Cells were treated for 24 or 48 hours. After treatment, cells were collected by trypsinization, washed with 1x PBS twice, and fixed in 70% ethanol at -20 °C overnight. After fixation, cells were washed once with 1x PBS and stained in PI staining solution (20 μg/ml Propidium Iodine in 1x PBS solution with 0.1 mg/ml RNase A and 0.1% Triton X-100) at 37 °C for 15 mins. Cells were then kept in staining solution at 4 °C overnight protected from light before being analyzed for cell cycle distribution with flow cytometry (BD LSR ll, BD Biosciences).

3.12 Proteasome activity assay

A total of 1 x 10^6 PANC-1 cells were seeded in 100-mm petri dishes and incubated in the cell culture incubator. The next day, the medium was replaced with fresh medium containing drugs. After 24 hours of treatment with C150 or DMSO, cells were lysed in proteasome activity lysis buffer (50 mM HEPES, 10 mM $NaCl_2$, 1.5 mM $MgCl_2$, 1 mM EDTA, 2 mM ATP, 1% Triton X-100) on ice for 1 hour. The supernatant was collected by centrifugation at 16,000 x g for 15 minutes and kept on ice. The Pierce BCA protein assay was performed to determine the protein concentrations in the cell lysates. In a black-wall 96-well plate, 150 μl fluorescent proteasome substrate Suc-LLVY-AMC (BML-P802-0005, Enzo Life Science, Farmingdale, NY) and 50 μl cell lysate were added per well to a final substrate concentration of 100 μM. The proteasome inhibitor epoxomicin (4 μM) was used in the negative control group. The plate was then placed in a fluorescent plate reader, incubated at 37 ºC, and read in the kinetics mode at 360/460 nm

every 20 minutes for 80 minutes. Fluorescent readings were then normalized to the protein amount in the cell lysate of each sample.

3.13 Native gel analysis for assembled proteasome

A total of 1 x 10^6 PANC-1 cells were seeded in 100-mm petri dishes and incubated in the cell culture incubator. The next day, the medium was replaced with fresh medium containing drugs. After 24 hours of treatment with C150 or DMSO, cells were lysed in proteasome activity assay lysis buffer, and supernatants were collected by centrifugation at 16,000 x g for 15 minutes. After the Pierce BCA protein assay, the supernatants were mixed with 2x non-denaturing loading buffer (161-0738, Bio-Rad). A total of 30 μg protein from each sample were loaded and separated in 4% Tris-Borate native gels at 100 V for 3.5 hours in running buffer (89 mM Tris, 89 mM boric acid, 2 mM EDTA, 5 mM $MgCl_2$, 1 mM ATP). The 4% Tris-Borate native gels were made as follows (10 ml): 7.5 ml H_2O + 1.333 ml 30% polyacrylamide (1610158, Bio-Rad) + 50 μl $MgCl_2$ (1 M) + 100 μl ATP (0.1 M) + 1 ml 10x Tris-Boric-EDTA buffer (161-0733, Bio-Rad) + 100 μl 10% APS + 10 μl TEMED. After electrophoresis, gels were soaked in 1x Tris-Glycine buffer with 0.1% SDS for 30 minutes. Proteins in gels were then transferred onto 0.2 μm PVDF membranes at 100 V for 3.5 hours at 4 °C in transfer buffer (1x Tris-Glycine buffer with 20% methanol). Subsequently, membranes were stained with Ponceau S to reveal protein bands, then washed in 0.1% TBST solution and blocked in 5% blocking grade milk in 0.1% TBST for 2 hours at room temperature before being incubated with anti-20s β-5 antibody and anti-19s PSMC-3 antibody overnight at 4 °C. Membranes were then washed in 0.1% TBST and incubated with HRP-conjugated anti-mouse secondary antibody (7076S, Cell Signaling Technology, Danvers, MA) with 1: 5000 dilution in 5% milk/0.1% TBST solution for 2 hours at room

temperature. Protein bands were detected with the Pierce ECL plus reagents (32132, Thermo Scientific).

3.14 Cell growth curve by MTT assay

Cells were seeded in 96-well plates at 5,000 cells/well and incubated in a cell culture incubator overnight. The next day, the medium was changed to fresh medium containing C150 at the indicated concentrations. Cells were incubated for 0, 24, 48, 72, and 96 hours and the MTT assay was performed.

3.15 Gemcitabine combination treatment

PANC-1 cells were seeded in a 96-well plate at 5,000 cells/well and incubated overnight. The next day, the medium was changed to fresh medium containing drug combinations in a matrix design as shown in **Figure 5.6B**. Cells were treated for 72 hours and viability was determined using the MTT assay. The combination index was calculated according to the Chou-Talalay's method [287] using CompuSyn software (https://www.combosyn.com.)

3.16 Immunofluorescent staining for LC-3 puncta

PANC-1 cells were seeded in 8-chamber microscope cell culture slides (PEZGS0816, MilliporeSigma) at 6 x 10^4 cells per chamber and incubated in the cell culture incubator. The next day, the medium was replaced with fresh medium containing drugs. After treatment, cells were washed twice in PBS and fixed in ice-cold 100% methanol at -20 °C for 15 min. Cells were then washed 3 times with PBS and blocked in 5% normal goat serum (5425S, Cell Signaling Technology, Danvers, MA) in PBS with 0.3% TritonX-100 for 1 hour at room temperature. Cells

were then incubated with anti-LC-3 antibody (3868S, Cell Signaling Technology, Danvers, MA) at 4 °C overnight in antibody incubation buffer (1x PBS with 0.3% TritonX-100 and 1% BSA). The next day, cells were incubated with Alexa-488 conjugated secondary antibody (4412S, Cell Signaling Technology, Danvers, MA) in antibody incubation buffer for 2 hours at room temperature and protected from light. After 3 washes with PBS, the slide was coverslipped with the anti-fade mounting solution with DAPI (8961S, Cell Signaling Technology, Danvers, MA), and cured in the dark overnight at room temperature to stain nuclei. The slides were then imaged with fluorescence microscopy at 600x magnification.

3.17 β-galactosidase staining for cellular senescence

The senescence β-galactosidase staining kit (9860S, Cell Signaling Technology, Danvers, MA) was utilized according to the manufacturer's protocol. Briefly, PANC-1 cells were seeded in a 24-well plate at 5 x 10^4 cells per well and incubated in a cell culture incubator overnight. The next day, the old medium was replaced with fresh medium containing drugs. Cells were treated for 24 or 48 hours. After treatment, cells were washed with PBS twice and fixed in 0.5 ml fixative solution for 15 minutes at room temperature. Following cell fixation, 0.5 ml staining solution with X-gal (1 mg/ml) at pH 6.0 was added to each well. Plates were sealed with parafilm, wrapped in aluminum foil, and incubated in a 37 °C dry oven for 24 hours. After removal of the staining solution, cells were washed 3 times with PBS and covered with 0.5 ml 70% glycerol. At least 5 random fields per well were imaged using a bright field light microscope at 200x magnification. Positively stained cells and total cells in each image were counted using the multi-point manual counting tool in ImageJ software.

3.18 Orthotopic mouse xenograft model for pancreatic cancer

All animal experiments were performed according to an Animal Care and Use Protocol (2018-2443) approved by the Institutional Animal Care and Use Committee at the University of Kansas Medical Center. Acute MTD (maximal tolerance dose) of C150 in mice was determined using 6 mice (Strain: BALB/cJ, 3 female, 3 male) starting at a one-time intraperitoneal (IP) dose of 20 mg/kg (in 20% H_2O + 20% DMSO + 60% PEG-400). All mice appeared lethargic and were sacrificed 2 hours after the injection. The dose was reduced to 10 mg/kg in another set of 6 mice and no sign of toxicity was observed. Then the dose was raised to 15 mg/kg and mice were monitored for 7 days and no sign of toxicity was observed. To further detect tolerance for sub-chronic administration of C150 at 15 mg/kg, 6 mice were given C150 at 15 mg/kg daily for 5 consecutive days. No signs of toxicity were observed, indicating good tolerance. Based on the data and taking a margin of safety, the treatment regimen was determined to be 15 mg/kg, 3 times weekly by IP injection.

Luciferase labeled PANC-1 cells (PANC-1-Luc) were established by the Preclinical Proof of Concept Core Laboratory at the University of Kansas Medical Center, Kansas City, KS. During tumor inoculation, 4-6 weeks-old female nude mice (Hsd: Athymic Nude-Foxn1nu, Harlan) were anesthetized with isoflurane inhalation (5% for induction and 2% for maintenance of anesthesia). A subcostal laparotomy was performed to expose the pancreas. A total of 4 x 10^5 PANC-1-Luc cells suspended in 50 μl cold 1x PBS were injected into the tail of the pancreas. The skin was then sealed with wound clips. Two weeks after tumor cell inoculation, mice were given 150 mg/ml of D-luciferin (Goldbio, St Louis, MO) by IP injection and were imaged using the IVIS imaging system (Waltham, MA). Mice were divided into 2 groups (vehicle: n = 10, treatment: n

= 9) based on imaging to ensure even tumor burdens in each group. Treatments then commenced with 15 mg/kg of C150 or vehicle (20% H_2O + 20% DMSO + 60% PEG-400) by IP injections 3x weekly. Mice were treated for six weeks and imaged weekly to monitor tumor size. Bodyweight was monitored weekly. At necropsy, tumor samples were weighed and fixed in 4% formaldehyde or frozen at -80 °C for future analysis. Body condition score (BCS) and clinical signs of pain and distress were used as indicators of toxicities. Mice reaching BCS2 or less or showing any of the signs below were considered showing toxicity: guarding, reduced movement, abnormal appearance (hunched), restlessness, circling, convulsion or blindness, rapid or labored breathing, hemorrhage, flaccid or spastic paralysis, unable to ambulate, recumbency or mutilation.

3.19 Syngeneic mouse model for pancreatic cancer

Female C57BL/6 mice (6-8 weeks old) were purchased from Jackson Laboratory (Bar Harbor, ME). For tumor cell implantation, mice were anesthetized by isoflurane inhalation. A subcostal laparotomy was performed to expose the pancreas. A total of 4 x 10^5 Pan02 mouse pancreatic cancer cells suspended in 50 μl PBS were injected into the tail of the pancreas. The skin was then sealed with wound clips. Twenty-one days after tumor cell inoculation, two random mice were sacrificed to confirm tumor formation. Subsequently, mice were randomly grouped into 2 groups (vehicle: n = 9, treatment: n = 8). Treatment was then started with 150 mg/kg of C150 or vehicle (5% Tween-80 + 95% H_2O) by oral gavage. Mice were treated 3 times a week for 2 weeks and monitored twice daily for signs of moribund state. The moribund state was determined using body score (< 2), or any signs of extreme lethargy, lack of responsiveness to manual stimulus, immobility, or hypothermia. When these signs were observed, the mice were humanely

sacrificed and counted as death events. Necropsy was then immediately performed, and tumors were weighed and collected upon sacrifice. If ascites were present, their volume was measured. Thirty-five days after tumor inoculation all surviving mice were humanely sacrificed, and tumors and ascites were collected and measured.

3.20 Statistics

All results are presented as mean ± SD unless stated otherwise. Statistical analysis was performed using the Student's t-test or the Mann-Whitney test for two-group comparisons. For multi-group comparisons, one-way ANOVA with the Tukey post hoc test was performed. The log-rank test was used for survival analysis. $P < 0.05$ was considered statistically significant.

Chapter 4. A novel inhibitor, C150, for pancreatic cancer epithelial-mesenchymal transition and tumor growth in mice

4.1 Introduction

Pancreatic ductal adenocarcinoma (PDAC) accounts for 90% of all pancreatic cancer cases [288] and is one of the most lethal cancers. The overall 5-year survival rate of PDAC patients is only 10% [4]. Despite numerous efforts, the treatment options are still limited, and treatment outcomes remain poor. Gemcitabine as a single agent has been the first-line chemotherapy for almost three decades [289] and provides only limited benefits on survival. Recently developed combination therapy of gemcitabine and nab-paclitaxel improved the median overall survival by a few months but also increased toxicities [10]. A non-gemcitabine combination regimen, FOLFIRINOX (oxaliplatin, irinotecan, fluorouracil, and leucovorin), also gained a small benefit in survival compared to gemcitabine, but toxicities are significant so that this regimen cannot be tolerated by many patients [7, 9]. The high mortality rate of PDAC is largely due to early metastasis that accounts for extremely poor treatment outcomes [5, 7]. Searching for new agents against pancreatic cancer is of great significance and urgency.

Emerging studies have shown that epithelial-to-mesenchymal transition (EMT) plays an important role in PDAC cell invasion, metastasis, tumor progression, and drug resistance [290, 291]. The initial steps of metastasis involve the dissemination of cancer cells from the tumor bulk and invasion through the extracellular matrix (ECM), during which EMT plays a critical role [292]. By initiating the EMT process, the apical-basal polarized carcinoma cells lose cell-cell adhesions and are converted to fibroblast-like mesenchymal cells, acquiring more mobility and invasiveness [82, 293, 294]. In a transgenic mouse model of pancreatic cancer, EMT was shown to happen at a very early stage of tumor formation and was associated with cancer cell dissemination and invasion prior to, and in parallel to, primary pancreatic tumor formation [135].

Moreover, in human tissue samples of pancreatic cancer, it has been found that the epithelial marker E-cadherin was weakly expressed in poorly differentiated tumors, and the mesenchymal marker N-cadherin was mainly expressed in the invasive front [96]. The EMT-promoting factor Snail was highly expressed in tumor tissues compared to normal tissues [96]. Snail represses expressions of epithelial molecules such as E-cadherin, Claudins, and ZO-1 [295-297], and promotes the expression of mesenchymal molecules such as Fibronectin, N-cadherin, and MMPs [82, 298-300]. Overexpression of Snail induced EMT and promoted pancreatic cancer cell invasion and metastasis in mouse models of pancreatic cancer [97]. These studies strongly demonstrated the significance of EMT in promoting pancreatic cancer progression. Thus, targeting EMT may be beneficial to the treatment of this disease.

Previously, we have established a high-throughput screening (HTS) assay for the discovery of compounds that had the potential to enhance E-cadherin expression [286]. Upon screening of combined libraries of ~47,000 compounds, we discovered several positive hits that could potentially inhibit EMT in pancreatic cancer cells [286]. Here, we aim to study one of the top hits, compound C150, a quinoline compound with a novel structure, for its activities in suppressing pancreatic cancer EMT and tumor progression in *vitro* and in *vivo.*

4.2 Results

4.2.1 C150 inhibited proliferation in multiple pancreatic cancer cell lines

The effect of C150 (**Fig 4.1A**) on cell viability was examined in a panel of human pancreatic cancer cell lines (PANC-1, BxPC-3, MIA PaCA-2, HPAF-II, L3.6 pl) and an immortalized human pancreatic duct epithelial cell line (hTERT-HPNE). Treatment for 48 hours resulted in a

significant decrease of cell viability in all tested pancreatic cancer cells. The 50% inhibitory concentration (IC_{50}) was ~1 μM for BxPC-3, MIA PaCA-2, HPAF-II, and L3.6 pl cells, and ~2.5 μM for PANC-1 cells. In contrast, the non-cancerous hTERT-HPNE cells were much more resistant to C150 treatment, with an IC_{50} of ~12.5 μM and not much more inhibition was observed when drug concentration was further increased (**Fig 4.1B**). These data indicate preferential cytotoxicity of C150 towards pancreatic cancer cells versus normal cells. To examine whether the reduced cell viability was due to apoptosis or suppression of proliferation, we treated PANC-1 cells with C150 at 1 μM and 2 μM for 48 hours. Two apoptosis markers, PARP and Caspase-3, were then examined by western blotting. Etoposide (50 μg/ml) was used as a positive control. Etoposide induced massive PARP and Caspase-3 cleavage, while C150 did not induce any PARP or Caspase-3 cleavage (**Fig 4.1C**), indicating that C150 did not induce apoptosis. In contrast, the cell proliferation marker, PCNA, was significantly decreased by the same C150 treatment (**Fig 4.2A**). Cell cycle analysis showed a G2/M phase arrest induced by C150 treatment, and no sub-G0 cells were detected (**Fig 4.2B**). The data suggested that C150 inhibited pancreatic cancer cell proliferation rather than inducing apoptosis, and the effect was well separated between cancer and normal cells.

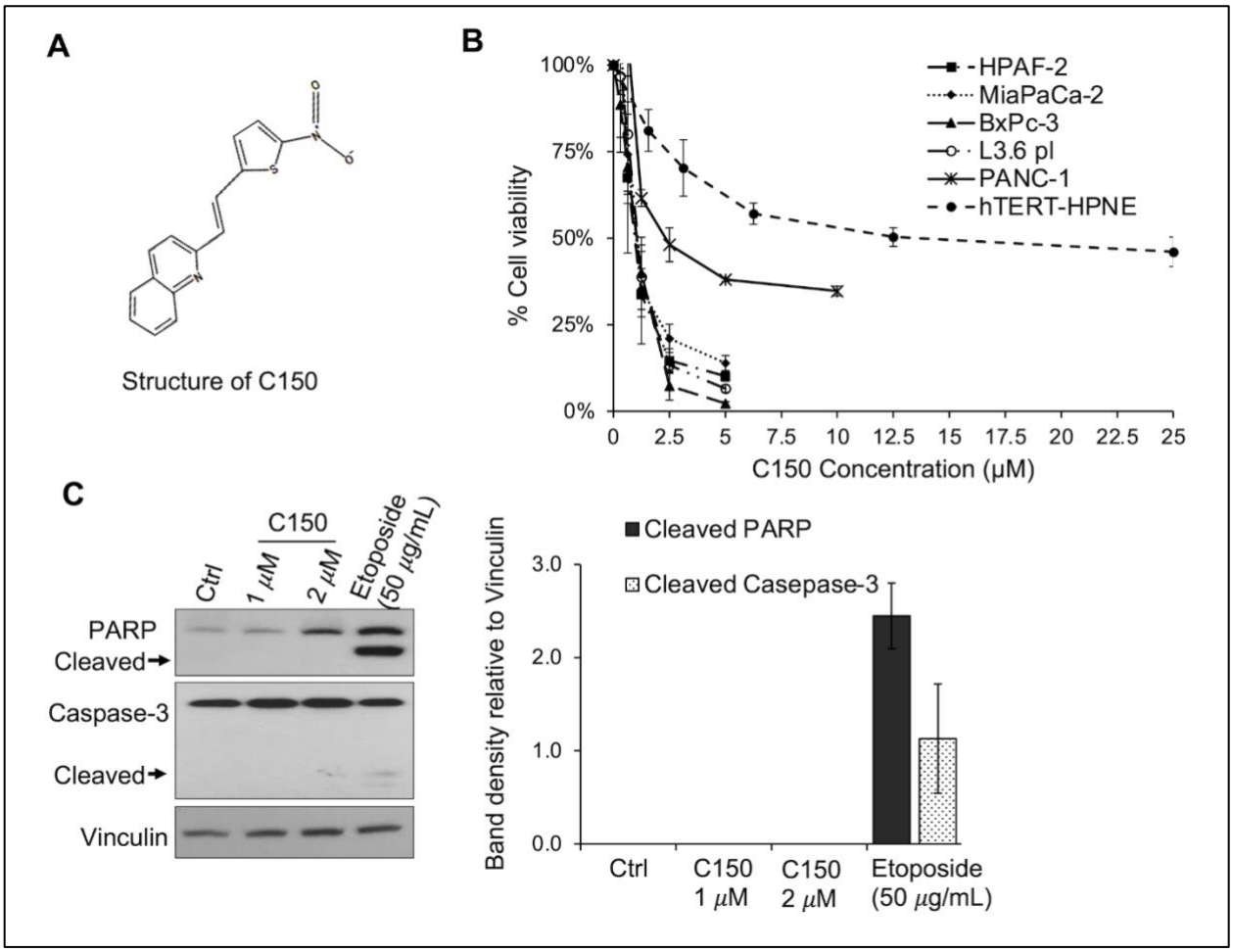

Figure 4.1 C150 reduced cell viability in pancreatic cancer cell lines but did not induce apoptosis. A. Structure of C150. **B.** Cell viability upon C150 treatment. Human pancreatic cancer cell lines HPAF-2, MiaPaCa2, BxPC-3, L3.6pl, PANC-1, and immortalized human normal pancreatic ductal epithelial cell line hTERT-HPNE were incubated with increasing concentrations of C150 for 48 h. Cell viability was analyzed using the MTT assay and normalized to untreated controls. **C.** Western blot of apoptosis markers. PANC-1 cells were treated with DMSO (Ctrl) or C150 (1 μM and 2 μM) or etoposide (50 μg/mL) for 48 hours. Vinculin was blotted as the loading control. Bar graphs show band densities of cleaved PARP and cleaved Caspase-3 relative to Vinculin. Data represent mean ± SD of at least 3 independent experiments in all graphs. * $p < 0.05$, ** $p < 0.01$ (vs. Ctrl) by One-way ANOVA-Tukey's test.

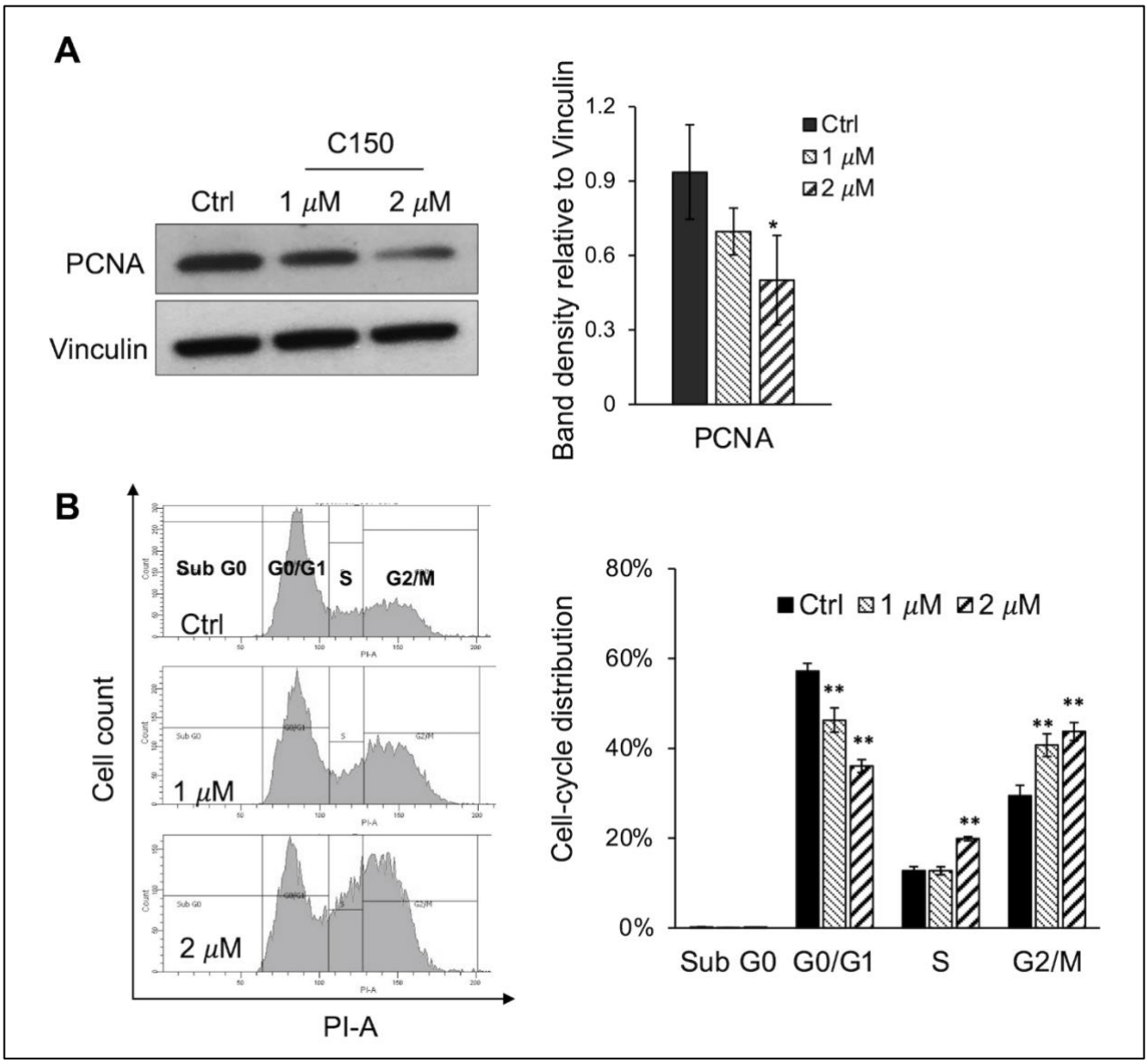

Figure 4.2 C150 inhibited PANC-1 cell proliferation and caused G2/M cell cycle arrest. A. Western blot of PCNA. PANC-1 cells were treated with DMSO (Ctrl) or C150 (1 μM and 2 μM) for 48 hours. Total cell lysates were analyzed for PCNA. Vinculin was blotted as loading control. Right panel bar graph shows band densities of PCNA relative to Vinculin. **B.** Cell cycle analysis. PANC-1 cells were treated with DMSO (Ctrl) or C150 (1 μM and 2 μM) for 48 hours. Cells were then collected, fixed in 70% ethanol, stained with propidium iodide (PI), and subjected to flow cytometry analysis. The left panel shows the representative figures of cell cycle distribution. The bar graph shows the percentage distribution of each cycle. Data represent mean ± SD of at least 3 independent experiments in all graphs. * $p < 0.05$, ** $p < 0.01$ (vs. Ctrl) by One-way ANOVA-Tukey's test.

4.2.2 C150 inhibited migration and invasion in pancreatic cancer cells

Pancreatic cancer cell migration was first evaluated in a wound-healing (scratch) assay. Treatment with C150 significantly inhibited PANC-1 cell migration at sub-toxic concentrations of 1 μM and 2 μM at both 12 hours and 24 hours (**Fig 4.3A**). Boyden chamber trans-well migration/invasion assays were then used to further assess the activity of C150 to inhibit cell migration (without Matrigel coating) and invasion (with Matrigel coating). A 48-hour treatment with C150 reduced the number of PANC-1 cells on the outside of the trans-well membrane in a concentration-dependent manner, with or without Matrigel coating (**Fig 4.3B**). These results were confirmed with another pancreatic cancer cell line, MiaPaCa-2 (**Fig 4.3C**). In parallel, the phosphorylation of Cofilin, an actin-binding protein, was increased upon treatment with 2 μM of C150 in PANC-1 cells (**Fig 4.4A**), indicating inhibition of cytoskeleton rearrangement and decrease of cell mobility [301]. These data indicated that both migration and invasion were inhibited by C150 treatment.

A three-dimensional (3D) cell invasion model was then utilized to better mimic *in vivo* conditions of pancreatic cancer invasion, in which a tumor spheroid was cultured with surrounding collagen-rich extracellular matrix (ECM). In this assay, PANC-1 cells were first cultured in complete growth medium in round-bottomed ultralow-attachment 96-well plates to form compact cell spheroids. The cell spheroids were then cultured in type I collagen matrix. After 72 hours in culture, cells at the perimeter of the spheroid disseminated and invaded into the surrounding collagen ECM, forming a radial-shaped area of invasion (**Fig 4.4B**). C150 treatment at 2 μM and 4 μM significantly inhibited the invasion of PANC-1 cells in this model (**Fig 4.4B**).

Taking together, both 2D and 3D culture data consistently showed that C150 inhibited pancreatic cancer cell migration and invasion *in vitro*.

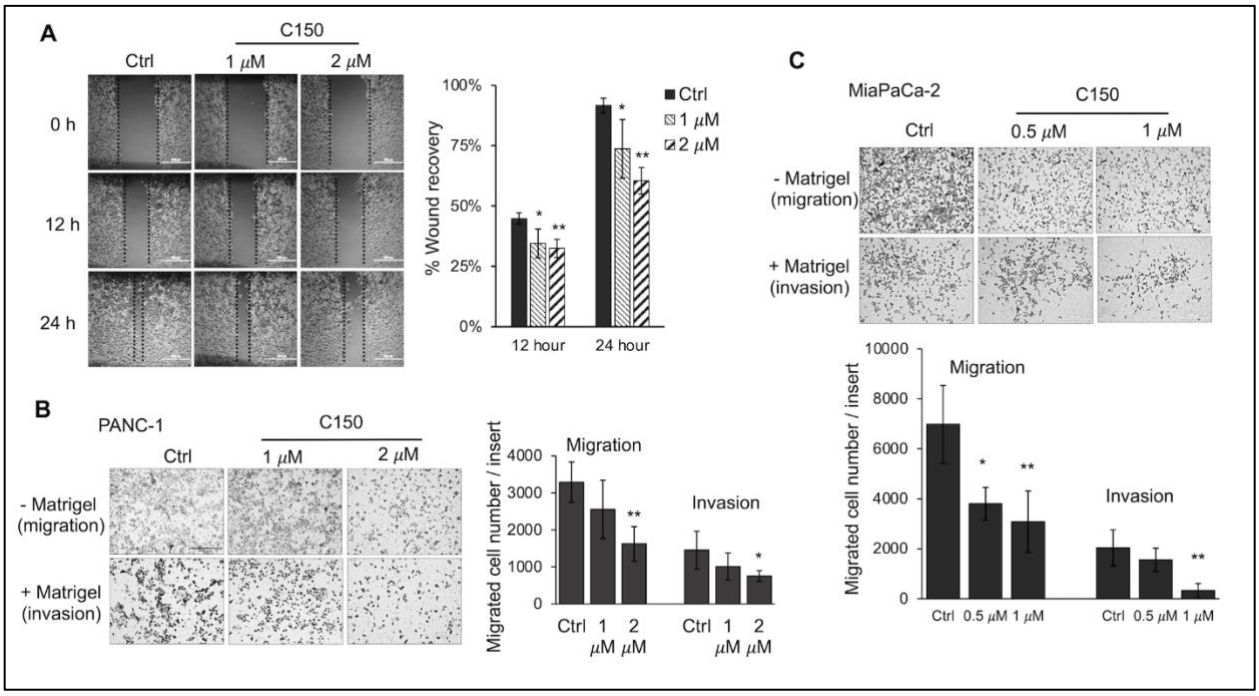

Figure 4.3 C150 inhibited pancreatic cancer cell migration and invasion in 2D assay. A. Scratch (wound-healing) assay. A monolayer of PANC-1 cells was treated with DMSO (Ctrl) or C150 (1μM and 2 μM) for 12 and 24 hours after a wound was made. Scale bar shows 500 μm. Bar graph shows the percentage of wound recovery (mean ± SD of 4 repeats). **B-C.** Trans-well migration and invasion of PANC-1 cells (**B**) and MiaPaCa-2 cells (**C**). Boyden chamber trans-well inserts were either un-coated (migration) or coated (invasion) with 0.1% Matrigel. Cells were treated with DMSO (Ctrl) or C150 (1 μM and 2 μM, 48 hours for PANC-1, and 0.5 μM and 1 μM, 24 hours for Mia PaCa-2). Bar graphs show the number of migrated or invaded cells per insert (mean ± SD of 2 independent experiments each done in triplicates). Scale bar shows 500 μm. * $p < 0.05$, ** $p < 0.01$ (*vs* Ctrl) by one-way ANOVA-Tukey's test.

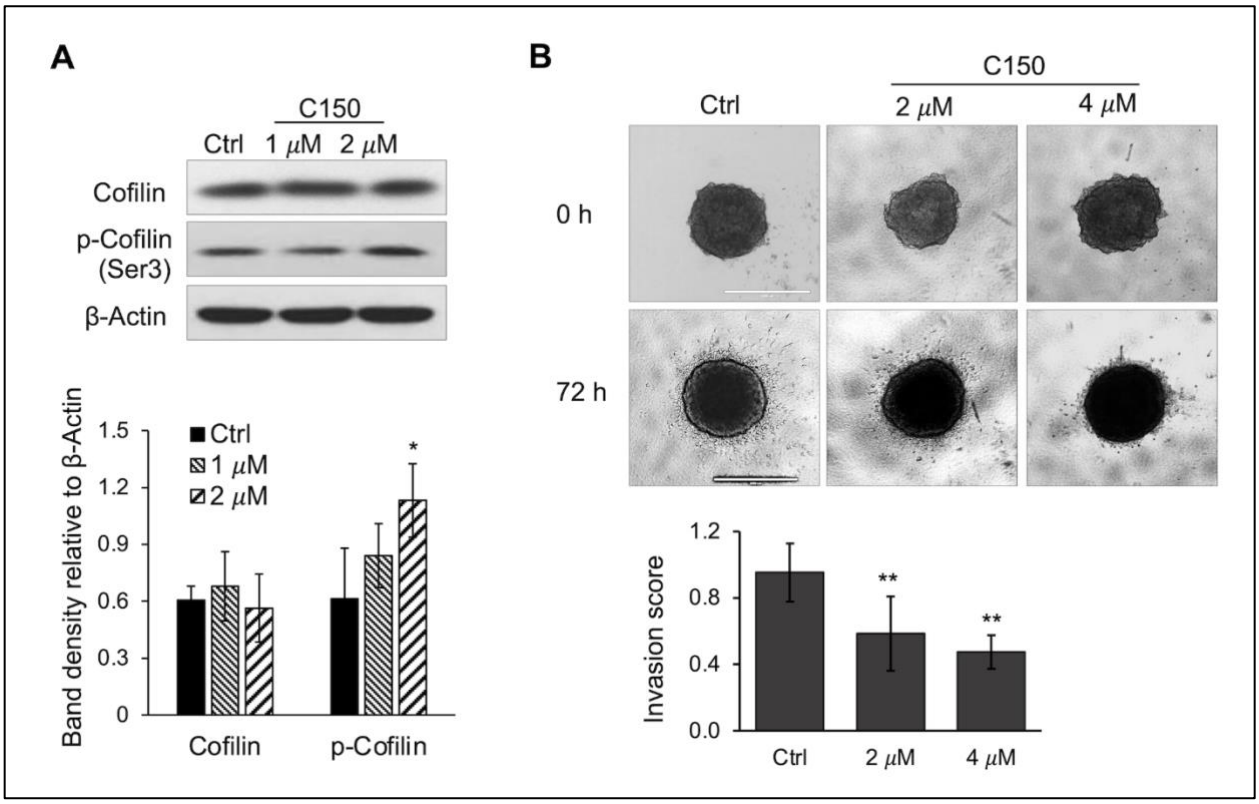

Figure 4.4 C150 inhibited PANC-1 cell invasion in 3D cell invasion assay. A. Western blots of Cofilin and p-Cofilin. PANC-1 cells were treated with DMSO (Ctrl) or C150 (1 μM and 2 μM) for 24 hours. Total cell lysates were subjected to immunoblotting against Cofilin and p-Cofilin (Ser-3). β-Actin was blotted as loading control. Bar graph shows the band densities relative to β-Actin (mean ± SD of 3 independent experiments). **B.** 3D invasion assay. PANC-1 cell spheroids were grown in collagen and treated with DMSO (Ctrl) or C150 (2 μM and 4 μM) for 72 hours. Scale bar shows 1000 μm. Bar graph shows the invasion score (mean ± SD of 2 independent experiments each done in 8 repeats). * $p < 0.05$, ** $p < 0.01$ (*vs* Ctrl) by one-way ANOVA-Tukey's test.

4.2.3 C150 suppressed EMT in pancreatic cancer cells

Multiple EMT markers were examined to investigate whether C150 inhibited pancreatic cancer EMT. Upon 24-hour treatment, C150 at 1 μM and 2 μM significantly increased the epithelial markers ZO-1 and Claudin-1 in PANC-1 cells and decreased the mesenchymal marker N-Cadherin (**Fig 4.5A**). The pro-EMT transcription factor Snail also decreased (**Fig 4.5A**). MMP-2 and MMP-9 are two matrix metalloproteases that contribute significantly to pancreatic cancer cell invasion by degrading the collagen-rich desmoplastic ECM in and surrounding the tumor [302-304]. We found that 24-hour treatment with C150 (1 μM and 2 μM) decreased the expression of MMP-2 and MMP-9 in PANC-1 cells as detected by RT-qPCR (**Fig 4.5B**). Furthermore, the activity of MMP-2 was significantly reduced by the same C150 treatment as detected by the gelatin zymography assay (**Fig 4.5C**). The activity of MMP-9 was not detected because of the overall low expression level of MMP-9 in PANC-1 cells.

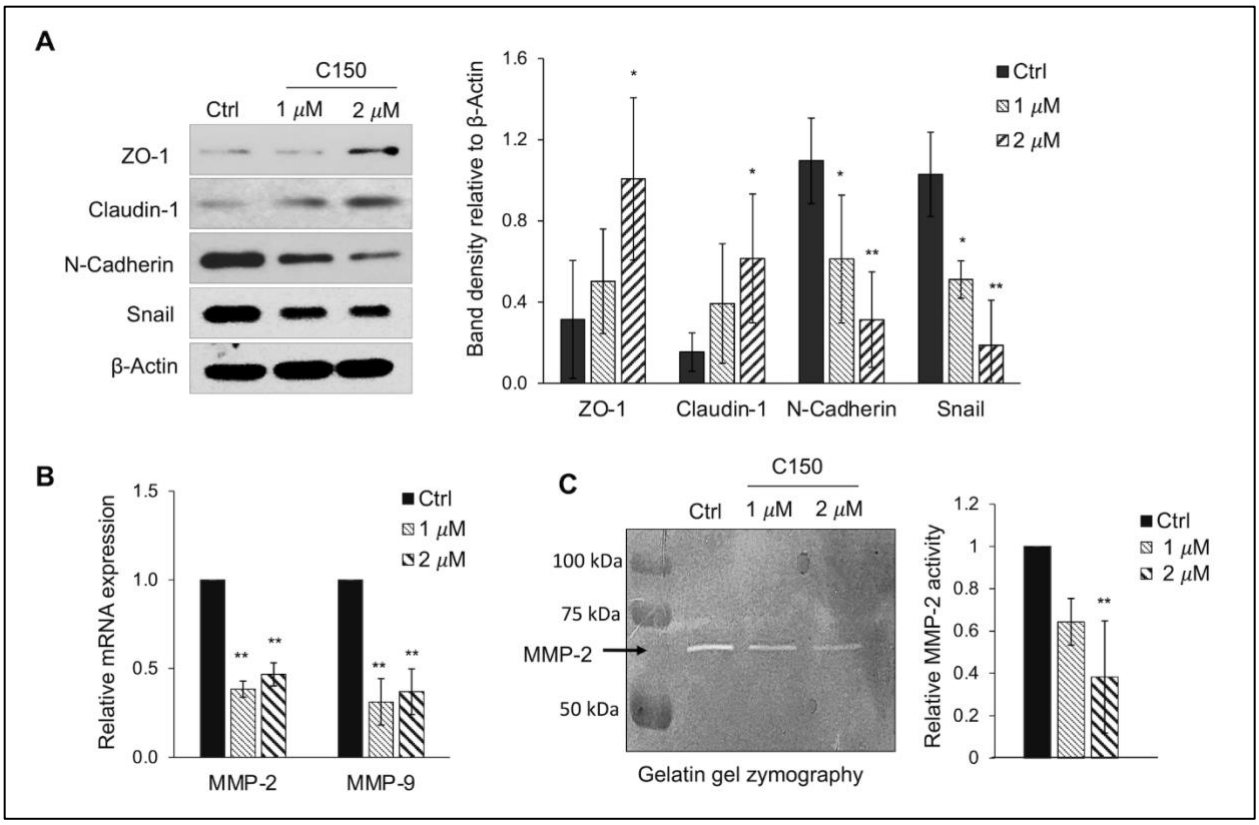

Figure 4.5 C150 inhibited EMT in PANC-1 cells. A. Western blots of EMT markers. PANC-1 cells were treated with DMSO (Ctrl) or C150 (1 μM and 2 μM) for 24 hours. Total cell lysates were subjected to immunoblotting against ZO-1, Claudin-1, Snail, and N-Cadherin. β-Actin was blotted as loading control. Bar graph shows the band densities relative to β-Actin. **B.** mRNA expression levels of MMP-2 and MMP-9. PANC-1 cells were treated with DMSO (Ctrl) or C150 (1 μM and 2 μM) for 24 hours. RT-qPCR results were quantified and normalized to the Ctrl group using the $2^{-\Delta\Delta Ct}$ method with GAPDH as the housekeeping gene. **C.** MMP-2 activity in gelatin zymography assay. PANC-1 cells were treated with DMSO (Ctrl) or C150 (1 μM and 2 μM) for 24 hours in FBS-free medium. The medium was then analyzed in a gelatin gel and proceeded with the enzyme activity zymography assay. The bright bands represent MMP-2 enzyme activity. Bar graph shows the relative enzyme activity normalized to the Ctrl group. Data represent mean ± SD of at least 3 independent experiments in all graphs. * $p < 0.05$, ** $p < 0.01$ (*vs.* Ctrl) by one-way ANOVA-Tukey's test.

4.2.4 C150 decreased Snail protein level by enhancing its proteasomal degradation

Snail is a master transcription factor that promotes EMT in pancreatic and many other cancers [81]. Accumulation of Snail protein in the nucleus facilitates the expression of genes that lead to the EMT phenotype. After a 24-hour treatment, C150 significantly decreased the nuclear Snail protein levels in PANC-1 cells (**Fig 4.6A**). Decrease in Snail protein levels may be a result of decreased expression, or enhanced protein degradation. We examined the mRNA expression level of Snail by RT-qPCR and the data showed that the mRNA level was not altered by C150 treatment (**Fig 4.6B**). We thus postulated that C150 decreased the Snail protein level by enhancing its proteasomal degradation. We treated PANC-1 cells with C150 in the presence of a proteasome inhibitor MG-132 (0.5 μM). The proteasome inhibitor MG-132 completely reversed C150-induced Snail decrease after a 16-hour treatment (**Fig 4.6C**). Moreover, when protein synthesis was blocked by puromycin (25 μg/ml) in PANC-1 cells, the presence of C150 (2 μM) accelerated Snail degradation (**Fig 4.7A**) and shortened the half-life of Snail protein from 2.7 hours in the absence of C150 to 2 hours (**Fig 4.7B**), supporting our hypothesis that C150 enhances Snail protein degradation.

We then overexpressed Snail in PANC-1 cells. The overexpression was confirmed by western blotting (**Fig 4.7C**), and cell migration was tested with the wound-healing assay. As expected, Snail overexpression increased cell migration, as the percentage of wound recovery was higher than that in the vector-transfected cells after 24 hours (**Fig 4.7C**). C150 (2 μM) treatment inhibited cell migration in both the empty vector-transfected cells and the Snail overexpressed cells (**Fig 4.7C**). The extent of the decrease in migration caused by C150 treatment had no difference between the vector-transfected cells and Snail overexpressed cells (15% decrease in

vector-transfected cells *vs*. 11% in Snail overexpressed cells, P > 0.05), suggesting that Snail overexpression did not dampen C150's effects on inhibiting PANC-1 cells migration. Taken together, the *in vitro* data showed that C150 enhanced degradation of Snail protein and inhibited pancreatic cancer cell EMT, resulting in inhibition of cell proliferation, migration, and invasion.

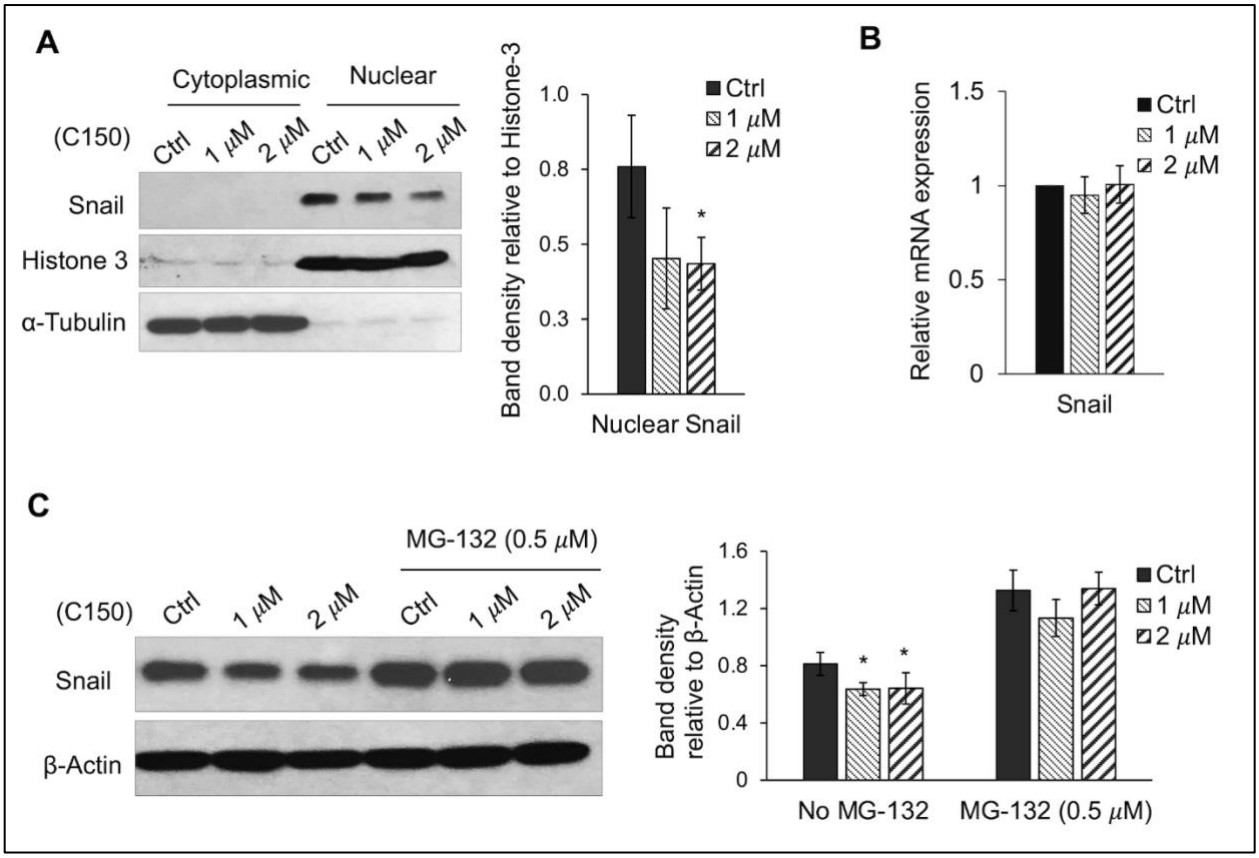

Figure 4.6 C150 enhanced Snail protein degradation. A. Cytoplasmic and nuclear protein levels of Snail. PANC-1 cells were treated with DMSO (Ctrl) or C150 (1 μM and 2 μM) for 24 hours. Cytoplasmic and nuclear fractions were subjected to immunoblotting against Snail. Histone-3 and α-tubulin were blotted as nuclear and cytoplasmic loading controls, respectively. Bar graph shows the band density of nuclear Snail relative to Histone-3. **B.** mRNA levels of Snail upon C150 treatment. PANC-1 cells were treated with DMSO (Ctrl) or C150 (1 μM and 2 μM) for 24 hours. RT-qPCR results were quantified and normalized to the control group using the $2^{-\Delta\Delta Ct}$ method with GAPDH as the housekeeping gene. **C.** Snail protein levels upon C150 and MG-132 treatment. PANC-1 cells were treated with C150 (1μM and 2 μM) alone or co-treated with C150 and MG-132 (0.5 μM) for 16 hours. Total lysates were subjected to immunoblotting against Snail. β-Actin was blotted as loading control. Bar graph shows the band densities of Snail relative to β-Actin. Data are presented as mean ± SD of 3 independent experiments. * $p < 0.05$, ** $p < 0.01$ by one-way ANOVA-Tukey's test.

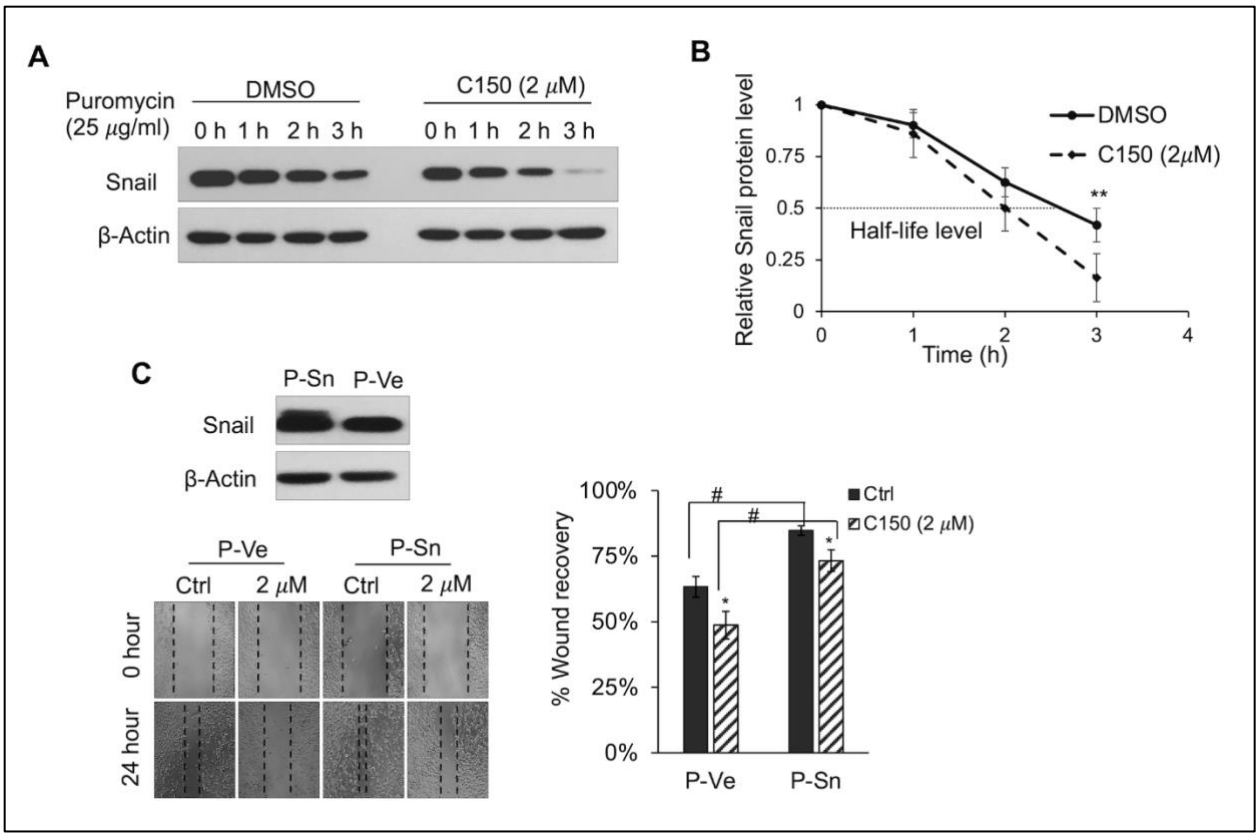

Figure 4.7 C150 accelerated Snail protein degradation in PANC-1 cells and inhibited migration in Snail-overexpressed PANC-1 cells. A. Snail protein levels post puromycin treatment. PANC-1 cells were treated with DMSO or C150 (2 μM) for 24 hours, then puromycin (25 μg/mL) was added to block protein synthesis. Cell lysates were collected at 0, 1, 2 or 3 hours after puromycin was added. β-Actin was blotted as loading control. **B.** Snail protein degradation curve. Snail band densities relative to β-Actin at indicated time points were quantified and normalized to that of the zero-hour time point in each group. **C.** Wound healing assay in PANC-1 cells with Snail overexpression. PANC-1 cells were transfected with Snail plasmid (P-Sn) or empty vector plasmid (P-Ve) for 48 hours. Overexpression of Snail was confirmed by western blotting. Transfected cells were then seeded for scratch assay with DMSO (Ctrl) or 2 μM C150 treatment for 24 hours. Bar graph shows the percentage of wound recovery. Data are presented as mean ± SD of 3 independent experiments. * $p < 0.05$, ** $p < 0.01$; # $p < 0.05$ by student's T-test.

4.2.5 C150 treatment reduced tumor growth in an orthotopic mouse model of pancreatic cancer

An orthotopic mouse model of pancreatic cancer was used to evaluate the *in vivo* effects of C150. Luciferase labeled PANC-1 cells (PANC-1-luc) were injected into the pancreas of nude mice. Two weeks after cell injection, mice were imaged to confirm tumor formation and were grouped based on tumor burden into vehicle (n = 10) and treatment group (n = 9), for each group to have equal tumor burdens. Mice were treated 3 times per week with 15 mg/kg of C150 (determined by dose-finding experiments described in Methods) or vehicle (20% DMSO + 20% H_2O + 60% PEG400) by intraperitoneal (IP) injection.

Six weeks of C150 treatment significantly reduced tumor burden compared to vehicle controls (**Fig 4.8A-B**). The final average tumor weight in the C150 treated group was significantly lower than that in the control group (**Fig 4.8C**). The expression of the proliferating cell nuclear antigen (PCNA) was significantly inhibited in C150-treated tumors compared to vehicle-treated tumors (**Fig 4.8D**), indicating a reduction of cell proliferation by C150 treatment. EMT markers in the tumor samples were examined by western blot. Consistent with *in vitro* data, the epithelial markers ZO-1 and Claudin-1 were elevated in the tumor tissues of C150-treated mice, while the pro-metastasis marker MMP-2 was decreased (**Fig 4.9 A-B**). Collectively, the *in vivo* data are consistent with the *in vitro* data, suggesting that C150 inhibited pancreatic cancer progression.

Toxicities were evaluated by body condition score (BCS) and clinical signs as described in Materials and Methods. All mice started at a BCS of 3. During the treatment, no mice showed observable clinical signs of toxicity or had BCS dropped to 2 or below. However, the average

body weight of the treatment group decreased compared to the control group (**Fig 4.9C**), indicating potential toxicities not evaluated here. Therefore, the toxicity profile and therapeutic window of C150 need further investigation.

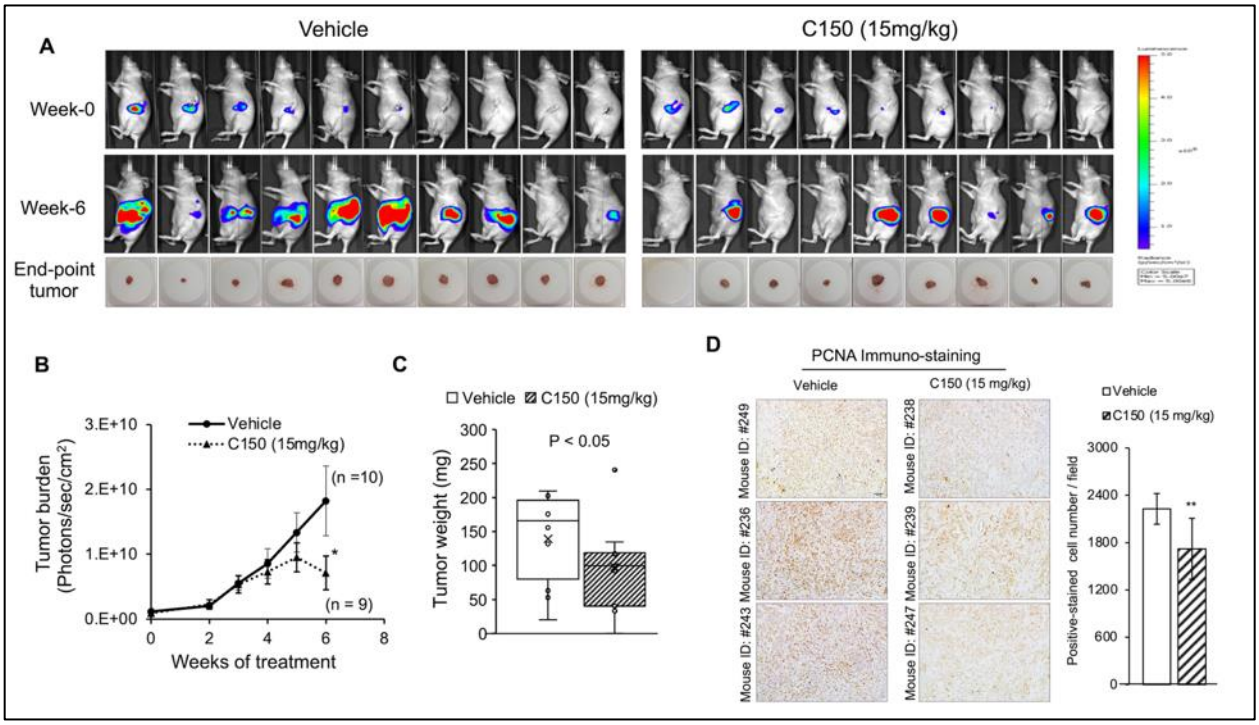

Figure 4.8 C150 reduced tumor growth in mice. A. Bioluminescence images of tumor burden in live mice at the beginning (Week-0) and the end (Week-6) of treatment. Actual tumors at necropsy are shown below the bioluminescence images. **B.** Longitudinal average tumor burden detected by imaging, quantified as photons/sec/cm^2 (mean ± SEM). **C.** Average tumor weight at necropsy (n=9 for C150 group, and n=10 for vehicle group). $P < 0.05$ by Mann-Whitney test. **D.** Immunohistochemistry staining for PCNA in tumor samples. Three random tumors each from the vehicle or the C150 group were analyzed. Scale bar shows 50 μm. Bar graph shows the quantification of positively stained cells, presented as mean ± SD of at least 5 different fields per sample of the 3 samples. ** $p < 0.01$ with t-test.

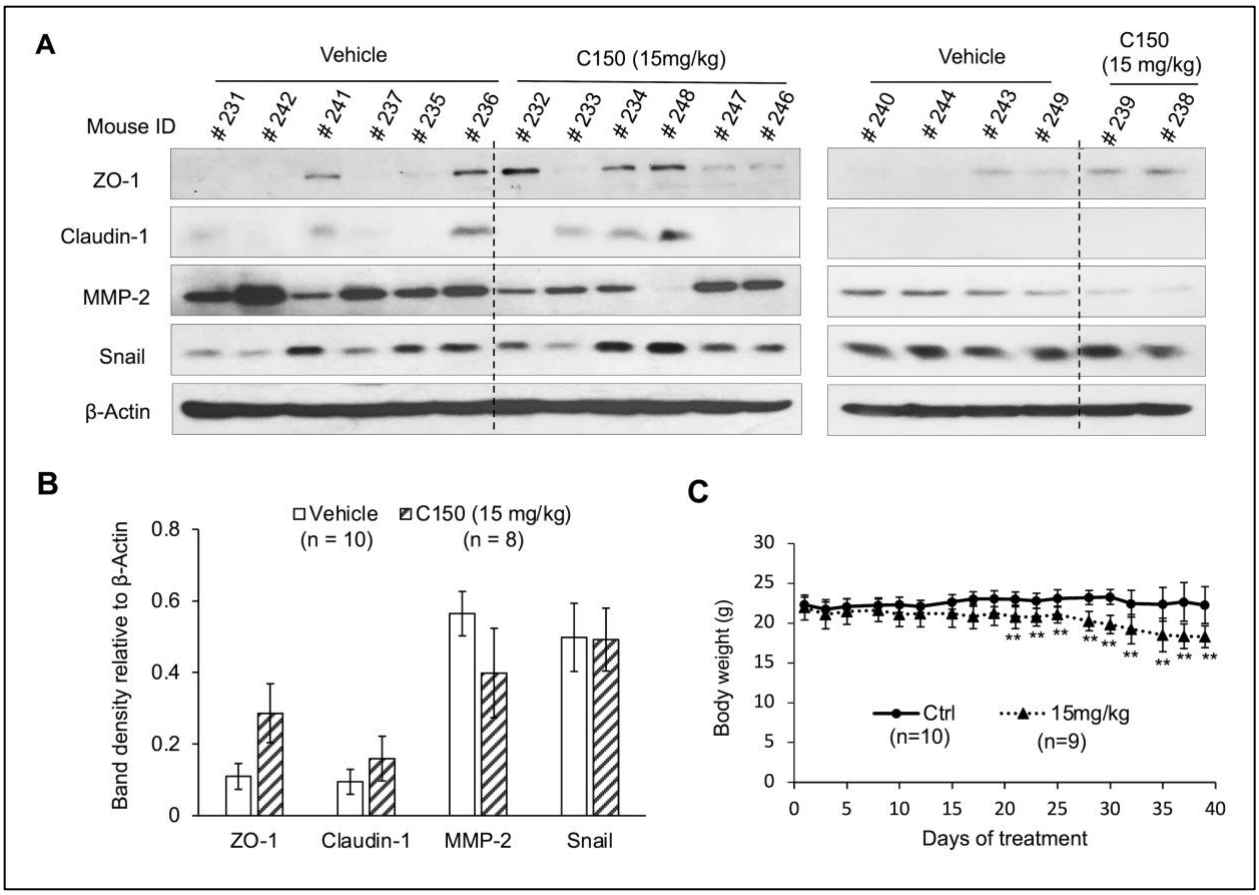

Figure 4.9 Western blot of EMT markers in tumor samples. A. Total lysates of tumor samples from all mice were analyzed. EMT marker ZO-1, Claudin-1, MMP-2 and Snail were probed. β-Actin was blotted as loading control. **B.** Quantification of band densities in western blot relative to β-Actin (mean ± SEM). **C**. Average body weight (mean ± SD). ** $p < 0.01$ by student's T-test.

4.3 Summary and discussion

There is increasing evidence for the critical role of EMT in promoting pancreatic cancer progression [291]. During EMT, cancer cells undergo serial molecular changes to turn off the expression of epithelial markers while upregulating mesenchymal markers, leading to the loss of cell-cell and cell-membrane adhesion [305]. In this study, we found that C150 treatment in PANC-1 cells increased the epithelial markers ZO-1 and Claudin-1, both of which are integral components of tight junctions in the epithelial phenotype. In contrast, the mesenchymal marker

N-cadherin decreased upon C150 treatment. These data indicate that C150 treatment suppressed the EMT process in PANC-1 cells. These mechanisms were further confirmed in a mouse model, with data showing that C150 treatment increased ZO-1 and Claudin-1 and decreased MMP-2 in tumor tissues, which was in line with the *in vitro* data, indicating EMT inhibition.

During the invasion stage, cancer cells need to degrade the basal membrane and the dense extracellular matrix (ECM). This process is mainly mediated by the matrix degradation enzymes of the family of metalloproteinases (MMPs) [306]. The production of MMPs by cancer cells is upregulated by EMT-promoting factors [292, 307]. In this study, we found that compound C150 significantly inhibited pancreatic cancer cell migration and invasion in multiple *in vitro* assays. The expression levels and activities of MMP-2 and MMP-9, two of the major metalloproteinases responsible for degrading collagen fibers in the tumor stroma, were downregulated by C150 treatment. This may be of particular importance in pancreatic cancer as the disease is well characterized with rich collagenous stroma [308].

The pro-EMT factor Snail was strongly decreased by C150 treatment. Snail directly regulates expressions of several epithelial/mesenchymal markers, including ZO-1, Claudin-1, and N-cadherin [82, 296, 297]. Ectopic expression of Snail resulted in EMT and promoted metastasis in mouse models of pancreatic cancer [97, 309]. The reduction of Snail protein level by C150 treatment provides a mechanism by which C150 inhibits EMT in pancreatic cancer cells. Further, silencing Snail was reported to result in cell cycle arrest and suppressed proliferation in cancer [310]. This observation is consistent with our *in vitro* and *in vivo* data that compound C150 decreased Snail and inhibited cell proliferation.

A limitation of our data is that changes of Snail were not detected in the mouse tumor samples. This is likely due to several reasons: The fast turn-over time of Snail protein [93, 311] and a late sample-collecting time of 48 hours after the last treatment may have resulted in the inability to detect changes in Snail protein levels. Also, tissues harvested from mouse tumors were a mixture of tumor cells, fibroblasts, blood vessels, immune cells, and other associated tissue cells. This could obscure the results. Further, after 6 weeks of treatment, the tumor cells with decreased Snail (assumed to be more sensitive) would have died or would not have proliferated. Therefore, in the residual tumor tissues, cells without changes in Snail expression or with minor changes are more likely to dominate the population, and therefore a decrease in Snail expression could not be detected. Nevertheless, multiple *in vitro* assays and Snail overexpression confirmed the role of Snail in the C150-mediated EMT-inhibiting effect.

Notably, we found that C150 induced a decrease of Snail protein through enhanced proteasomal degradation but did not inhibit its expression. Our data show that Snail mRNA remained unchanged and the decrease in protein was prevented by a proteasome inhibitor. Snail protein degradation is tightly controlled by its phosphorylation and ubiquitination status [80, 312]. Multiple pathways have been reported to regulate Snail phosphorylation, among them is the GSK3β mediated pathway [92]. GSK3β phosphorylates Snail at two different sites, priming it for nuclear exportation, ubiquitination, and subsequent proteasomal degradation [92]. However, we found that C150 significantly increased Serine-9 phosphorylation of GSK3β (**Fig 4.10**), which inhibits its kinase function [313, 314]. Therefore Serine-9 phosphorylation of GSK3β would likely increase Snail protein stability rather than decrease it. Thus, we speculated that

C150-induced Snail degradation is not likely to be mediated by the GSK3β pathway. Many regulatory pathways and kinases are involved in the regulation of Snail protein stability [82, 312]. With the molecular target of C150 unknown, the exact mechanism by which C150 increased Snail proteasomal degradation is unclear and needs further investigation.

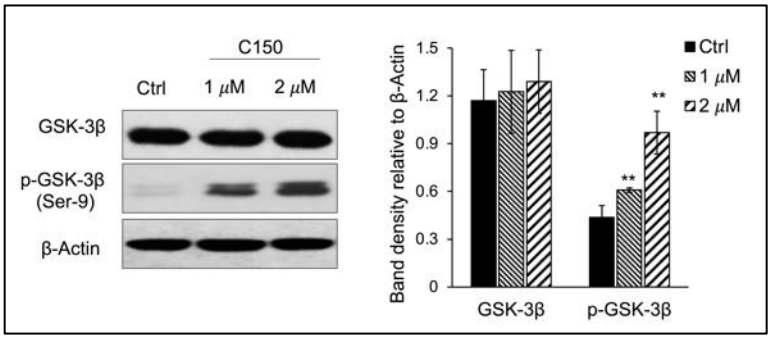

Figure 4.10 C150 treatment increased Serine-9 phosphorylation of GSK-3β. PANC-1 cells were treated with DMSO (Ctrl) or C150 at 1 μM and 2 μM for 24 hours. GSK-3**β** and p-GSK-3**β** were probed. β-Actin was blotted as loading control. Right panel bar graph shows the quantification of band densities relative to β-Actin. Data are presented as mean ±SD of 3 independent experiments. ** $p < 0.01$ by one-way ANOVA-Tukey's test

Taken together, we report for the first time that the novel compound C150 inhibited pancreatic cancer cell migration and invasion *in vitro*, suppressed EMT, and reduced tumor growth in mice. The data suggest that C150 can serve as a drug lead for comprehensive inhibition in pancreatic cancer growth and metastasis. Future investigations could involve target identification of C150 and in-depth mechanistic studies, as well as defining its toxicity profiles. Analogs of C150 may be developed and tested for improved efficacy, reduced toxicity, and improved PK and other drug-like properties.

Chapter 5. The EMT inhibitor C150 inhibits pancreatic cancer through induction of ER stress and proteasome assembly

5.1 Introduction

The homeostasis between protein loading and protein folding in the endoplasmic reticulum (ER) is essential for cell survival. Cellular insults that perturb this homeostasis lead to misfolded protein accumulation and ER stress [177]. In response to ER stress, cells activate the unfolded protein response (UPR) pathways to restore homeostasis in the ER in an effort to survive [178]. The UPR is controlled by three ER-membrane bound proteins, protein kinase RNA-like ER kinase (PERK), inositol-requiring protein 1α (IRE1α) and activating transcription factor 6 (ATF-6) [178]. Activation of PERK, IRE1α and ATF-6 activates their direct downstream transcription factors, ATF-4, XBP1-s, and spliced-ATF-6 respectively, leading to increased gene expressions of chaperone proteins to enhance the protein folding capacity in the ER [315, 316]. In addition, PERK activation results in the attenuation of mRNA translation through eIF2α phosphorylation, therefore reducing new protein load to the ER [317]. Finally, ER stress also activates the ER associated degradation (ERAD) pathway to facilitate misfolded protein removal through the ubiquitin-proteasome system and autophagy [318, 319]. By increasing the level of protein folding chaperones, reducing protein synthesis, and enhancing misfolded protein removal through ERAD, the UPR signaling functions as a pro-survival mechanism to restore ER homeostasis [319]. However, severe or prolonged ER stress that goes beyond the UPR rescue would lead to cell proliferation arrest, cell death, and senescence [250, 320, 321].

As the major protein degradation system in the cell, proteasome levels, and activities are often elevated upon proteomic stresses, such as misfolded protein accumulation under ER stress, to facilitate the clearance of misfolded or damaged proteins [322]. The two major forms of proteasomes in the cell are the 20s proteasome and the 26s proteasome, both of which are multi-

subunit protein complexes. The 20s proteasome is made up of two sets of seven different α subunits (α_{1-7}) forming a ring and two sets of seven different β subunits (β_{1-7}) forming a ring. These rings are arranged as $\alpha_{1-7}\beta_{1-7}\beta_{1-7}\alpha_{1-7}$. The 26s proteasome is composed of a 20s proteasome flanked at one or both of its ends by a 19s regulatory particle (19s RP) that is made up of 19 different subunits [207]. Therefore, the assembly of a full 26s proteasome requires the steps of 20s proteasome assembly, 19s RP assembly, and the docking of 19sRP to the 20s proteasome [208]. The 26s proteasome serves as the main complex for cellular protein degradation in an ATP- and ubiquitin-dependent manner [209], while the 20s is also capable of degrading a portion of cellular proteins independent of ATP and ubiquitin [211, 212].

Because of the essential role of ER balance in cell survival, disrupting ER balance has been proposed as a potential therapeutic approach in cancer treatment [323, 324]. We have shown in chapter 4 that the quinoline compound C150 enhanced the proteasome-mediated degradation of Snail protein in pancreatic cancer cells, causing EMT inhibition and reduced cell invasion. In this chapter, we further reveal that C150 induced profound ER stress in pancreatic cancer cells and led to an increase in proteasome assembly, cellular autophagy, and attenuation of mRNA translation. C150 treatment arrested pancreatic cancer cells in the G2/M phase, induced cellular senescence, and increased cellular sensitivity to gemcitabine treatment. C150 treatment significantly increased survival and reduced tumor growth in a syngeneic pancreatic cancer mouse model.

5.2 Results

5.2.1 C150 increased proteasome activity in PANC-1 cells by increasing proteasome assembly

We have previously reported that C150 enhanced proteasomal degradation of the pro-EMT transcription factor Snail in PANC-1 cells. In addition, we found that β-catenin, TP53, and Sox2 protein levels were also reduced by C150 treatment (**Fig 5.1**).

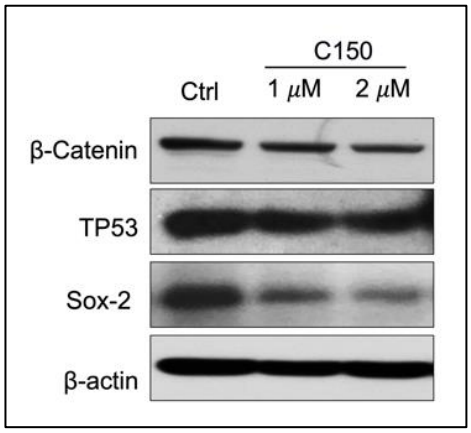

Figure 5.1 C150 decreased β-Catenin, TP53, and Sox-2 protein levels. PANC-1 cells were treated with DMSO (Ctrl) or C150 (1 μM and 2 μM) for 24 hours. Total cell lysates were analyzed and probed for β–catenin, TP53, and Sox-2. β-Actin was blotted as loading control.

All of these transcription factors are proteasome substrates [325-327]. Therefore, we postulated that C150 increased proteasome activity in the cell. To examine cellular proteasome activity upon C150 treatment, PANC-1 cells were first treated with C150 (1 μM and 2 μM) for 24 hours. Cell lysates were collected in non-denaturing buffer and incubated with a proteasome substrate, Suc-LLVY-AMC, which generates fluorescence upon proteasomal degradation. The results showed that lysates from C150-treated cells exhibited a significantly higher proteasome activity compared to the DMSO-treated group (Ctrl) in a concentration-dependent manner (**Fig 5.2A**). This increase was completely attenuated when a specific proteasome inhibitor epoxomicin was added to the cell lysates (**Fig 5.2B**). To examine whether C150 directly increased the activity of proteasomes, un-treated PANC-1 cell lysates were incubated with C150 and the proteasome substrate. The direct incubation of C150 in non-treated cell lysates did not have any effect on

proteasome activity (**Fig 5.2C**). These data suggested that the C150-mediated increase of the proteasome activity was dependent on a cellular process that requires the integrity of the cell but was not through direct interaction of C150 with the proteasomes.

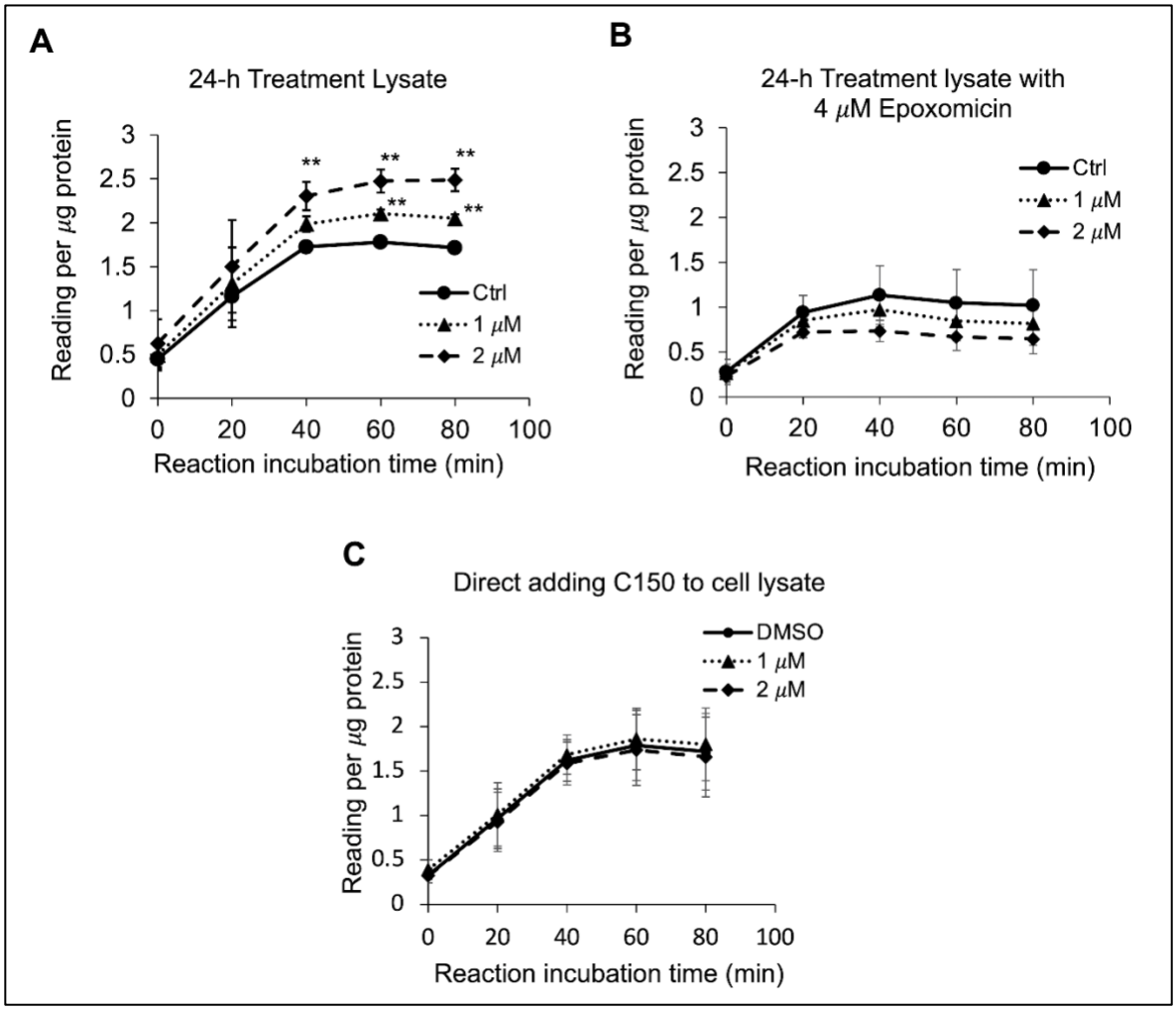

Figure 5.2 C150 enhanced proteasome activity. A-B. Proteasome activity in C150-treated PANC-1 cell lysates in the absence (**A**) or presence (**B**) of epoxomicin (4 μM). PANC-1 cells were treated with C150 (1 μM and 2 μM) or DMSO (Ctrl) for 24 hours. Cell lysates were then collected and incubated with the proteasome substrate Suc-LLVY-AMC at 37 ºC in the absence (**A**) or in the presence (**B**) of 4 μM epoxomicin and the fluorescence signal was detected every 20 minutes for 80 minutes at 360/460 nm. Fluorescence signal intensity was corrected for protein amounts in the lysates. **C.** Proteasome activity in non-treated PANC-1 cell lysates incubated with C150. DMSO (Ctrl) or C150 (1 μM and 2 μM) was directly added into lysates of non-treated PANC-1 cells and incubated at room temperature for 30 minutes before mixing with Suc-LLVY-AMC substrate. Data are presented as mean ± SD of 3 independent experiments each done in triplicates. * $P < 0.05$, ** $P < 0.01$ (*vs*. Ctrl) by one-way ANOVA with Tukey HSD test.

We then investigated the total levels of assembled 20s and 26s proteasomes in the PANC-1 cells treated with C150. Anti-β-5 subunit antibody was used to detect the 20s proteasomes. Because the 26s proteasome is composed of a 20s flanked by one or two 19s caps at its ends, an anti-PSMC-3 subunit for 19s RP was also used to show the 1-cap or 2-caped 26s proteasomes. Native gel protein electrophoresis and western blots showed that the assembled 20s proteasomes and 2-cap 26s proteasomes were both elevated upon C150 treatment (**Fig 5.3A**). To determine if the increased 20s and 26s proteasome levels were the results of increased expressions of their subunits, we tested a panel of 20s and 19s subunits by western blotting. All the examined subunits remained unchanged by C150 treatment (**Fig 5.3B**). Because the abundance of proteasomes in the cell is also regulated by their assembly [322, 328], we then examined the expressions of nine proteasome assembly chaperones by RT-qPCR. We found that 24-hour C150 treatment (1 μM and 2 μM) significantly increased the expressions of the chaperone PAC-1, PAC-3, PSMD-5, PSMD-10, and PAAF-1. The other four chaperones showed a trend to increase but this increase was not significant (**Fig 5.3C**). Taken together, the data suggested that C150 enhanced proteasome activity in PANC-1 cells by increasing proteasome assembly.

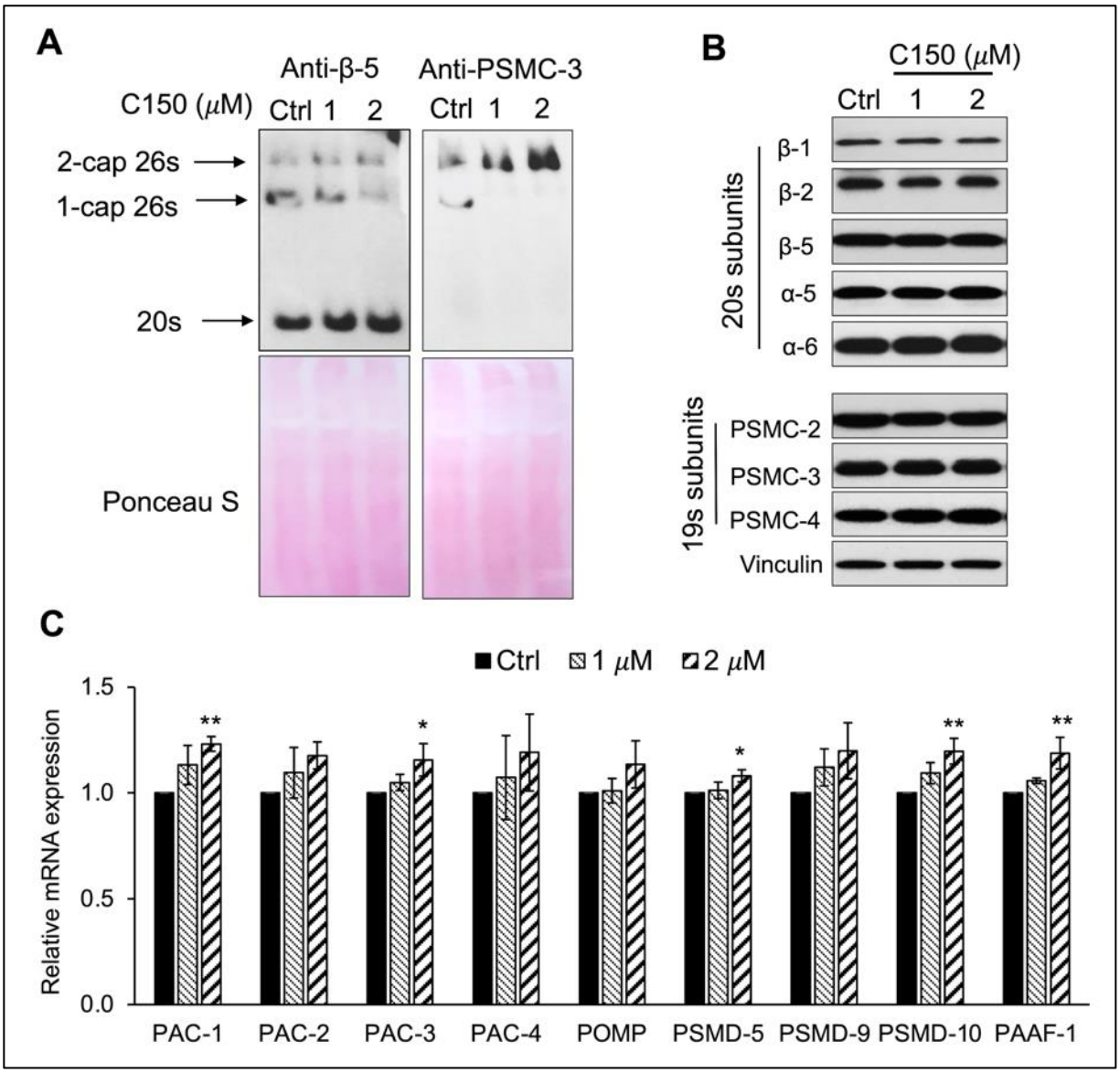

Figure 5.3 C150 increased proteasome assembly. PANC-1 cells were treated with C150 (1 μM and 2 μM) or DMSO (Ctrl) for 24 hours. **A.** Native gel blots for assembled 20s and 26s proteasome. Anti β-5 antibody was used to show 20s and anti-PSMC-3 to show 26s proteasomes. Lower panels show Ponceau S staining. **B.** Western blots of proteasome subunits. Total cell lysates were analyzed for proteasome subunits. Vinculin was a loading control. **C.** RT-qPCR for mRNA expressions of proteasome assembly chaperones. Results were quantified and normalized to the Ctrl group using the $2^{-\Delta\Delta Ct}$ method with GAPDH as a housekeeping gene. Data are presented as mean ± SD of 3 independent experiments each done in triplicates. * $P < 0.05$, ** $P < 0.01$ (*vs*. Ctrl) by one-way ANOVA with Tukey HSD test.

5.2.2 C150 induced ER stress, increased autophagy, and attenuated protein synthesis in PANC-1 cell

An increase of proteasome levels can be induced by ER stress [224, 225]. We next investigated whether C150 treatment can induce ER stress in PANC-1 cells. A 24-hour treatment with C150 (1 μM and 2 μM) resulted in a profound upregulation of the ER stress makers, Bip, ATF-4, and XBP-1s (**Fig 5.4A**). During ER stress response, autophagy is often initiated to further assist the removal of misfolded and damaged proteins [329]. Our data showed that C150 treatment significantly increased LC-3II, and LC-3II level was further enhanced by the additional treatment of chloroquine at 20 μM for 4 hours (**Fig 5.4B**), suggesting an increased autophagy flux by C150 treatment. The increased autophagy was further confirmed by immunostaining of LC-3 puncta in the cells (**Fig 5.4C**). Furthermore, the phosphorylation of the translation initiation factor eIF2α was significantly increased upon C150 treatment (**Fig 5.4D**), indicating a reduction of protein synthesis in response to the ER stress [173]. To confirm protein synthesis attenuation, we performed a puromycin incorporation assay [330]. Puromycin can effectively incorporate into newly synthesized peptides and later be detected using western blotting [331]. PANC-1 cells were treated with C150 (1 μM and 2 μM) for 24 hours, and then pulsed with 2 μM puromycin for 20 minutes. The C150-treated cells exhibited a significantly lower level of incorporated puromycin (**Fig 5.4E**), indicating reduced protein synthesis.

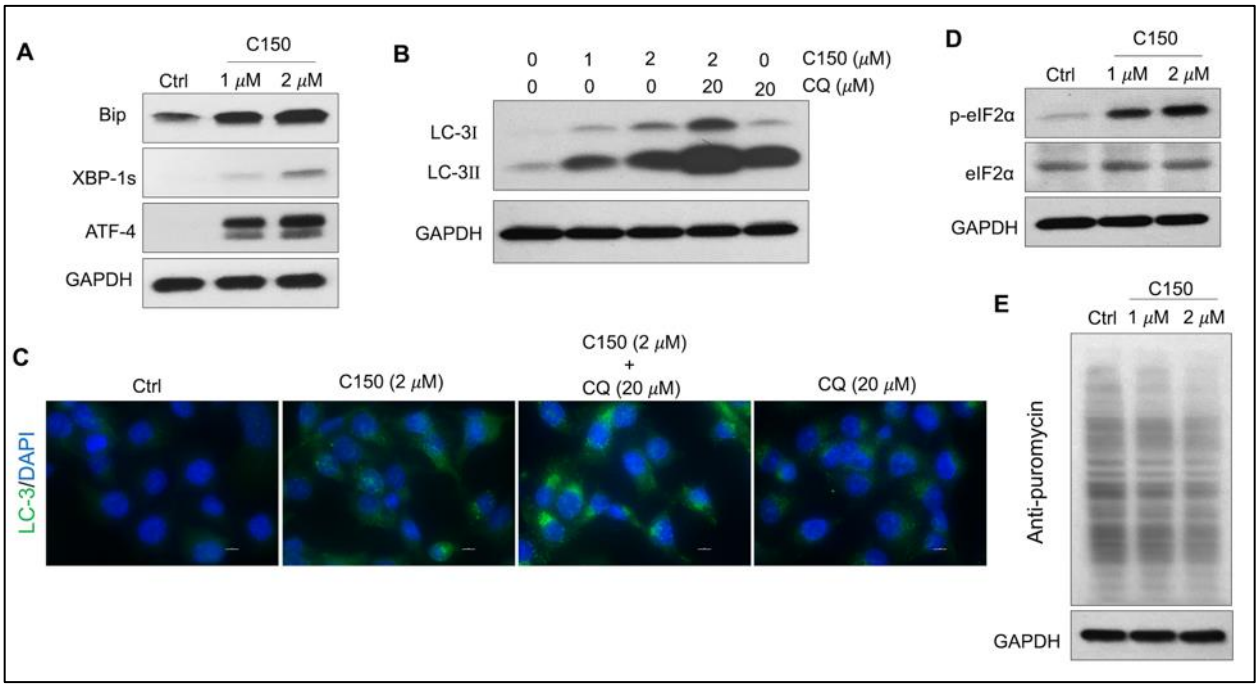

Figure 5.4. C150 induced ER stress and resulted in autophagy and attenuation of protein translation in PANC-1 cells. PANC-1 cells were treated with DMSO (Ctrl) or C150 (1 μM and 2 μM) for 24 hours. **A.** Western blots of ER stress makers, Bip, XBP-1s, and ATF-4. GAPDH was blotted as loading control. **B.** Western blots of the autophagy marker LC-3. CQ, chloroquine (20 μM, 4 hours treatment). **C.** Immunofluorescence staining for LC-3 puncta. Cells were fixed and stained against LC-3 (green). Cell nuclei were stained with DAPI (blue). Scale bar, 10 μm. CQ, chloroquine (20 μM, 4 hours treatment). **D.** Western blots of eIF2α and p-eIF2α. **E.** Puromycin incorporation showing protein synthesis inhibition. PANC-1 cells were treated with 2 μM puromycin for 20 minutes after 24 hours treatment with C150 or DMSO (Ctrl). Total cell lysates were analyzed and blotted with anti-puromycin antibody. GAPDH was blotted as loading control.

5.2.3 C150 caused G2/M cell cycle arrest, induced cell senescence, and synergized with gemcitabine in PANC-1 cells

It was reported that ER stress was able to induce cell cycle arrest [320, 332]. Upon C150 treatment (1 μM and 2 μM) for 24 and 48 hours in PANC-1 cells, there was a robust increase of the cell population in the G2/M phase as demonstrated by PI cell cycle analysis (**Fig 5.5A-B**), suggesting a G2/M cell cycle arrest under C150 treatment. Cell growth curves showed significantly reduced proliferation rates by C150 treatment (**Fig 5.5C**). Sustained cell cycle arrest commonly results in apoptosis and/or cell senescence [333]. Our previous data in **Chapter 4** have shown that C150 treatment did not induce apoptosis. Notably, data here showed that C150 treatments at 24 and 48 hours effectively induced senescence in PANC-1 cells, indicated by the increased β-galactosidase (SA-β-galactosidase) staining at pH 6.0 (**Fig 5.6A**). Induction of senescence was reported to sensitize pancreatic cancer cells to chemotherapeutic agents [334]. We found that the combination treatment of C150 with gemcitabine more effectively reduced PANC-1 cell viability compared to single-agent treatment (**Fig 5.6B**). Strong synergistic effects were shown when C150 was added to gemcitabine, with the Chou-Talalay's combination index(CI) [287] being far less than 1 (**Fig 5.6C**).

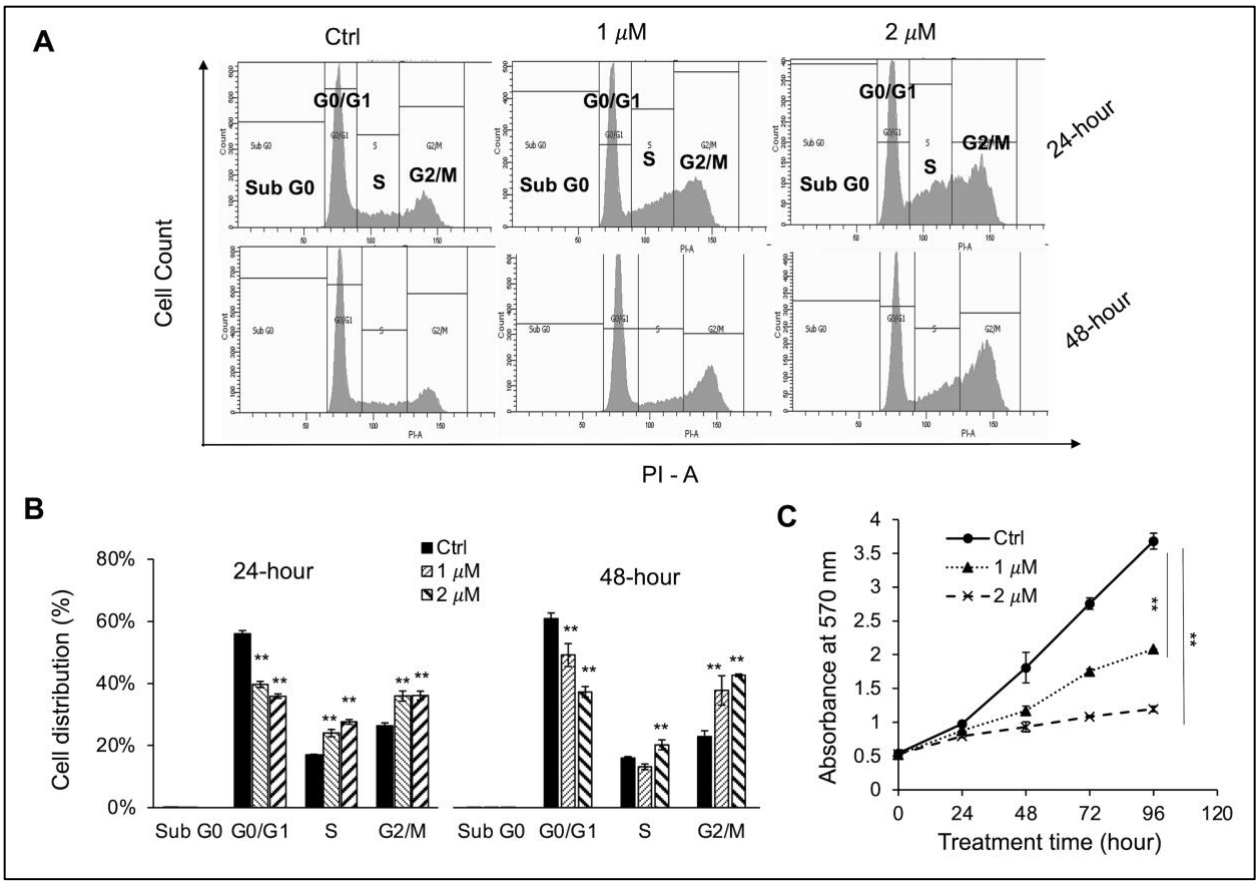

Figure 5.5 C150 caused G2/M cell cycle arrest and inhibited proliferation in PANC-1 cells. **A.** Cell cycle analysis. PANC-1 cells were treated with DMSO (Ctrl) or C150 (1 μM and 2 μM) for 24 and 48 hours. Cells were stained with propidium iodide (PI) and analyzed for cell cycle distributions with flow cytometry. **B.** Bar graph shows the quantification of the percentage of cells in each cell cycle. Data are presented as mean ± SD of 3 independent experiments. **C.** Cell growth curve. PANC-1 cells were seeded at 5,000 cells per well in 96-well plates in triplicates and cultured for 0, 24, 48, 72, and 96 hours with C150 treatments. Viable cells were detected by the MTT assay. Data are presented as mean ± SD of 3 experiments. * $P < 0.05$, ** $P < 0.01$ (*vs.* Ctrl) by one-way ANOVA with Tukey HSD test.

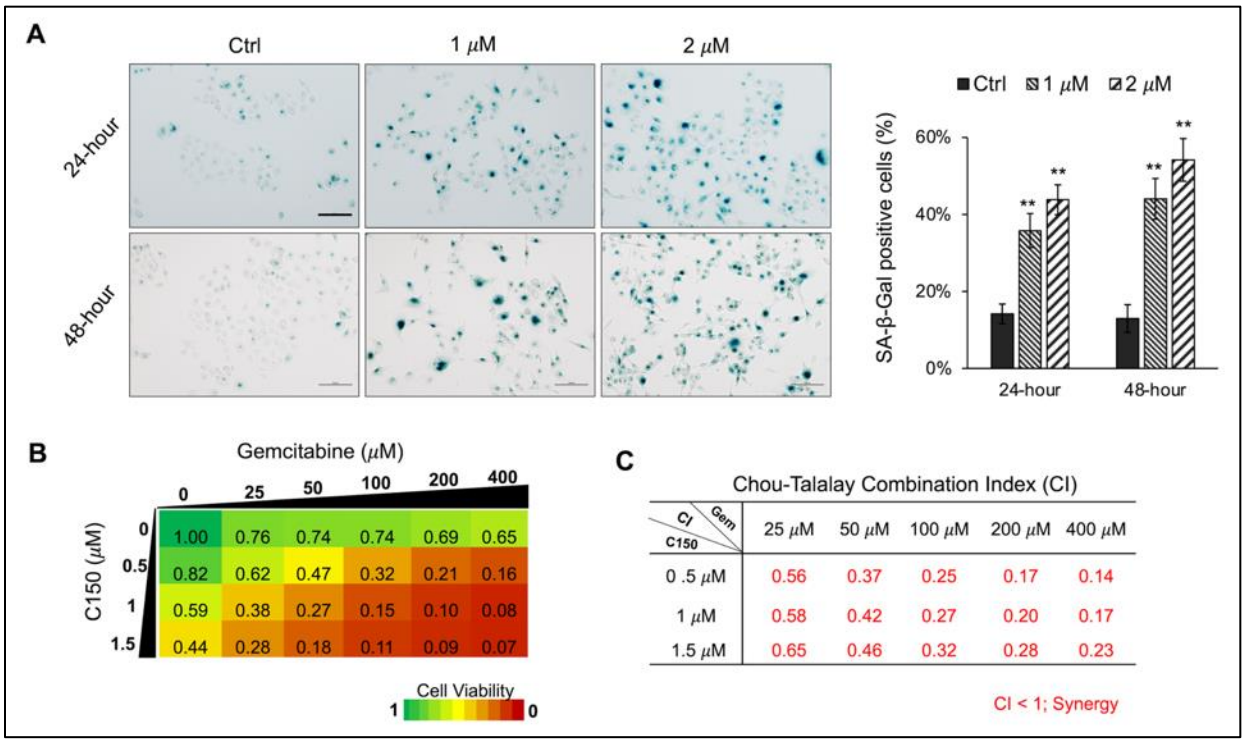

Figure 5.6 C150 induced senescence and synergized with gemcitabine in PANC-1 cells. A. SA-β-galactosidase staining at pH 6.0 for cell senescence. Senescent cells were identified by the green-blue staining under bright field light microscopy with 200x magnification. Scale bar, 100 μm. Bar graph shows the percentage of senescent cells per imaging field with five random fields in each sample. Data are presented as mean ± SD of two independent experiments each done in triplicates. **B.** Heatmap of cell viabilities under combination treatment of C150 with gemcitabine in PANC-1 cells. PANC-1 cells were treated with C150 and gemcitabine at the indicated concentrations for 72 hours. Cell viability was detected using MTT assay. Data are presented as mean viability from three independent experiments each done in duplicates. **C.** Combination Index. The drug combination index was calculated from the cell viability data in (**B**) according to the Chou-Talalay's method. Mean CI values from three experiments were presented. * $P < 0.05$, ** $P < 0.01$ (*vs*. Ctrl) by one-way ANOVA with Tukey HSD test.

5.2.4 C150 reduced tumor growth and increased survival in a syngeneic pancreatic cancer mouse model

A syngeneic pancreatic cancer mouse model was used to evaluate the activity of C150 *in vivo*. Compared to xenografts in immune-compromised mice, a syngeneic model preserves the intact immune functions, which plays an important role in cancer progression and responses to treatment. Pan02 mouse pancreatic cancer cells were orthotopically injected into the pancreas of C57BL/6 mice. Three weeks (21 days) after cell implantation, mice were treated with C150 (150 mg/kg) or vehicle by oral gavage three times a week for 2 weeks. Data showed that C150 treatments significantly improved the survival rate of mice 35 days after tumor inoculation (80% survival), when almost all the vehicle-treated mice had died (10% survival) **(Fig 5.7A**). The tumor weight at necropsy was significantly reduced by C150 treatment (n = 8) compared to vehicle-treated controls (n = 9) (**Fig 5.7B**). Moreover, 89% (8/9) of mice in the vehicle-treated group developed ascites, whereas only 50% (4/8) in the C150 group had ascites (**Fig 5.7C**). In mice having ascites, the average volume was lower in C150 treated mice (**Fig 5.7D**). The expression levels of ER markers were examined in tumor tissues. Consistent with our *in vitro* data, the ER stress markers Bip, cleaved-ATF6, ATF4, and XBP-1s were elevated in C150 treated tumors compared to vehicle-treated controls (**Fig. 5.8A-B**). Lamin B1 was decreased (**Fig. 5.8A-B**), indicating cellular senescence in C150-treated tumors [335].

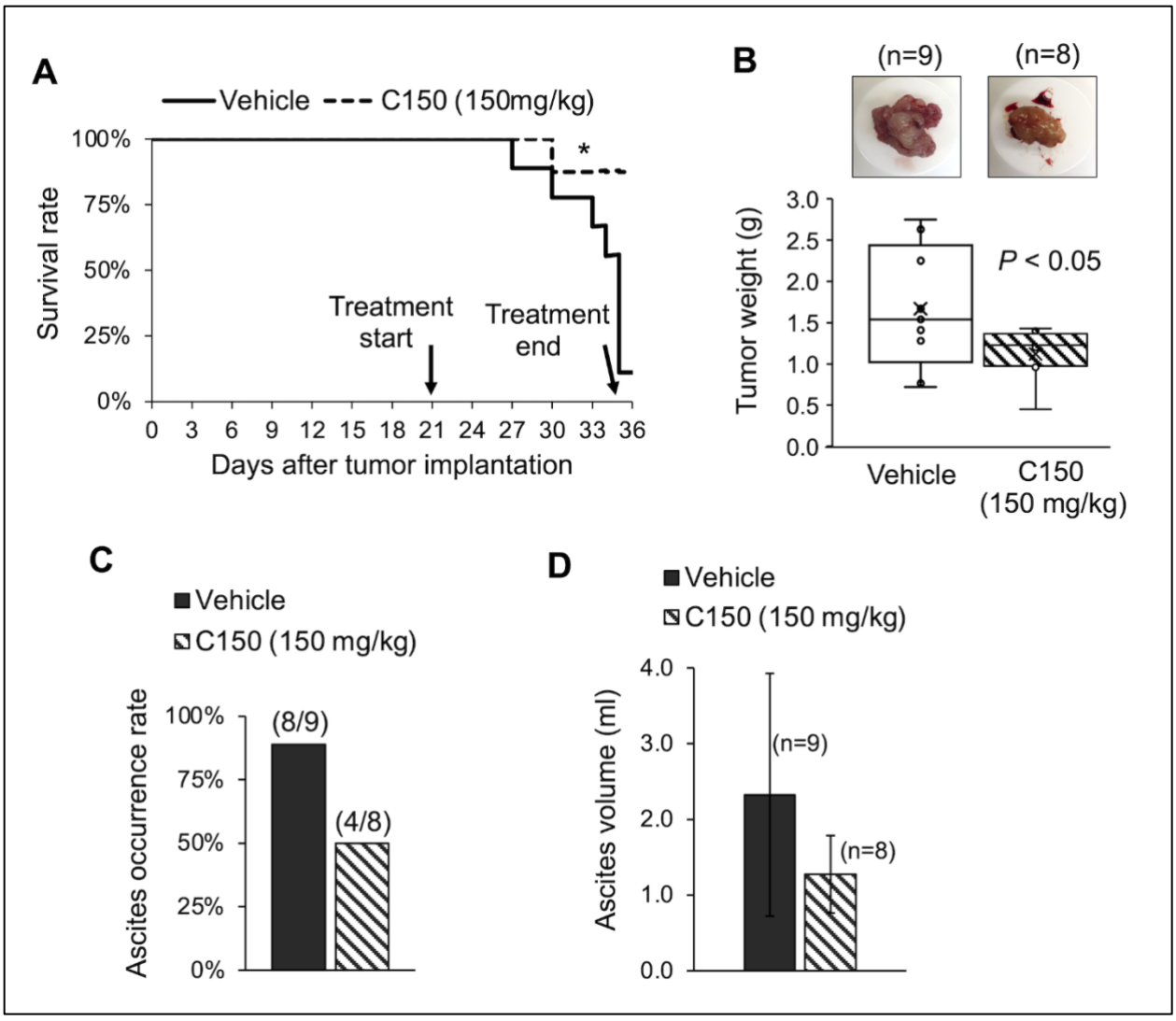

Figure 5.7 C150 treatment increased survival rate and reduced tumor growth in a syngeneic mouse model. A. Kaplan-Meier survival curve of tumor-bearing mice. * $p < 0.05$ (*vs.* vehicle) by log-Rank test. **B.** Tumor weight at necropsy (n = 9 for vehicle, n = 8 for C150). $p < 0.05$ by student t-test. **C.** Ascites occurrence rate. **D**. Average volume of ascites presented as mean ± SD (n = 9 for vehicle, n = 8 for C150). Data are presented as mean ± SD.

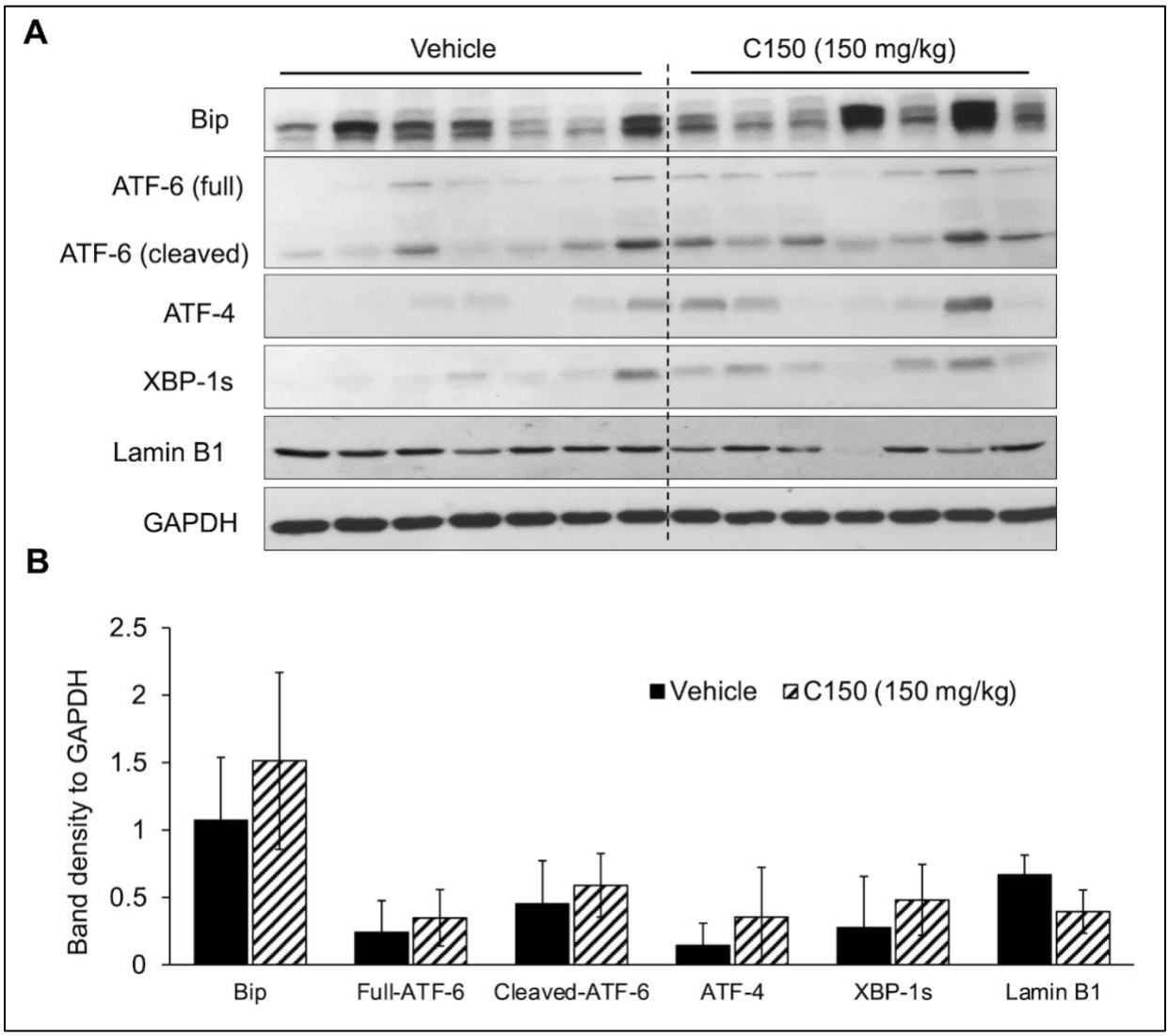

Figure 5.8 C150 induced ER stress in mouse tumor samples. A. Western blotting of ER stress and senescence markers in mouse tumor tissues. Tumors from seven mice in each group were analyzed. GAPDH was blotted as loading control. **B.** Bar graph shows the quantification of band density relative to GAPDH. Data are presented as mean ± SD.

5.3 Summary and discussion

Interrupting ER homeostasis has been shown to be an effective way to inhibit tumor progress because of the vital role the ER plays in cellular protein homeostasis and cell survival [284, 336]. Due to high proliferation demand and the hypoxic microenvironment, cancer cells are under higher endogenous ER stress, resulting in a higher endogenous activation level of UPR signaling [337]. As such, pancreatic tumor tissues have higher Bip and ATF-6 expression levels than the normal tissues [275]. The high basal activation of UPR renders pancreatic cancers more vulnerable to the disturbance of ER balance. Disrupting UPR signaling by either inhibiting or further activating it would both impede the cellular capacity to rescue ER stress in cancer cells, leading to catastrophic effects in cancer cells [281, 284, 338]. In agreement with this notion, our study found that C150 induced profound ER stress and further aggravated UPR signals in pancreatic cancer cells, which subsequently impeded cell proliferation, triggered cell cycle arrest, and led to pancreatic cancer cell senescence.

Findings in our study showed that C150 treatment significantly increased proteasome activity by enhancing proteasome assembly. Increased proteasome activity under ER stress is a pro-survival response of pancreatic cancer cells to restore the ER proteomic homeostasis [339]. However, C150-mediated increase of proteasome activity accelerated the degradation of several critical transcription factors in the EMT/CSC/cell death pathways, such as Snail, β-catenin, Sox2, and TP53, as detected in this study. It is possible that many other important proteins in cancer cell growth/proliferation, invasion, and stemness are also influenced. The degradation of Snail and the other regulatory proteins consequently led to inhibition in EMT and cell invasion in pancreatic cancer cells. These results indicated that the increased proteasome activity under

C150-induced ER stress may have a broad effect on degrading proteins important to pancreatic oncogenesis, resulting in comprehensive inhibition of pancreatic cancer progression through multiple pathways.

Cellular senescence is effectively evaded in pancreatic cancer due to the highly frequent loss-of-function mutations of CDKN2A and p53 [55, 340]. Re-introduction of senescence has been reported as an effective approach to inhibit pancreatic cancer growth [341, 342]. In our study, C150 successfully induced senescence regardless of the mutations of CDKN2A and p53 in PANC-1 cells [343]. Senescence was also detected in Pan02 orthotopic mouse xenografts treated with C150, as shown by the decreased level of Lamin B1. Tumor growth was significantly inhibited, and survival of mice was improved. Moreover, C150-induced senescence drastically sensitized PANC-1 cells to gemcitabine treatment. Therefore, C150 holds a great promise in combination treatment with gemcitabine in pancreatic cancer. This synergy may be extended to other drugs too. Further investigations are worthwhile to validate the synergistic effects in animal studies.

Chapter 6. Discussion and future directions

Pancreatic cancer is a devastating disease that will soon become the third leading cause of cancer-related deaths [4]. Despite our increasing understandings of the genetic makeup and molecular pathways of this disease, the prognosis of pancreatic cancer remains very poor. One of the reasons for such unsatisfactory prognosis is the highly metastatic nature of pancreatic cancer. Metastasis is a major hurdle for effective pancreatic cancer treatment and for improving the survival of patients. More than 80% of cases are presented with metastasis upon diagnosis [5]. Even in patients who have undergone surgery with the primary tumor resected, relapse of the disease would eventfully occur with metastasis [7]. Metastasis is a complex stepwise process that involves cancer cell dissemination, tissue invasion, intravasation, blood circulation, extravasation to pre-metastatic niche, and finally the formation of new metastatic colonies [344]. It has become increasingly evident that EMT plays a critical role in promoting pancreatic cancer metastasis, especially during the cell dissemination and tissue invasion steps [115, 135]. During cell dissemination, cancer cells undergo EMT to shed off their epithelial features, resulting in loss of cell-cell adhesion, cell dissemination from primary tumor, and gain of cell mobility. The EMT-ed cancer cells are not only more mobile, but they also actively secret proteases such as MMPs to remodel to the ECM, clearing the path for invasion through the dense stroma tissue [344].

The critical role of EMT in the pancreatic cancer invasion-metastasis cascade has granted the potential benefits of targeting EMT for its treatment. In efforts of testing this hypothesis and identifying pharmacological inhibitors for pancreatic cancer EMT, we here studied a hit compound (C150) from a previously reported high-throughput screening assay [286]. Our data in **Chapter 4** clearly indicated that C150 significantly reduced pancreatic cancer cell invasion in multiple 2D and 3D cell culture models. EMT was significantly inhibited both *in vitro* and *in*

vivo by C150 treatment, demonstrated by the decreased levels of Snail and N-cadherin combined with increased ZO-1 and Claudin-1. MMP-2 and MMP-9, which are two major enzymes responsible for ECM degradation in pancreatic cancer cell invasion and are direct downstream target genes of Snail [345-348], were also downregulated. C150 was also able to decrease cell migration in Snail-overexpressing cells. The data in **Chapter 4** consistently and clearly showed that pharmacological inhibition of EMT is an effective way to inhibit pancreatic cancer cell invasion.

More importantly, the EMT-TF Snail was significantly downregulated by C150 without changes in its gene expression (**Chapter 4**). Instead, C150 enhanced proteasome assembly downstream of ER stress (**Chapter 5**). Hence, it is likely that C150-induced Snail downregulation is independent of, and not affected by the upstream signals that direct Snail gene expression. The benefits of this could be that C150-induced inhibition of EMT would not be impeded by alterations in EMT-stimulating factors such as hypoxia or growth factors, which all stimulate Snail gene expression. C150 also decreased β-catenin, Sox-2, and TP53 (**Chapter 5**), all of which are important factors in EMT/CSC/proliferation/death control. These data indicate that the inhibition in pancreatic cancer progression induced by C150 could comprehensively include regulations in EMT, CSC, cell proliferation, and cell death, the details of which are worth further investigations.

Pancreatic cancer cells are under a higher baseline level of ER stress compared to normal pancreatic tissues, likely due to the hypoxic microenvironment [269]. These cancer cells trigger basal levels of UPR activation as an adaptation and survival strategy, as shown by the elevated

Bip and ATF-6 expressions in tumor tissues [275, 276]. The basal activation of UPR keeps pancreatic cancer cells on a delicate balance between survival and death [240]. Inhibiting or further aggravating UPR has both been shown to be detrimental for pancreatic cancer cells [281, 284, 285]. Our data in **Chapter 5** showed that C150 induced profound ER stress in pancreatic cancer cells, and further activated their UPR signaling. As a result, it enhanced proteasome assembly and activity and subsequently led to cell cycle arrest and cellular senescence. With the increased proteasome activity, Snail degradation was accelerated, which led to EMT inhibition as shown in **Chapter 4**. The increased proteasome activity also decreased TP53, Sox-2, and β-catenin. Furthermore, autophagy was also triggered as an additional protein degradation mechanism. A reasonable presumption is that the signaling proteins important in cell growth, proliferation, mobility, and such would also be degraded. As such, induction of ER stress by C150 may have a broad effect on enhancing cellular proteolysis and may comprehensively inhibit pancreatic cancer progression through various pathways, including EMT and CSC. To further elucidate the core pathways affected, future studies could include proteomic profiling and transcriptome analysis to identify the major pathway(s) affected by the interruption of ER balance under C150 treatment. Findings from this study linked ER stress and pancreatic cancer EMT and demonstrated the vulnerability of pancreatic cancer cells to disrupted ER balance. The study argued strongly for the feasibility of inducing ER stress for comprehensive inhibition in pancreatic cancer cell growth and invasion.

The enhanced ER stress and inhibition of EMT by C150 in this study also provided opportunities to overcome gemcitabine resistance in pancreatic cancer cells. Pancreatic cancer patients develop resistance to gemcitabine quickly, posing a major issue to pancreatic cancer treatment [349]. The

exact mechanism of gemcitabine resistance is not yet fully understood, but some principles have been proposed, which include activation of EMT, downregulation of gemcitabine activating enzymes, and upregulation of ABC drug efflux transporters [147, 350]. Data in **Chapter 5** showed that C150 drastically sensitized pancreatic cancer cells to gemcitabine treatment. Strong synergies were observed at various combination ratios. This strong *in vitro* synergy needs to be validated with *in vivo* tests in future studies. The role of ER stress and the exact molecular mechanism by which C150 synergizes with gemcitabine are also worth further investigation.

Our studies highlighted the compound C150 as a drug lead for pancreatic cancer. Oral administration of C150 was effective and showed less toxicity compared to IP injection. In addition, because of the poor water solubility of C150, oral administration would be a preferred route for future studies. To further advance C150 as a drug-lead, pharmacokinetic studies are needed to understand the ADME (absorption, distribution, metabolism, and excretion) features of C150 *in vivo*. This includes, but is not limited to, the level of absorption (bioavailability), maximum plasma drug concentration (C_{max}), and half-life, all of which have not been determined in the studies here. Moreover, the first-pass effect by liver metabolism can be a major problem for orally administered drugs. Currently, we do not know whether the *in vivo* effectiveness of C150 was mediated directly by C150 or by its metabolites, which grants further investigations. Possible future experiments are 1) incubating C150 with mouse liver homogenates followed by collecting samples for mass spectrometry analysis, or 2) collecting blood samples from mice after oral administration of C150 for mass spectrometry analysis. Through these analyses, potential metabolites could be identified and tested for *in vitro* and *in vivo* effects.

Analogs of C150 should also be developed and tested. We have tested seven C150 analogs, but without identifying a more effective compound than C150 (**Fig 6.1**). In the future, more analogs with structural diversities should be tested to better understand the structure-activity-relationship (SAR), so that further optimization can be based on this information to improve its drug-like properties.

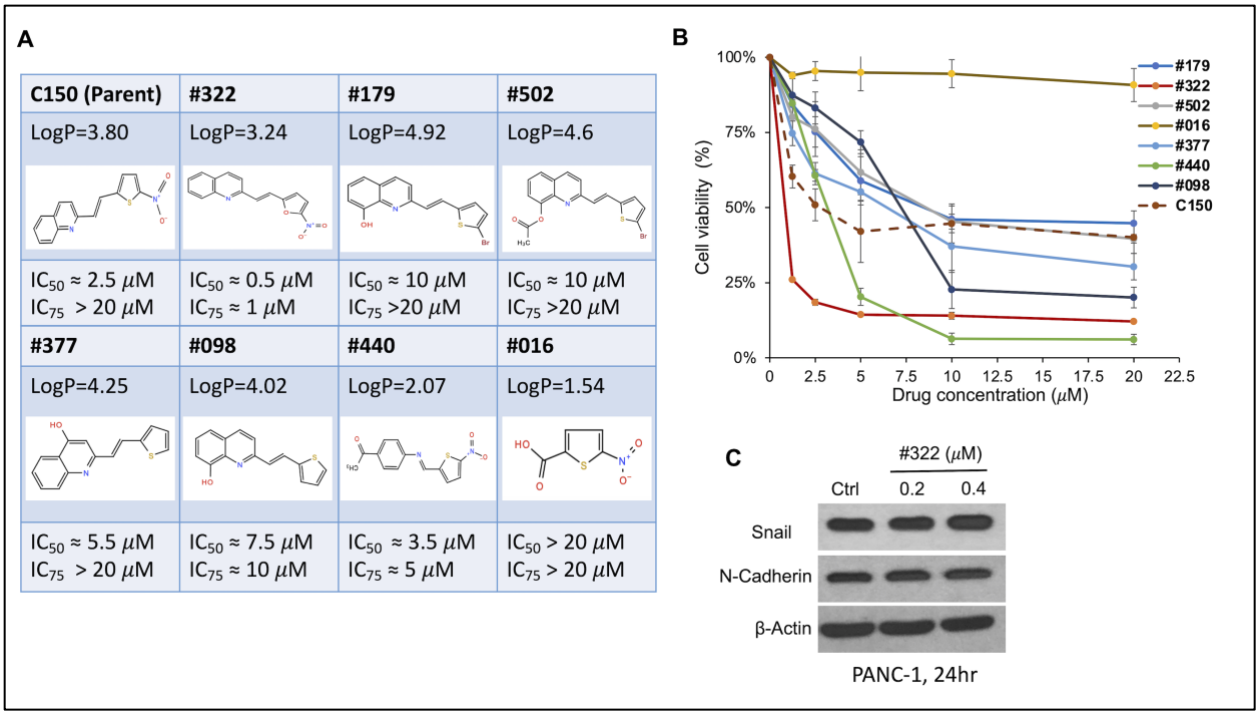

Figure 6.1 Test of seven C150 analogs on cell viability and EMT inhibition in PANC-1 cells. **A.** Analogue structures and estimated IC_{50} values. **B.** Cell viabilities detected by the MTT assay. PANC-1 cells were treated for 48 hours. Data are presented as mean ± SD of three experiments. **C.** Snail and N-Cadherin western blotting. PANC-1 cell treated with #322 for 24 hours. Total cell lysates were analyzed for Snail and N-Cadherin. β–actin is the loading control.

*** Note**: Although analog #322 showed higher activity in reducing cell viability with a lower IC_{50} value than C150, #322 treatment at concentrations close to its IC_{50} in PANC-1 cells failed to decrease Snail and N-cadherin. Thus, #322 is less potent than C150 in terms of EMT inhibition.

There are some limitations of the studies presented here. One is that the molecular target for C150 was not identified. The exact mechanism(s) by which C150 induced ER stress remain

unknown. Future efforts need to focus on identifying the molecular target of C150. One promising method for target identification is through the compound-centric chemical proteomics (CCCP) assay [351]. In this assay, the drug candidate (C150 here) and a non-active control compound will be chemically linked to immobilized beads, such as Sepharose or agarose beads. Linking should not block the compound's activity. Cell lysates are incubated with control-beads and C150-beads for target-compound binding, and the potential binding targets are eluted. Elutes are separated in SDS-PAGE gels and the specific binding band(s) is analyzed by mass spectrometry to reveal the protein identities. The identified target(s) can then be validated by *in vitro* target validation assays, such as the surface plasmon resonance (SPR) assay and the cellular thermo shift assay (CESTA). If the target protein structure is available, using the structure-based rational drug design would then allow us to develop more potent analogs and help us to better understand the structure-activity relations (SAR) of C150. These studies could potentially lead to the discovery of a more active compound with better solubility and pharmacodynamic/pharmacokinetic profiles.

Another limitation is that the animal model used in this study did not represent pancreatic cancer metastasis well. We did not use the tail vein injection of cancer cells, because that model bypasses the initial dissemination and intravasation steps where EMT is required. We used the orthotopic transplantation of human pancreatic cancer cells into the mouse pancreases, however, metastases were not found even in the vehicle-treated mice (**Chapter 4**). A possible explanation for this inconclusive result is the harsh vehicle solution used in this study. Due to the poor water solubility of C150, the compound was dissolved in a vehicle solution composed of 20% DMSO + 60% PEG-400 + 20% H_2O. This harsh vehicle itself may have restricted tumor metastasis in

the control mice. As a result, even the vehicle-treated mice did not develop metastases. Given the profound anti-invasion effect of C150 *in vitro,* a more appropriate formulation that minimizes the vehicle effects needs to be developed. One such potential formulation could be liposomes. By encapsulating C150 in liposome droplets, the compound may be more effectively delivered through IP injections and more readily absorbed, with little or no impacts from the vehicle itself.

The immunocompromised mouse xenograft model used in **Chapter 4** also has its inherent limitations. Although this model itself might not be the reason for the absence of metastases in vehicle-treated mice because the same mouse model demonstrated high metastatic rates in our other studies [352, 353], it should be noted that the immunological microenvironment in the tumor stroma contributes significantly to pancreatic cancer metastasis [354]. Therefore, an alternative is to use genetically engineered mouse models. One such model is the KPC mouse model (LSL-KrasG12D/+; LSL-Trp53R172H/+; Pdx1-Cre) that spontaneously develops tumors in the pancreas by driving Cre-mediated KRAS and TP53 mutations [37]. These mice develop advanced PDAC that closely resembles the human disease progression around 16 weeks of age [355]. The advantages of this model are the intact immune system and the close resemblance to human disease progression in metastasis. However, it may not be an ideal treatment model for the study of drug efficacy, due to several reasons: 1) the difficulty of monitoring *in vivo* tumor growth; 2) the individual variances in the time of tumor formation, making "when to start treatment" a challenge; 3) large numbers of KPC mice would be needed for the treatment study in order to reach statistical significance, which would make it very costly and time-consuming. Another immune-intact model, the syngeneic mouse model, was used in our study (**Chapter 5**) by orthotopically implanting Pan02 murine pancreatic cancer cells. Tumors in this model hardly

metastasized but developed ascites instead. In the future, a possible solution for using the immune-intact mouse model could be to collect cancer cells from KPC mice and implant these cells orthotopically into the KPC background strain of mice. Tumors from this model have been shown by other studies to effectively metastasize to the liver [356].

In summary, our studies here linked pancreatic cancer EMT and ER homeostasis and support the feasibility to target ER homeostasis for inhibition of EMT and induction of cellular senescence. This provides an opportunity for combination with other drugs for synergistic effects. The studies suggest that targeting EMT and ER homeostasis potentially can overcome the major challenges of metastasis and drug resistance in pancreatic cancer treatment. These studies also highlight compound C150 as an EMT inhibitor and inducer of ER stress in pancreatic cancer cells. C150 inhibited cell invasion, promoted cellular senescence, exhibited a preferential growth inhibition in pancreatic cancer cells versus normal cells, and increased chemotherapy sensitivity. C150 also inhibited pancreatic cancer growth in an orthotopic xenograft model and improved survival rates in mice bearing syngeneic pancreatic cancers. Our study indicates that C150, as the first of its class, is a promising drug-lead to be further developed for pancreatic cancer treatment.

References

1. Bardeesy, N. and R.A. DePinho, *Pancreatic cancer biology and genetics.* Nature Reviews Cancer, 2002. **2**(12): p. 897-909.
2. Orth, M., et al., *Pancreatic ductal adenocarcinoma: biological hallmarks, current status, and future perspectives of combined modality treatment approaches.* Radiation Oncology, 2019. **14**(1): p. 141.
3. Kleeff, J., et al., *Pancreatic cancer.* Nat Rev Dis Primers, 2016. **2**: p. 16022.
4. Siegel, R.L., et al., *Cancer Statistics, 2021.* CA: A Cancer Journal for Clinicians, 2021. **71**(1): p. 7-33.
5. Loos, M., et al., *Surgical treatment of pancreatic cancer.* Ann N Y Acad Sci, 2008. **1138**: p. 169-80.
6. Winter, J.M., et al., *Survival after Resection of Pancreatic Adenocarcinoma: Results from a Single Institution over Three Decades.* Annals of Surgical Oncology, 2012. **19**(1): p. 169-175.
7. Kamisawa, T., et al., *Pancreatic cancer.* The Lancet, 2016. **388**(10039): p. 73-85.
8. Burris, H.r., et al., *Improvements in survival and clinical benefit with gemcitabine as first-line therapy for patients with advanced pancreas cancer: a randomized trial.* Journal of clinical oncology, 1997. **15**(6): p. 2403-2413.
9. Conroy, T., et al., *FOLFIRINOX versus gemcitabine for metastatic pancreatic cancer.* N Engl J Med, 2011. **364**(19): p. 1817-25.
10. Von Hoff, D.D., et al., *Increased survival in pancreatic cancer with nab-paclitaxel plus gemcitabine.* N Engl J Med, 2013. **369**(18): p. 1691-703.
11. Chan, K.K.W., et al., *Real-world outcomes of FOLFIRINOX vs gemcitabine and nab-paclitaxel in advanced pancreatic cancer: A population-based propensity score-weighted analysis.* Cancer Medicine, 2020. **9**(1): p. 160-169.
12. Mizrahi, J.D., et al., *Pancreatic cancer.* The Lancet, 2020. **395**(10242): p. 2008-2020.
13. Yamaguchi, J., et al., *Cells of origin of pancreatic neoplasms.* Surgery Today, 2018. **48**(1): p. 9-17.
14. Hezel, A.F., et al., *Genetics and biology of pancreatic ductal adenocarcinoma.* Genes Dev, 2006. **20**(10): p. 1218-49.
15. Tomasello, G., et al., *Outcome of head compared to body and tail pancreatic cancer: a systematic review and meta-analysis of 93 studies.* Journal of Gastrointestinal Oncology, 2019. **10**(2): p. 259-269.
16. van Erning, F.N., et al., *Association of the location of pancreatic ductal adenocarcinoma (head, body, tail) with tumor stage, treatment, and survival: a population-based analysis.* Acta Oncol, 2018. **57**(12): p. 1655-1662.
17. Brosens, L.A., et al., *Pancreatic adenocarcinoma pathology: changing "landscape".* J Gastrointest Oncol, 2015. **6**(4): p. 358-74.
18. Basturk, O., et al., *A Revised Classification System and Recommendations From the Baltimore Consensus Meeting for Neoplastic Precursor Lesions in the Pancreas.* Am J Surg Pathol, 2015. **39**(12): p. 1730-41.

19. Makohon-Moore, A. and C.A. Iacobuzio-Donahue, *Pancreatic cancer biology and genetics from an evolutionary perspective.* Nature Reviews Cancer, 2016. **16**(9): p. 553-565.
20. Ren, B., X. Liu, and A.A. Suriawinata, *Pancreatic Ductal Adenocarcinoma and Its Precursor Lesions: Histopathology, Cytopathology, and Molecular Pathology.* The American Journal of Pathology, 2019. **189**(1): p. 9-21.
21. Sipos, B., et al., *Pancreatic Intraepithelial Neoplasia Revisited and Updated.* Pancreatology, 2009. **9**(1): p. 45-54.
22. Löhr, M., et al., *Frequency of K-ras Mutations in Pancreatic Intraductal Neoplasias Associated with Pancreatic Ductal Adenocarcinoma and Chronic Pancreatitis: A Meta-Analysis.* Neoplasia, 2005. **7**(1): p. 17-23.
23. Hruban, R.H., A. Maitra, and M. Goggins, *Update on pancreatic intraepithelial neoplasia.* International journal of clinical and experimental pathology, 2008. **1**(4): p. 306-316.
24. Hosoda, W., et al., *Genetic analyses of isolated high-grade pancreatic intraepithelial neoplasia (HG-PanIN) reveal paucity of alterations in TP53 and SMAD4.* J Pathol, 2017. **242**(1): p. 16-23.
25. Erkan, M., et al., *The role of stroma in pancreatic cancer: diagnostic and therapeutic implications.* Nat Rev Gastroenterol Hepatol, 2012. **9**(8): p. 454-67.
26. Pothula, S.P., et al., *Key role of pancreatic stellate cells in pancreatic cancer.* Cancer Lett, 2016. **381**(1): p. 194-200.
27. Apte, M.V., et al., *A starring role for stellate cells in the pancreatic cancer microenvironment.* Gastroenterology, 2013. **144**(6): p. 1210-9.
28. Korc, M., *Pancreatic cancer-associated stroma production.* Am J Surg, 2007. **194**(4 Suppl): p. S84-6.
29. Shields, M.A., et al., *Biochemical role of the collagen-rich tumour microenvironment in pancreatic cancer progression.* Biochem J, 2012. **441**(2): p. 541-52.
30. Biankin, A.V., et al., *Pancreatic cancer genomes reveal aberrations in axon guidance pathway genes.* Nature, 2012. **491**(7424): p. 399-405.
31. Witkiewicz, A.K., et al., *Whole-exome sequencing of pancreatic cancer defines genetic diversity and therapeutic targets.* Nature Communications, 2015. **6**(1): p. 6744.
32. Karnoub, A.E. and R.A. Weinberg, *Ras oncogenes: split personalities.* Nature Reviews Molecular Cell Biology, 2008. **9**(7): p. 517-531.
33. Bryant, K.L., et al., *KRAS: feeding pancreatic cancer proliferation.* Trends in Biochemical Sciences, 2014. **39**(2): p. 91-100.
34. Ying, H., et al., *Genetics and biology of pancreatic ductal adenocarcinoma.* Genes & development, 2016. **30**(4): p. 355-385.
35. Hingorani, S.R., et al., *Preinvasive and invasive ductal pancreatic cancer and its early detection in the mouse.* Cancer Cell, 2003. **4**(6): p. 437-450.
36. Aguirre, A.J., et al., *Activated Kras and Ink4a/Arf deficiency cooperate to produce metastatic pancreatic ductal adenocarcinoma.* Genes Dev, 2003. **17**(24): p. 3112-26.
37. Hingorani, S.R., et al., *Trp53R172H and KrasG12D cooperate to promote chromosomal instability and widely metastatic pancreatic ductal adenocarcinoma in mice.* Cancer Cell, 2005. **7**(5): p. 469-83.
38. Schutte, M., et al., *Abrogation of the Rb/p16 tumor-suppressive pathway in virtually all pancreatic carcinomas.* Cancer Res, 1997. **57**(15): p. 3126-30.

39. Caldas, C., et al., *Frequent somatic mutations and homozygous deletions of the p16 (MTS1) gene in pancreatic adenocarcinoma.* Nat Genet, 1994. **8**(1): p. 27-32.
40. Yachida, S., et al., *Clinical significance of the genetic landscape of pancreatic cancer and implications for identification of potential long-term survivors.* Clinical cancer research : an official journal of the American Association for Cancer Research, 2012. **18**(22): p. 6339-6347.
41. Sharpless, N.E. and R.A. DePinho, *The INK4A/ARF locus and its two gene products.* Current Opinion in Genetics & Development, 1999. **9**(1): p. 22-30.
42. Saiki, Y. and A. Horii, *Molecular pathology of pancreatic cancer.* Pathol Int, 2014. **64**(1): p. 10-9.
43. Rhim, A.D. and B.Z. Stanger, *Molecular biology of pancreatic ductal adenocarcinoma progression: aberrant activation of developmental pathways.* Progress in molecular biology and translational science, 2010. **97**: p. 41-78.
44. Sharpless, N.E., *INK4a/ARF: a multifunctional tumor suppressor locus.* Mutat Res, 2005. **576**(1-2): p. 22-38.
45. Bertoli, C., J.M. Skotheim, and R.A.M. de Bruin, *Control of cell cycle transcription during G1 and S phases.* Nature reviews. Molecular cell biology, 2013. **14**(8): p. 518-528.
46. Pomerantz, J., et al., *The Ink4a tumor suppressor gene product, p19Arf, interacts with MDM2 and neutralizes MDM2's inhibition of p53.* Cell, 1998. **92**(6): p. 713-23.
47. Zhang, Y., Y. Xiong, and W.G. Yarbrough, *ARF promotes MDM2 degradation and stabilizes p53: ARF-INK4a locus deletion impairs both the Rb and p53 tumor suppression pathways.* Cell, 1998. **92**(6): p. 725-34.
48. Baugh, E.H., et al., *Why are there hotspot mutations in the TP53 gene in human cancers?* Cell Death & Differentiation, 2018. **25**(1): p. 154-160.
49. Cadwell, C. and G.P. Zambetti, *The effects of wild-type p53 tumor suppressor activity and mutant p53 gain-of-function on cell growth.* Gene, 2001. **277**(1): p. 15-30.
50. Strano, S., et al., *Mutant p53: an oncogenic transcription factor.* Oncogene, 2007. **26**(15): p. 2212-2219.
51. Muller, P.A.J. and K.H. Vousden, *p53 mutations in cancer.* Nature Cell Biology, 2013. **15**(1): p. 2-8.
52. Weisz, L., M. Oren, and V. Rotter, *Transcription regulation by mutant p53.* Oncogene, 2007. **26**(15): p. 2202-2211.
53. Escobar-Hoyos, L.F., et al., *Altered RNA Splicing by Mutant p53 Activates Oncogenic RAS Signaling in Pancreatic Cancer.* Cancer Cell, 2020. **38**(2): p. 198-211.e8.
54. Weissmueller, S., et al., *Mutant p53 Drives Pancreatic Cancer Metastasis through Cell-Autonomous PDGF Receptor β Signaling.* Cell, 2014. **157**(2): p. 382-394.
55. Morton, J.P., et al., *Mutant p53 drives metastasis and overcomes growth arrest/senescence in pancreatic cancer.* Proceedings of the National Academy of Sciences, 2010. **107**(1): p. 246.
56. Padua, D. and J. Massagué, *Roles of TGFβ in metastasis.* Cell Research, 2009. **19**(1): p. 89-102.
57. Peng, B., et al., *Suppression of tumorigenesis and induction of p15(ink4b) by Smad4/DPC4 in human pancreatic cancer cells.* Clin Cancer Res, 2002. **8**(11): p. 3628-38.
58. Zhang, Y., P.B. Alexander, and X.-F. Wang, *TGF-β Family Signaling in the Control of Cell Proliferation and Survival.* Cold Spring Harbor perspectives in biology, 2017. **9**(4): p. a022145.

59. Siegel, P.M. and J. Massagué, *Cytostatic and apoptotic actions of TGF-β in homeostasis and cancer.* Nature Reviews Cancer, 2003. **3**(11): p. 807-820.
60. Blackford, A., et al., *SMAD4 gene mutations are associated with poor prognosis in pancreatic cancer.* Clinical cancer research : an official journal of the American Association for Cancer Research, 2009. **15**(14): p. 4674-4679.
61. Bardeesy, N., et al., *Smad4 is dispensable for normal pancreas development yet critical in progression and tumor biology of pancreas cancer.* Genes Dev, 2006. **20**(22): p. 3130-46.
62. Ijichi, H., et al., *Aggressive pancreatic ductal adenocarcinoma in mice caused by pancreas-specific blockade of transforming growth factor-beta signaling in cooperation with active Kras expression.* Genes Dev, 2006. **20**(22): p. 3147-60.
63. Izeradjene, K., et al., *Kras(G12D) and Smad4/Dpc4 haploinsufficiency cooperate to induce mucinous cystic neoplasms and invasive adenocarcinoma of the pancreas.* Cancer Cell, 2007. **11**(3): p. 229-43.
64. Wilentz, R.E., et al., *Loss of expression of Dpc4 in pancreatic intraepithelial neoplasia: evidence that DPC4 inactivation occurs late in neoplastic progression.* Cancer Res, 2000. **60**(7): p. 2002-6.
65. Jones, S., et al., *Core signaling pathways in human pancreatic cancers revealed by global genomic analyses.* Science (New York, N.Y.), 2008. **321**(5897): p. 1801-1806.
66. Gillson, J., et al., *Small Molecule KRAS Inhibitors: The Future for Targeted Pancreatic Cancer Therapy?* Cancers, 2020. **12**(5): p. 1341.
67. Parrales, A. and T. Iwakuma, *Targeting Oncogenic Mutant p53 for Cancer Therapy.* Frontiers in Oncology, 2015. **5**(288).
68. Kalluri, R. and R.A. Weinberg, *The basics of epithelial-mesenchymal transition.* J Clin Invest, 2009. **119**(6): p. 1420-8.
69. Lim, J. and J.P. Thiery, *Epithelial-mesenchymal transitions: insights from development.* Development, 2012. **139**(19): p. 3471.
70. Thiery, J.P., et al., *Epithelial-mesenchymal transitions in development and disease.* Cell, 2009. **139**(5): p. 871-90.
71. Nieto, M.A., et al., *EMT: 2016.* Cell, 2016. **166**(1): p. 21-45.
72. Ye, X. and R.A. Weinberg, *Epithelial-Mesenchymal Plasticity: A Central Regulator of Cancer Progression.* Trends Cell Biol, 2015. **25**(11): p. 675-86.
73. Huber, M.A., N. Kraut, and H. Beug, *Molecular requirements for epithelial-mesenchymal transition during tumor progression.* Curr Opin Cell Biol, 2005. **17**(5): p. 548-58.
74. Peinado, H. and A. Cano, *A hypoxic twist in metastasis.* Nat Cell Biol, 2008. **10**(3): p. 253-4.
75. Shintani, Y., et al., *Collagen I promotes epithelial-to-mesenchymal transition in lung cancer cells via transforming growth factor-beta signaling.* Am J Respir Cell Mol Biol, 2008. **38**(1): p. 95-104.
76. Du, B. and J.S. Shim, *Targeting Epithelial-Mesenchymal Transition (EMT) to Overcome Drug Resistance in Cancer.* Molecules, 2016. **21**(7).
77. Dongre, A. and R.A. Weinberg, *New insights into the mechanisms of epithelial-mesenchymal transition and implications for cancer.* Nat Rev Mol Cell Biol, 2019. **20**(2): p. 69-84.
78. Stemmler, M.P., et al., *Non-redundant functions of EMT transcription factors.* Nature Cell Biology, 2019. **21**(1): p. 102-112.

79. Manzanares, M., A. Locascio, and M.A. Nieto, *The increasing complexity of the Snail gene superfamily in metazoan evolution.* Trends in Genetics, 2001. **17**(4): p. 178-181.
80. Díaz, V.M., R. Viñas-Castells, and A. García de Herreros, *Regulation of the protein stability of EMT transcription factors.* Cell Adhesion & Migration, 2014. **8**(4): p. 418-428.
81. Nieto, M.A., *The snail superfamily of zinc-finger transcription factors.* Nature Reviews Molecular Cell Biology, 2002. **3**(3): p. 155-166.
82. Lamouille, S., J. Xu, and R. Derynck, *Molecular mechanisms of epithelial–mesenchymal transition.* Nature Reviews Molecular Cell Biology, 2014. **15**: p. 178.
83. Xu, J., S. Lamouille, and R. Derynck, *TGF-beta-induced epithelial to mesenchymal transition.* Cell Res, 2009. **19**(2): p. 156-72.
84. Yook, J.I., et al., *A Wnt-Axin2-GSK3beta cascade regulates Snail1 activity in breast cancer cells.* Nat Cell Biol, 2006. **8**(12): p. 1398-406.
85. Sahlgren, C., et al., *Notch signaling mediates hypoxia-induced tumor cell migration and invasion.* Proc Natl Acad Sci U S A, 2008. **105**(17): p. 6392-7.
86. Julien, S., et al., *Activation of NF-kappaB by Akt upregulates Snail expression and induces epithelium mesenchyme transition.* Oncogene, 2007. **26**(53): p. 7445-56.
87. Kim, H.J., et al., *Constitutively active type I insulin-like growth factor receptor causes transformation and xenograft growth of immortalized mammary epithelial cells and is accompanied by an epithelial-to-mesenchymal transition mediated by NF-kappaB and snail.* Mol Cell Biol, 2007. **27**(8): p. 3165-75.
88. Catalanotto, C., C. Cogoni, and G. Zardo, *MicroRNA in Control of Gene Expression: An Overview of Nuclear Functions.* International journal of molecular sciences, 2016. **17**(10): p. 1712.
89. Ru, P., et al., *miRNA-29b suppresses prostate cancer metastasis by regulating epithelial-mesenchymal transition signaling.* Mol Cancer Ther, 2012. **11**(5): p. 1166-73.
90. Zhang, J., et al., *miR-30 inhibits TGF-β1-induced epithelial-to-mesenchymal transition in hepatocyte by targeting Snail1.* Biochem Biophys Res Commun, 2012. **417**(3): p. 1100-5.
91. Liu, Y.N., et al., *MiR-1 and miR-200 inhibit EMT via Slug-dependent and tumorigenesis via Slug-independent mechanisms.* Oncogene, 2013. **32**(3): p. 296-306.
92. Zhou, B.P., et al., *Dual regulation of Snail by GSK-3β-mediated phosphorylation in control of epithelial–mesenchymal transition.* Nature Cell Biology, 2004. **6**(10): p. 931-940.
93. Zheng, H., et al., *PKD1 phosphorylation-dependent degradation of SNAIL by SCF-FBXO11 regulates epithelial-mesenchymal transition and metastasis.* Cancer Cell, 2014. **26**(3): p. 358-373.
94. Yang, Z., et al., *Pak1 Phosphorylation of Snail, a Master Regulator of Epithelial-to-Mesenchyme Transition, Modulates Snail's Subcellular Localization and Functions.* Cancer Research, 2005. **65**(8): p. 3179.
95. Zhang, K., et al., *Lats2 kinase potentiates Snail1 activity by promoting nuclear retention upon phosphorylation.* The EMBO Journal, 2012. **31**(1): p. 29.
96. Hotz, B., et al., *Epithelial to Mesenchymal Transition: Expression of the Regulators Snail, Slug, and Twist in Pancreatic Cancer.* Clinical Cancer Research, 2007. **13**(16): p. 4769-4776.
97. Nishioka, R., et al., *SNAIL induces epithelial-to-mesenchymal transition in a human pancreatic cancer cell line (BxPC3) and promotes distant metastasis and invasiveness in vivo.* Exp Mol Pathol, 2010. **89**(2): p. 149-57.

98. Vandewalle, C., F. Van Roy, and G. Berx, *The role of the ZEB family of transcription factors in development and disease.* Cell Mol Life Sci, 2009. **66**(5): p. 773-87.
99. Postigo, A.A. and D.C. Dean, *ZEB represses transcription through interaction with the corepressor CtBP.* Proceedings of the National Academy of Sciences, 1999. **96**(12): p. 6683.
100. Sánchez-Tilló, E., et al., *ZEB1 represses E-cadherin and induces an EMT by recruiting the SWI/SNF chromatin-remodeling protein BRG1.* Oncogene, 2010. **29**(24): p. 3490-3500.
101. Postigo, A.A., et al., *Regulation of Smad signaling through a differential recruitment of coactivators and corepressors by ZEB proteins.* The EMBO Journal, 2003. **22**(10): p. 2453-2462.
102. Sánchez-Tilló, E., et al., *β-catenin/TCF4 complex induces the epithelial-to-mesenchymal transition (EMT)-activator ZEB1 to regulate tumor invasiveness.* Proceedings of the National Academy of Sciences, 2011. **108**(48): p. 19204.
103. Shirakihara, T., M. Saitoh, and K. Miyazono, *Differential regulation of epithelial and mesenchymal markers by deltaEF1 proteins in epithelial mesenchymal transition induced by TGF-beta.* Mol Biol Cell, 2007. **18**(9): p. 3533-44.
104. Xiong, H., et al., *Roles of STAT3 and ZEB1 proteins in E-cadherin down-regulation and human colorectal cancer epithelial-mesenchymal transition.* J Biol Chem, 2012. **287**(8): p. 5819-32.
105. Zhang, W., et al., *HIF-1α Promotes Epithelial-Mesenchymal Transition and Metastasis through Direct Regulation of ZEB1 in Colorectal Cancer.* PLOS ONE, 2015. **10**(6): p. e0129603.
106. Guaita, S., et al., *Snail induction of epithelial to mesenchymal transition in tumor cells is accompanied by MUC1 repression and ZEB1 expression.* J Biol Chem, 2002. **277**(42): p. 39209-16.
107. Dave, N., et al., *Functional cooperation between Snail1 and twist in the regulation of ZEB1 expression during epithelial to mesenchymal transition.* The Journal of biological chemistry, 2011. **286**(14): p. 12024-12032.
108. Gregory, P.A., et al., *The miR-200 family and miR-205 regulate epithelial to mesenchymal transition by targeting ZEB1 and SIP1.* Nature Cell Biology, 2008. **10**(5): p. 593-601.
109. Long, J., D. Zuo, and M. Park, *Pc2-mediated sumoylation of Smad-interacting protein 1 attenuates transcriptional repression of E-cadherin.* J Biol Chem, 2005. **280**(42): p. 35477-89.
110. Llorens, M.C., et al., *Phosphorylation Regulates Functions of ZEB1 Transcription Factor.* J Cell Physiol, 2016. **231**(10): p. 2205-17.
111. Abshire, C.F., J.L. Carroll, and A.M. Dragoi, *FLASH protects ZEB1 from degradation and supports cancer cells' epithelial-to-mesenchymal transition.* Oncogenesis, 2016. **5**(8): p. e254-e254.
112. Zhou, Z., et al., *USP51 promotes deubiquitination and stabilization of ZEB1.* Am J Cancer Res, 2017. **7**(10): p. 2020-2031.
113. Chen, B., et al., *Prognostic value of ZEB-1 in solid tumors: a meta-analysis.* BMC Cancer, 2019. **19**(1): p. 635.
114. Kurahara, H., et al., *Epithelial-mesenchymal transition and mesenchymal-epithelial transition via regulation of ZEB-1 and ZEB-2 expression in pancreatic cancer.* J Surg Oncol, 2012. **105**(7): p. 655-61.

115. Krebs, A.M., et al., *The EMT-activator Zeb1 is a key factor for cell plasticity and promotes metastasis in pancreatic cancer.* Nature Cell Biology, 2017. **19**: p. 518.
116. Chang, A.T., et al., *An evolutionarily conserved DNA architecture determines target specificity of the TWIST family bHLH transcription factors.* Genes Dev, 2015. **29**(6): p. 603-16.
117. Yang, F., et al., *SET8 promotes epithelial-mesenchymal transition and confers TWIST dual transcriptional activities.* Embo j, 2012. **31**(1): p. 110-23.
118. Qin, Q., et al., *Normal and disease-related biological functions of Twist1 and underlying molecular mechanisms.* Cell Research, 2012. **22**(1): p. 90-106.
119. Yang, M.-H., et al., *Direct regulation of TWIST by HIF-1α promotes metastasis.* Nature Cell Biology, 2008. **10**(3): p. 295-305.
120. Nairismägi, M.-L., et al., *The Proto-Oncogene TWIST1 Is Regulated by MicroRNAs.* PLOS ONE, 2013. **8**(5): p. e66070.
121. Dong, P., et al., *MicroRNA-106b modulates epithelial–mesenchymal transition by targeting TWIST1 in invasive endometrial cancer cell lines.* Molecular Carcinogenesis, 2014. **53**(5): p. 349-359.
122. Bing, L., et al., *MicroRNA-543 suppresses endometrial cancer oncogenicity via targeting FAK and TWIST1 expression.* Archives of Gynecology and Obstetrics, 2014. **290**(3): p. 533-541.
123. Lin, Y., et al., *MicroRNA-33b Inhibits Breast Cancer Metastasis by Targeting HMGA2, SALL4 and Twist1.* Scientific Reports, 2015. **5**(1): p. 9995.
124. Wang, J., et al., *The Aurora-A–Twist1 axis promotes highly aggressive phenotypes in pancreatic carcinoma.* Journal of Cell Science, 2017. **130**(6): p. 1078.
125. Su, Y.-W., et al., *IL-6 Stabilizes Twist and Enhances Tumor Cell Motility in Head and Neck Cancer Cells through Activation of Casein Kinase 2.* PLOS ONE, 2011. **6**(4): p. e19412.
126. Hong, J., et al., *Phosphorylation of Serine 68 of Twist1 by MAPKs Stabilizes Twist1 Protein and Promotes Breast Cancer Cell Invasiveness.* Cancer Research, 2011. **71**(11): p. 3980.
127. Li, C.-W., et al., *AKT1 Inhibits Epithelial-to-Mesenchymal Transition in Breast Cancer through Phosphorylation-Dependent Twist1 Degradation.* Cancer Research, 2016. **76**(6): p. 1451.
128. Zhong, J., et al., *Degradation of the transcription factor Twist, an oncoprotein that promotes cancer metastasis.* Discovery medicine, 2013. **15**(80): p. 7-15.
129. Ohuchida, K., et al., *Twist, a novel oncogene, is upregulated in pancreatic cancer: Clinical implication of Twist expression in pancreatic juice.* International Journal of Cancer, 2007. **120**(8): p. 1634-1640.
130. Chen, S., et al., *Hypoxia induces TWIST-activated epithelial–mesenchymal transition and proliferation of pancreatic cancer cells in vitro and in nude mice.* Cancer Letters, 2016. **383**(1): p. 73-84.
131. Satoh, K., et al., *Up-regulation of MSX2 enhances the malignant phenotype and is associated with twist 1 expression in human pancreatic cancer cells.* Am J Pathol, 2008. **172**(4): p. 926-39.
132. Chaffer, C.L. and R.A. Weinberg, *A perspective on cancer cell metastasis.* Science, 2011. **331**(6024): p. 1559-64.
133. Brabletz, T., *To differentiate or not--routes towards metastasis.* Nat Rev Cancer, 2012. **12**(6): p. 425-36.

134. Lambert, A.W., D.R. Pattabiraman, and R.A. Weinberg, *Emerging Biological Principles of Metastasis.* Cell, 2017. **168**(4): p. 670-691.
135. Rhim, Andrew D., et al., *EMT and Dissemination Precede Pancreatic Tumor Formation.* Cell, 2012. **148**(1): p. 349-361.
136. Pattabiraman, D.R. and R.A. Weinberg, *Tackling the cancer stem cells - what challenges do they pose?* Nat Rev Drug Discov, 2014. **13**(7): p. 497-512.
137. Rodriguez-Aznar, E., et al., *EMT and Stemness-Key Players in Pancreatic Cancer Stem Cells.* Cancers (Basel), 2019. **11**(8).
138. Li, C., et al., *Identification of pancreatic cancer stem cells.* Cancer Res, 2007. **67**(3): p. 1030-7.
139. Hermann, P.C., et al., *Distinct populations of cancer stem cells determine tumor growth and metastatic activity in human pancreatic cancer.* Cell Stem Cell, 2007. **1**(3): p. 313-23.
140. Kim, M.P., et al., *ALDH Activity Selectively Defines an Enhanced Tumor-Initiating Cell Population Relative to CD133 Expression in Human Pancreatic Adenocarcinoma.* PLOS ONE, 2011. **6**(6): p. e20636.
141. Shiozawa, Y., et al., *Cancer stem cells and their role in metastasis.* Pharmacology & therapeutics, 2013. **138**(2): p. 285-293.
142. Wang, Z., et al., *Pancreatic cancer: understanding and overcoming chemoresistance.* Nat Rev Gastroenterol Hepatol, 2011. **8**(1): p. 27-33.
143. Mani, S.A., et al., *The epithelial-mesenchymal transition generates cells with properties of stem cells.* Cell, 2008. **133**(4): p. 704-15.
144. Wang, Z., et al., *Acquisition of epithelial-mesenchymal transition phenotype of gemcitabine-resistant pancreatic cancer cells is linked with activation of the notch signaling pathway.* Cancer Res, 2009. **69**(6): p. 2400-7.
145. Wellner, U., et al., *The EMT-activator ZEB1 promotes tumorigenicity by repressing stemness-inhibiting microRNAs.* Nat Cell Biol, 2009. **11**(12): p. 1487-95.
146. Zhou, W., et al., *Snail contributes to the maintenance of stem cell-like phenotype cells in human pancreatic cancer.* PloS one, 2014. **9**(1): p. e87409-e87409.
147. Arumugam, T., et al., *Epithelial to mesenchymal transition contributes to drug resistance in pancreatic cancer.* Cancer Res, 2009. **69**(14): p. 5820-8.
148. Chang, T.H., et al., *Slug confers resistance to the epidermal growth factor receptor tyrosine kinase inhibitor.* Am J Respir Crit Care Med, 2011. **183**(8): p. 1071-9.
149. Kajita, M., K.N. McClinic, and P.A. Wade, *Aberrant expression of the transcription factors snail and slug alters the response to genotoxic stress.* Mol Cell Biol, 2004. **24**(17): p. 7559-66.
150. Dean, M., T. Fojo, and S. Bates, *Tumour stem cells and drug resistance.* Nat Rev Cancer, 2005. **5**(4): p. 275-84.
151. Singh, A. and J. Settleman, *EMT, cancer stem cells and drug resistance: an emerging axis of evil in the war on cancer.* Oncogene, 2010. **29**(34): p. 4741-51.
152. Abdullah, L.N. and E.K. Chow, *Mechanisms of chemoresistance in cancer stem cells.* Clin Transl Med, 2013. **2**(1): p. 3.
153. Shah, A.N., et al., *Development and characterization of gemcitabine-resistant pancreatic tumor cells.* Ann Surg Oncol, 2007. **14**(12): p. 3629-37.
154. Du, Z., et al., *Pancreatic Cancer Cells Resistant to Chemoradiotherapy Rich in "Stem-Cell-Like" Tumor Cells.* Digestive Diseases and Sciences, 2011. **56**(3): p. 741-750.

155. Malek, R., et al., *Therapeutic Targeting of Epithelial Plasticity Programs: Focus on the Epithelial-Mesenchymal Transition.* Cells Tissues Organs, 2017. **203**(2): p. 114-127.
156. Feng, X.H. and R. Derynck, *Specificity and versatility in tgf-beta signaling through Smads.* Annu Rev Cell Dev Biol, 2005. **21**: p. 659-93.
157. Halder, S.K., R.D. Beauchamp, and P.K. Datta, *A specific inhibitor of TGF-beta receptor kinase, SB-431542, as a potent antitumor agent for human cancers.* Neoplasia, 2005. **7**(5): p. 509-21.
158. Nagaraj, N.S. and P.K. Datta, *Targeting the transforming growth factor-beta signaling pathway in human cancer.* Expert Opin Investig Drugs, 2010. **19**(1): p. 77-91.
159. Park, C.Y., D.K. Kim, and Y.Y. Sheen, *EW-7203, a novel small molecule inhibitor of transforming growth factor-beta (TGF-beta) type I receptor/activin receptor-like kinase-5, blocks TGF-beta1-mediated epithelial-to-mesenchymal transition in mammary epithelial cells.* Cancer Sci, 2011. **102**(10): p. 1889-96.
160. Melisi, D., et al., *TGFβ receptor inhibitor galunisertib is linked to inflammation- and remodeling-related proteins in patients with pancreatic cancer.* Cancer Chemother Pharmacol, 2019. **83**(5): p. 975-991.
161. Siddiquee, K., et al., *Selective chemical probe inhibitor of Stat3, identified through structure-based virtual screening, induces antitumor activity.* Proc Natl Acad Sci U S A, 2007. **104**(18): p. 7391-6.
162. Liu, J., et al., *Targeting Wnt-driven cancer through the inhibition of Porcupine by LGK974.* Proc Natl Acad Sci U S A, 2013. **110**(50): p. 20224-9.
163. Olmeda, D., et al., *Snail silencing effectively suppresses tumour growth and invasiveness.* Oncogene, 2007. **26**(13): p. 1862-74.
164. Yang, J., et al., *Twist, a master regulator of morphogenesis, plays an essential role in tumor metastasis.* Cell, 2004. **117**(7): p. 927-39.
165. da Silva, S.D., et al., *TWIST1 is a molecular marker for a poor prognosis in oral cancer and represents a potential therapeutic target.* Cancer, 2014. **120**(3): p. 352-62.
166. Arima, Y., et al., *Induction of ZEB proteins by inactivation of RB protein is key determinant of mesenchymal phenotype of breast cancer.* J Biol Chem, 2012. **287**(11): p. 7896-906.
167. Khan, M.A., et al., *Thymoquinone inhibits cancer metastasis by downregulating TWIST1 expression to reduce epithelial to mesenchymal transition.* Oncotarget, 2015. **6**(23): p. 19580-91.
168. Ismail, I.A., et al., *2-Hydroxycinnamaldehyde inhibits the epithelial-mesenchymal transition in breast cancer cells.* Breast Cancer Res Treat, 2013. **137**(3): p. 697-708.
169. Shintani, Y., et al., *ADH-1 suppresses N-cadherin-dependent pancreatic cancer progression.* Int J Cancer, 2008. **122**(1): p. 71-7.
170. Tanaka, H., et al., *Monoclonal antibody targeting of N-cadherin inhibits prostate cancer growth, metastasis and castration resistance.* Nat Med, 2010. **16**(12): p. 1414-20.
171. Thaiparambil, J.T., et al., *Withaferin A inhibits breast cancer invasion and metastasis at sub-cytotoxic doses by inducing vimentin disassembly and serine 56 phosphorylation.* Int J Cancer, 2011. **129**(11): p. 2744-55.
172. Gupta, P.B., et al., *Identification of selective inhibitors of cancer stem cells by high-throughput screening.* Cell, 2009. **138**(4): p. 645-659.
173. Walter, P. and D. Ron, *The Unfolded Protein Response: From Stress Pathway to Homeostatic Regulation.* Science, 2011. **334**(6059): p. 1081.

174. van Anken, E. and I. Braakman, *Versatility of the endoplasmic reticulum protein folding factory.* Crit Rev Biochem Mol Biol, 2005. **40**(4): p. 191-228.
175. Lin, J.H., P. Walter, and T.S.B. Yen, *Endoplasmic reticulum stress in disease pathogenesis.* Annual review of pathology, 2008. **3**: p. 399-425.
176. Hetz, C. and F.R. Papa, *The Unfolded Protein Response and Cell Fate Control.* Mol Cell, 2018. **69**(2): p. 169-181.
177. Schröder, M. and R.J. Kaufman, *ER stress and the unfolded protein response.* Mutat Res, 2005. **569**(1-2): p. 29-63.
178. Hetz, C., *The unfolded protein response: controlling cell fate decisions under ER stress and beyond.* Nature Reviews Molecular Cell Biology, 2012. **13**(2): p. 89-102.
179. Ali, M.M.U., et al., *Structure of the Ire1 autophosphorylation complex and implications for the unfolded protein response.* The EMBO Journal, 2011. **30**(5): p. 894-905.
180. Bertolotti, A., et al., *Dynamic interaction of BiP and ER stress transducers in the unfolded-protein response.* Nature Cell Biology, 2000. **2**(6): p. 326-332.
181. Adams, C.J., et al., *Structure and Molecular Mechanism of ER Stress Signaling by the Unfolded Protein Response Signal Activator IRE1.* Frontiers in Molecular Biosciences, 2019. **6**(11).
182. Oikawa, D., et al., *Activation of mammalian IRE1alpha upon ER stress depends on dissociation of BiP rather than on direct interaction with unfolded proteins.* Exp Cell Res, 2009. **315**(15): p. 2496-504.
183. Calfon, M., et al., *IRE1 couples endoplasmic reticulum load to secretory capacity by processing the XBP-1 mRNA.* Nature, 2002. **415**(6867): p. 92-6.
184. Acosta-Alvear, D., et al., *XBP1 Controls Diverse Cell Type- and Condition-Specific Transcriptional Regulatory Networks.* Molecular Cell, 2007. **27**(1): p. 53-66.
185. Hollien, J., et al., *Regulated Ire1-dependent decay of messenger RNAs in mammalian cells.* J Cell Biol, 2009. **186**(3): p. 323-31.
186. Hollien, J. and J.S. Weissman, *Decay of endoplasmic reticulum-localized mRNAs during the unfolded protein response.* Science, 2006. **313**(5783): p. 104-7.
187. Upton, J.P., et al., *IRE1α cleaves select microRNAs during ER stress to derepress translation of proapoptotic Caspase-2.* Science, 2012. **338**(6108): p. 818-22.
188. Ron, D., *Translational control in the endoplasmic reticulum stress response.* The Journal of clinical investigation, 2002. **110**(10): p. 1383-1388.
189. Carrara, M., et al., *Noncanonical binding of BiP ATPase domain to Ire1 and Perk is dissociated by unfolded protein CH1 to initiate ER stress signaling.* Elife, 2015. **4**.
190. Ma, K., K.M. Vattem, and R.C. Wek, *Dimerization and release of molecular chaperone inhibition facilitate activation of eukaryotic initiation factor-2 kinase in response to endoplasmic reticulum stress.* J Biol Chem, 2002. **277**(21): p. 18728-35.
191. Kaufman, R.J., *Regulation of mRNA translation by protein folding in the endoplasmic reticulum.* Trends in Biochemical Sciences, 2004. **29**(3): p. 152-158.
192. Spriggs, K.A., M. Bushell, and A.E. Willis, *Translational Regulation of Gene Expression during Conditions of Cell Stress.* Molecular Cell, 2010. **40**(2): p. 228-237.
193. Tsai, Y.C. and A.M. Weissman, *The Unfolded Protein Response, Degradation from the Endoplasmic Reticulum, and Cancer.* Genes & Cancer, 2010. **1**(7): p. 764-778.
194. Zhang, K. and R.J. Kaufman, *Identification and characterization of endoplasmic reticulum stress-induced apoptosis in vivo.* Methods Enzymol, 2008. **442**: p. 395-419.

195. Haze, K., et al., *Mammalian Transcription Factor ATF6 Is Synthesized as a Transmembrane Protein and Activated by Proteolysis in Response to Endoplasmic Reticulum Stress.* Molecular Biology of the Cell, 1999. **10**(11): p. 3787-3799.
196. Shen, J., et al., *ER Stress Regulation of ATF6 Localization by Dissociation of BiP/GRP78 Binding and Unmasking of Golgi Localization Signals.* Developmental Cell, 2002. **3**(1): p. 99-111.
197. Ye, J., et al., *ER Stress Induces Cleavage of Membrane-Bound ATF6 by the Same Proteases that Process SREBPs.* Molecular Cell, 2000. **6**(6): p. 1355-1364.
198. Wu, J., et al., *ATF6alpha optimizes long-term endoplasmic reticulum function to protect cells from chronic stress.* Dev Cell, 2007. **13**(3): p. 351-64.
199. Yamamoto, K., et al., *Transcriptional induction of mammalian ER quality control proteins is mediated by single or combined action of ATF6alpha and XBP1.* Dev Cell, 2007. **13**(3): p. 365-76.
200. Teske, B.F., et al., *The eIF2 kinase PERK and the integrated stress response facilitate activation of ATF6 during endoplasmic reticulum stress.* Molecular Biology of the Cell, 2011. **22**(22): p. 4390-4405.
201. Olzmann, J.A., R.R. Kopito, and J.C. Christianson, *The mammalian endoplasmic reticulum-associated degradation system.* Cold Spring Harb Perspect Biol, 2013. **5**(9).
202. Fujita, E., et al., *Two endoplasmic reticulum-associated degradation (ERAD) systems for the novel variant of the mutant dysferlin: ubiquitin/proteasome ERAD(I) and autophagy/lysosome ERAD(II).* Hum Mol Genet, 2007. **16**(6): p. 618-29.
203. Houck, S.A., et al., *Quality control autophagy degrades soluble ERAD-resistant conformers of the misfolded membrane protein GnRHR.* Mol Cell, 2014. **54**(1): p. 166-179.
204. Chino, H. and N. Mizushima, *ER-Phagy: Quality Control and Turnover of Endoplasmic Reticulum.* Trends in Cell Biology, 2020. **30**(5): p. 384-398.
205. Ciechanover, A., *Intracellular protein degradation: from a vague idea thru the lysosome and the ubiquitin-proteasome system and onto human diseases and drug targeting.* Biochim Biophys Acta, 2012. **1824**(1): p. 3-13.
206. Wójcik, C. and G.N. DeMartino, *Intracellular localization of proteasomes.* Int J Biochem Cell Biol, 2003. **35**(5): p. 579-89.
207. Tanaka, K., *The proteasome: overview of structure and functions.* Proceedings of the Japan Academy. Series B, Physical and biological sciences, 2009. **85**(1): p. 12-36.
208. Murata, S., H. Yashiroda, and K. Tanaka, *Molecular mechanisms of proteasome assembly.* Nature Reviews Molecular Cell Biology, 2009. **10**(2): p. 104-115.
209. Collins, G.A. and A.L. Goldberg, *The Logic of the 26S Proteasome.* Cell, 2017. **169**(5): p. 792-806.
210. Pickart, C.M., *Mechanisms Underlying Ubiquitination.* Annual Review of Biochemistry, 2001. **70**(1): p. 503-533.
211. Baugh, J.M., E.G. Viktorova, and E.V. Pilipenko, *Proteasomes Can Degrade a Significant Proportion of Cellular Proteins Independent of Ubiquitination.* Journal of Molecular Biology, 2009. **386**(3): p. 814-827.
212. Kumar Deshmukh, F., et al., *The Contribution of the 20S Proteasome to Proteostasis.* Biomolecules, 2019. **9**(5): p. 190.
213. Brodsky, J.L. and A.A. McCracken, *ER protein quality control and proteasome-mediated protein degradation.* Semin Cell Dev Biol, 1999. **10**(5): p. 507-13.

214. Fabre, B., et al., *Identification of proteins regulated by the proteasome following induction of endoplasmic reticulum stress.* Biochemical and Biophysical Research Communications, 2019. **517**(2): p. 188-192.
215. Qi, L., B. Tsai, and P. Arvan, *New Insights into the Physiological Role of Endoplasmic Reticulum-Associated Degradation.* Trends in Cell Biology, 2017. **27**(6): p. 430-440.
216. Okuda-Shimizu, Y. and L.M. Hendershot, *Characterization of an ERAD pathway for nonglycosylated BiP substrates, which require Herp.* Molecular cell, 2007. **28**(4): p. 544-554.
217. Cormier, J.H., et al., *EDEM1 Recognition and Delivery of Misfolded Proteins to the SEL1L-Containing ERAD Complex.* Molecular Cell, 2009. **34**(5): p. 627-633.
218. Schoebel, S., et al., *Cryo-EM structure of the protein-conducting ERAD channel Hrd1 in complex with Hrd3.* Nature, 2017. **548**(7667): p. 352-355.
219. Kikkert, M., et al., *Human HRD1 is an E3 ubiquitin ligase involved in degradation of proteins from the endoplasmic reticulum.* J Biol Chem, 2004. **279**(5): p. 3525-34.
220. Ye, Y., H.H. Meyer, and T.A. Rapoport, *The AAA ATPase Cdc48/p97 and its partners transport proteins from the ER into the cytosol.* Nature, 2001. **414**(6864): p. 652-6.
221. Cullinan, S.B., et al., *Nrf2 Is a Direct PERK Substrate and Effector of PERK-Dependent Cell Survival.* Molecular and Cellular Biology, 2003. **23**(20): p. 7198.
222. Lee, S., et al., *Involvement of the Nrf2-proteasome pathway in the endoplasmic reticulum stress response in pancreatic β-cells.* Toxicology and Applied Pharmacology, 2012. **264**(3): p. 431-438.
223. Digaleh, H., M. Kiaei, and F. Khodagholi, *Nrf2 and Nrf1 signaling and ER stress crosstalk: implication for proteasomal degradation and autophagy.* Cellular and Molecular Life Sciences, 2013. **70**(24): p. 4681-4694.
224. Rousseau, A. and A. Bertolotti, *An evolutionarily conserved pathway controls proteasome homeostasis.* Nature, 2016. **536**(7615): p. 184-189.
225. Lee, W., et al., *iRhom1 regulates proteasome activity via PAC1/2 under ER stress.* Scientific Reports, 2015. **5**(1): p. 11559.
226. Senft, D. and Z.e.A. Ronai, *UPR, autophagy, and mitochondria crosstalk underlies the ER stress response.* Trends in Biochemical Sciences, 2015. **40**(3): p. 141-148.
227. Mizushima, N. and M. Komatsu, *Autophagy: Renovation of Cells and Tissues.* Cell, 2011. **147**(4): p. 728-741.
228. Dikic, I. and Z. Elazar, *Mechanism and medical implications of mammalian autophagy.* Nature Reviews Molecular Cell Biology, 2018. **19**(6): p. 349-364.
229. Olsvik, H.L., et al., *FYCO1 Contains a C-terminally Extended, LC3A/B-preferring LC3-interacting Region (LIR) Motif Required for Efficient Maturation of Autophagosomes during Basal Autophagy.* The Journal of biological chemistry, 2015. **290**(49): p. 29361-29374.
230. Johansen, T. and T. Lamark, *Selective Autophagy: ATG8 Family Proteins, LIR Motifs and Cargo Receptors.* Journal of Molecular Biology, 2020. **432**(1): p. 80-103.
231. B'Chir, W., et al., *The eIF2α/ATF4 pathway is essential for stress-induced autophagy gene expression.* Nucleic acids research, 2013. **41**(16): p. 7683-7699.
232. Hosokawa, N., et al., *Nutrient-dependent mTORC1 association with the ULK1-Atg13-FIP200 complex required for autophagy.* Mol Biol Cell, 2009. **20**(7): p. 1981-91.
233. Jung, C.H., et al., *ULK-Atg13-FIP200 complexes mediate mTOR signaling to the autophagy machinery.* Mol Biol Cell, 2009. **20**(7): p. 1992-2003.

234. Jin, H.-O., et al., *Activating transcription factor 4 and CCAAT/enhancer-binding protein-β negatively regulate the mammalian target of rapamycin via Redd1 expression in response to oxidative and endoplasmic reticulum stress.* Free Radical Biology and Medicine, 2009. **46**(8): p. 1158-1167.
235. Qin, L., et al., *ER stress negatively regulates AKT/TSC/mTOR pathway to enhance autophagy.* Autophagy, 2010. **6**(2): p. 239-47.
236. Shaw, R.J., *LKB1 and AMP-activated protein kinase control of mTOR signalling and growth.* Acta Physiol (Oxf), 2009. **196**(1): p. 65-80.
237. Egan, D.F., et al., *Phosphorylation of ULK1 (hATG1) by AMP-activated protein kinase connects energy sensing to mitophagy.* Science, 2011. **331**(6016): p. 456-61.
238. Shen, S., et al., *Bufalin induces the interplay between apoptosis and autophagy in glioma cells through endoplasmic reticulum stress.* Int J Biol Sci, 2014. **10**(2): p. 212-24.
239. Shore, G.C., F.R. Papa, and S.A. Oakes, *Signaling cell death from the endoplasmic reticulum stress response.* Curr Opin Cell Biol, 2011. **23**(2): p. 143-9.
240. Hetz, C., K. Zhang, and R.J. Kaufman, *Mechanisms, regulation and functions of the unfolded protein response.* Nature Reviews Molecular Cell Biology, 2020. **21**(8): p. 421-438.
241. Urra, H., et al., *When ER stress reaches a dead end.* Biochimica et Biophysica Acta (BBA) - Molecular Cell Research, 2013. **1833**(12): p. 3507-3517.
242. Harding, H.P., et al., *Regulated Translation Initiation Controls Stress-Induced Gene Expression in Mammalian Cells.* Molecular Cell, 2000. **6**(5): p. 1099-1108.
243. McCullough, K.D., et al., *Gadd153 Sensitizes Cells to Endoplasmic Reticulum Stress by Down-Regulating Bcl2 and Perturbing the Cellular Redox State.* Molecular and Cellular Biology, 2001. **21**(4): p. 1249.
244. Puthalakath, H., et al., *ER Stress Triggers Apoptosis by Activating BH3-Only Protein Bim.* Cell, 2007. **129**(7): p. 1337-1349.
245. Reimertz , C., et al., *Gene expression during ER stress–induced apoptosis in neurons : induction of the BH3-only protein Bbc3/PUMA and activation of the mitochondrial apoptosis pathway.* Journal of Cell Biology, 2003. **162**(4): p. 587-597.
246. Li, J., B. Lee, and A.S. Lee, *Endoplasmic reticulum stress-induced apoptosis: multiple pathways and activation of p53-up-regulated modulator of apoptosis (PUMA) and NOXA by p53.* J Biol Chem, 2006. **281**(11): p. 7260-70.
247. Han, D., et al., *IRE1α Kinase Activation Modes Control Alternate Endoribonuclease Outputs to Determine Divergent Cell Fates.* Cell, 2009. **138**(3): p. 562-575.
248. Urano, F., et al., *Coupling of Stress in the ER to Activation of JNK Protein Kinases by Transmembrane Protein Kinase IRE1.* Science, 2000. **287**(5453): p. 664.
249. Hu, P., et al., *Autocrine Tumor Necrosis Factor Alpha Links Endoplasmic Reticulum Stress to the Membrane Death Receptor Pathway through IRE1α-Mediated NF-κB Activation and Down-Regulation of TRAF2 Expression.* Molecular and Cellular Biology, 2006. **26**(8): p. 3071.
250. Pluquet, O., A. Pourtier, and C. Abbadie, *The unfolded protein response and cellular senescence. A Review in the Theme: Cellular Mechanisms of Endoplasmic Reticulum Stress Signaling in Health and Disease.* American Journal of Physiology-Cell Physiology, 2014. **308**(6): p. C415-C425.
251. He, S. and N.E. Sharpless, *Senescence in Health and Disease.* Cell, 2017. **169**(6): p. 1000-1011.

252. Herranz, N. and J. Gil, *Mechanisms and functions of cellular senescence.* The Journal of clinical investigation, 2018. **128**(4): p. 1238-1246.
253. d'Adda di Fagagna, F., *Living on a break: cellular senescence as a DNA-damage response.* Nat Rev Cancer, 2008. **8**(7): p. 512-22.
254. Serrano, M., G.J. Hannon, and D. Beach, *A new regulatory motif in cell-cycle control causing specific inhibition of cyclin D/CDK4.* Nature, 1993. **366**(6456): p. 704-707.
255. Sharpless, N.E. and C.J. Sherr, *Forging a signature of in vivo senescence.* Nature Reviews Cancer, 2015. **15**(7): p. 397-408.
256. Narita, M., et al., *Rb-mediated heterochromatin formation and silencing of E2F target genes during cellular senescence.* Cell, 2003. **113**(6): p. 703-16.
257. Dimri, G.P., et al., *A biomarker that identifies senescent human cells in culture and in aging skin in vivo.* Proceedings of the National Academy of Sciences of the United States of America, 1995. **92**(20): p. 9363-9367.
258. Kurz, D.J., et al., *Senescence-associated (beta)-galactosidase reflects an increase in lysosomal mass during replicative ageing of human endothelial cells.* Journal of Cell Science, 2000. **113**(20): p. 3613.
259. Lee, B.Y., et al., *Senescence-associated beta-galactosidase is lysosomal beta-galactosidase.* Aging Cell, 2006. **5**(2): p. 187-95.
260. Itahana, K., J. Campisi, and G.P. Dimri, *Methods to detect biomarkers of cellular senescence: the senescence-associated beta-galactosidase assay.* Methods Mol Biol, 2007. **371**: p. 21-31.
261. Abbadie, C. and O. Pluquet, *Unfolded Protein Response (UPR) Controls Major Senescence Hallmarks.* Trends in Biochemical Sciences, 2020. **45**(5): p. 371-374.
262. Liu, J., et al., *Receptor for advanced glycation end-products promotes premature senescence of proximal tubular epithelial cells via activation of endoplasmic reticulum stress-dependent p21 signaling.* Cellular Signalling, 2014. **26**(1): p. 110-121.
263. Sasaki, M., et al., *A possible involvement of endoplasmic reticulum stress in biliary epithelial autophagy and senescence in primary biliary cirrhosis.* Journal of Gastroenterology, 2015. **50**(9): p. 984-995.
264. Sayers, C.M., et al., *Identification and Characterization of a Potent Activator of p53-Independent Cellular Senescence via a Small-Molecule Screen for Modifiers of the Integrated Stress Response.* Molecular Pharmacology, 2013. **83**(3): p. 594.
265. Kim, H.S., et al., *The p38-activated ER stress-ATF6α axis mediates cellular senescence.* The FASEB Journal, 2019. **33**(2): p. 2422-2434.
266. Druelle, C., et al., *ATF6α regulates morphological changes associated with senescence in human fibroblasts.* Oncotarget, 2016. **7**(42): p. 67699-67715.
267. Denoyelle, C., et al., *Anti-oncogenic role of the endoplasmic reticulum differentially activated by mutations in the MAPK pathway.* Nat Cell Biol, 2006. **8**(10): p. 1053-63.
268. Moenner, M., et al., *Integrated Endoplasmic Reticulum Stress Responses in Cancer.* Cancer Research, 2007. **67**(22): p. 10631.
269. Feldman, D.E., V. Chauhan, and A.C. Koong, *The Unfolded Protein Response: A Novel Component of the Hypoxic Stress Response in Tumors.* Molecular Cancer Research, 2005. **3**(11): p. 597.
270. Fernandez, P.M., et al., *Overexpression of the glucose-regulated stress gene GRP78 in malignant but not benign human breast lesions.* Breast Cancer Research and Treatment, 2000. **59**(1): p. 15-26.

271. Shuda, M., et al., *Activation of the ATF6, XBP1 and grp78 genes in human hepatocellular carcinoma: a possible involvement of the ER stress pathway in hepatocarcinogenesis.* Journal of Hepatology, 2003. **38**(5): p. 605-614.
272. Song, M.S., et al., *Induction of Glucose-regulated Protein 78 by Chronic Hypoxia in Human Gastric Tumor Cells through a Protein Kinase C-ε/ERK/AP-1 Signaling Cascade.* Cancer Research, 2001. **61**(22): p. 8322.
273. Fujimoto, T., et al., *Overexpression of Human X-box Binding Protein 1 (XBP-1) in Colorectal Adenomas and Adenocarcinomas.* Anticancer Research, 2007. **27**(1A): p. 127.
274. Tsai, H.Y., et al., *Endoplasmic reticulum ribosome-binding protein 1 (RRBP1) overexpression is frequently found in lung cancer patients and alleviates intracellular stress-induced apoptosis through the enhancement of GRP78.* Oncogene, 2013. **32**(41): p. 4921-4931.
275. Niu, Z., et al., *Elevated GRP78 expression is associated with poor prognosis in patients with pancreatic cancer.* Scientific Reports, 2015. **5**(1): p. 16067.
276. Martinez-Useros, J., et al., *Identification of Poor-outcome Biliopancreatic Carcinoma Patients With Two-marker Signature Based on ATF6α and p-p38 "STARD Compliant".* Medicine, 2015. **94**(45): p. e1972-e1972.
277. Hazari, Y.M., et al., *Emerging tale of UPR and cancer: an essentiality for malignancy.* Tumor Biology, 2016. **37**(11): p. 14381-14390.
278. Sano, R. and J.C. Reed, *ER stress-induced cell death mechanisms.* Biochimica et Biophysica Acta (BBA) - Molecular Cell Research, 2013. **1833**(12): p. 3460-3470.
279. Vandewynckel, Y.-P., et al., *The Paradox of the Unfolded Protein Response in Cancer.* Anticancer Research, 2013. **33**(11): p. 4683.
280. Ojha, R. and R.K. Amaravadi, *Targeting the unfolded protein response in cancer.* Pharmacological Research, 2017. **120**: p. 258-266.
281. Chien, W., et al., *Selective inhibition of unfolded protein response induces apoptosis in pancreatic cancer cells.* Oncotarget, 2014. **5**(13): p. 4881-4894.
282. Atkins, C., et al., *Characterization of a Novel PERK Kinase Inhibitor with Antitumor and Antiangiogenic Activity.* Cancer Research, 2013. **73**(6): p. 1993.
283. Chiu, T.L. and C.C. Su, *Tanshinone IIA increases protein expression levels of PERK, ATF6, IRE1α, CHOP, caspase-3 and caspase-12 in pancreatic cancer BxPC-3 cell-derived xenograft tumors.* Mol Med Rep, 2017. **15**(5): p. 3259-3263.
284. Mujumdar, N., et al., *Triptolide activates unfolded protein response leading to chronic ER stress in pancreatic cancer cells.* American Journal of Physiology-Gastrointestinal and Liver Physiology, 2014. **306**(11): p. G1011-G1020.
285. Mujumdar, N., et al., *Triptolide Induces Cell Death in Pancreatic Cancer Cells by Apoptotic and Autophagic Pathways.* Gastroenterology, 2010. **139**(2): p. 598-608.
286. Polireddy, K., et al., *Targeting Epithelial-Mesenchymal Transition for Identification of Inhibitors for Pancreatic Cancer Cell Invasion and Tumor Spheres Formation.* PLoS One, 2016. **11**(10): p. e0164811.
287. Chou, T.C., *Drug combination studies and their synergy quantification using the Chou-Talalay method.* Cancer Res, 2010. **70**(2): p. 440-6.
288. (IARC), I.A.f.R.o.C., *World Cancer Report*, in *World Cancer Report 2014*, C.P.W. Bernard W. Steward, Editor. 2014.

289. 3rd, H.A.B., et al., *Improvements in survival and clinical benefit with gemcitabine as first-line therapy for patients with advanced pancreas cancer: a randomized trial.* Journal of Clinical Oncology, 1997. **15**(6): p. 2403-2413.
290. Wang, S., S. Huang, and Y.L. Sun, *Epithelial-Mesenchymal Transition in Pancreatic Cancer: A Review.* BioMed Research International, 2017. **2017**: p. 10.
291. Beuran, M., et al., *The epithelial to mesenchymal transition in pancreatic cancer: A systematic review.* Pancreatology, 2015. **15**(3): p. 217-225.
292. Tsai, J.H. and J. Yang, *Epithelial-mesenchymal plasticity in carcinoma metastasis.* Genes Dev, 2013. **27**(20): p. 2192-206.
293. Thiery, J.P., *Epithelial–mesenchymal transitions in tumour progression.* Nature Reviews Cancer, 2002. **2**(6): p. 442-454.
294. Kalluri, R. and R.A. Weinberg, *The basics of epithelial-mesenchymal transition.* The Journal of Clinical Investigation, 2009. **119**(6): p. 1420-1428.
295. Batlle, E., et al., *The transcription factor snail is a repressor of E-cadherin gene expression in epithelial tumour cells.* Nat Cell Biol, 2000. **2**(2): p. 84-9.
296. Ikenouchi, J., et al., *Regulation of tight junctions during the epithelium-mesenchyme transition: direct repression of the gene expression of claudins/occludin by Snail.* Journal of Cell Science, 2003. **116**(10): p. 1959-1967.
297. Ohkubo, T. and M. Ozawa, *The transcription factor Snail downregulates the tight junction components independently of E-cadherin downregulation.* J Cell Sci, 2004. **117**(Pt 9): p. 1675-85.
298. Jorda, M., et al., *Upregulation of MMP-9 in MDCK epithelial cell line in response to expression of the Snail transcription factor.* J Cell Sci, 2005. **118**(Pt 15): p. 3371-85.
299. Shields, M.A., et al., *Pancreatic cancer cells respond to type I collagen by inducing snail expression to promote membrane type 1 matrix metalloproteinase-dependent collagen invasion.* J Biol Chem, 2011. **286**(12): p. 10495-504.
300. Yokoyama, K., et al., *Increased invasion and matrix metalloproteinase-2 expression by Snail-induced mesenchymal transition in squamous cell carcinomas.* Int J Oncol, 2003. **22**(4): p. 891-8.
301. Sumi, T., et al., *Cofilin phosphorylation and actin cytoskeletal dynamics regulated by rho- and Cdc42-activated LIM-kinase 2.* J Cell Biol, 1999. **147**(7): p. 1519-32.
302. Koshiba, T., et al., *Detection of matrix metalloproteinase activity in human pancreatic cancer.* Surgery Today, 1997. **27**(4): p. 302-304.
303. Määttä, M., et al., *Differential Expression of Matrix Metalloproteinase (MMP)-2, MMP-9, and Membrane Type 1-MMP in Hepatocellular and Pancreatic Adenocarcinoma: Implications for Tumor Progression and Clinical Prognosis.* Clinical Cancer Research, 2000. **6**(7): p. 2726.
304. Neesse, A., et al., *Stromal biology and therapy in pancreatic cancer.* Gut, 2011. **60**(6): p. 861-868.
305. Ye, X. and R.A. Weinberg, *Epithelial-Mesenchymal Plasticity: A Central Regulator of Cancer Progression.* Trends Cell Biol, 2015. **25**(11): p. 675-686.
306. Jablonska-Trypuc, A., M. Matejczyk, and S. Rosochacki, *Matrix metalloproteinases (MMPs), the main extracellular matrix (ECM) enzymes in collagen degradation, as a target for anticancer drugs.* J Enzyme Inhib Med Chem, 2016. **31**(sup1): p. 177-183.

307. Gordon, K.J., et al., *Bone morphogenetic proteins induce pancreatic cancer cell invasiveness through a Smad1-dependent mechanism that involves matrix metalloproteinase-2.* Carcinogenesis, 2009. **30**(2): p. 238-48.
308. Hidalgo, M., *Pancreatic cancer.* N Engl J Med, 2010. **362**(17): p. 1605-17.
309. Yin, T., et al., *Expression of Snail in Pancreatic Cancer Promotes Metastasis and Chemoresistance.* Journal of Surgical Research, 2007. **141**(2): p. 196-203.
310. Yang, X., et al., *Silencing Snail suppresses tumor cell proliferation and invasion by reversing epithelial-to-mesenchymal transition and arresting G2/M phase in non-small cell lung cancer.* Int J Oncol, 2017. **50**(4): p. 1251-1260.
311. de Herreros, A.G., et al., *Snail family regulation and epithelial mesenchymal transitions in breast cancer progression.* Journal of mammary gland biology and neoplasia, 2010. **15**(2): p. 135-147.
312. Yu, Q., B.P. Zhou, and Y. Wu, *The regulation of snail: on the ubiquitin edge.* Cancer Cell Microenviron, 2017. **4**(2).
313. Frame, S., P. Cohen, and R.M. Biondi, *A common phosphate binding site explains the unique substrate specificity of GSK3 and its inactivation by phosphorylation.* Mol Cell, 2001. **7**(6): p. 1321-7.
314. Hermida, M.A., J. Dinesh Kumar, and N.R. Leslie, *GSK3 and its interactions with the PI3K/AKT/mTOR signalling network.* Adv Biol Regul, 2017. **65**: p. 5-15.
315. Zhao, L. and S.L. Ackerman, *Endoplasmic reticulum stress in health and disease.* Curr Opin Cell Biol, 2006. **18**(4): p. 444-52.
316. Kaufman, R.J., *Molecular chaperones and the heat shock response. Sponsored by Cold Spring Harbor Laboratory, 6-10 May 1998.* Biochim Biophys Acta, 1999. **1423**(1): p. R13-27.
317. Wek, R.C. and D.R. Cavener, *Translational control and the unfolded protein response.* Antioxid Redox Signal, 2007. **9**(12): p. 2357-71.
318. Travers, K.J., et al., *Functional and genomic analyses reveal an essential coordination between the unfolded protein response and ER-associated degradation.* Cell, 2000. **101**(3): p. 249-58.
319. Ron, D. and P. Walter, *Signal integration in the endoplasmic reticulum unfolded protein response.* Nature Reviews Molecular Cell Biology, 2007. **8**(7): p. 519-529.
320. Brewer, J.W. and J.A. Diehl, *PERK mediates cell-cycle exit during the mammalian unfolded protein response.* Proceedings of the National Academy of Sciences, 2000. **97**(23): p. 12625.
321. Shore, G.C., F.R. Papa, and S.A. Oakes, *Signaling cell death from the endoplasmic reticulum stress response.* Current Opinion in Cell Biology, 2011. **23**(2): p. 143-149.
322. Rousseau, A. and A. Bertolotti, *Regulation of proteasome assembly and activity in health and disease.* Nature Reviews Molecular Cell Biology, 2018. **19**(11): p. 697-712.
323. Verfaillie, T., A.D. Garg, and P. Agostinis, *Targeting ER stress induced apoptosis and inflammation in cancer.* Cancer Letters, 2013. **332**(2): p. 249-264.
324. Schonthal, A.H., *Targeting endoplasmic reticulum stress for cancer therapy.* Front Biosci (Schol Ed), 2012. **4**: p. 412-31.
325. Aberle, H., et al., *beta-catenin is a target for the ubiquitin-proteasome pathway.* The EMBO journal, 1997. **16**(13): p. 3797-3804.
326. Love, I.M., D. Shi, and S.R. Grossman, *p53 Ubiquitination and proteasomal degradation.* Methods Mol Biol, 2013. **962**: p. 63-73.

327. Fang, L., et al., *A Methylation-Phosphorylation Switch Determines Sox2 Stability and Function in ESC Maintenance or Differentiation*. Molecular Cell, 2014. **55**(4): p. 537-551.
328. Bedford, L., et al., *Assembly, structure, and function of the 26S proteasome.* Trends in Cell Biology, 2010. **20**(7): p. 391-401.
329. Deegan, S., et al., *Stress-induced self-cannibalism: on the regulation of autophagy by endoplasmic reticulum stress.* Cell Mol Life Sci, 2013. **70**(14): p. 2425-41.
330. Schmidt, E.K., et al., *SUnSET, a nonradioactive method to monitor protein synthesis.* Nat Methods, 2009. **6**(4): p. 275-7.
331. Goodman, C.A. and T.A. Hornberger, *Measuring protein synthesis with SUnSET: a valid alternative to traditional techniques?* Exercise and sport sciences reviews, 2013. **41**(2): p. 107-115.
332. Bourougaa, K., et al., *Endoplasmic Reticulum Stress Induces G2 Cell-Cycle Arrest via mRNA Translation of the p53 Isoform p53/47.* Molecular Cell, 2010. **38**(1): p. 78-88.
333. Gire, V. and V. Dulic, *Senescence from G2 arrest, revisited.* Cell cycle (Georgetown, Tex.), 2015. **14**(3): p. 297-304.
334. Ruscetti, M., et al., *Senescence-Induced Vascular Remodeling Creates Therapeutic Vulnerabilities in Pancreas Cancer.* Cell, 2020. **181**(2): p. 424-441.e21.
335. Freund, A., et al., *Lamin B1 loss is a senescence-associated biomarker.* Molecular biology of the cell, 2012. **23**(11): p. 2066-2075.
336. Schönthal, A.H., *Pharmacological targeting of endoplasmic reticulum stress signaling in cancer.* Biochemical Pharmacology, 2013. **85**(5): p. 653-666.
337. Oakes, S.A., *Endoplasmic Reticulum Stress Signaling in Cancer Cells.* The American Journal of Pathology, 2020. **190**(5): p. 934-946.
338. Dauer, P., et al., *Inhibition of Sp1 prevents ER homeostasis and causes cell death by lysosomal membrane permeabilization in pancreatic cancer.* Scientific Reports, 2017. **7**(1): p. 1564.
339. Hwang, J. and L. Qi, *Quality Control in the Endoplasmic Reticulum: Crosstalk between ERAD and UPR pathways.* Trends in Biochemical Sciences, 2018. **43**(8): p. 593-605.
340. Ag Moir, J., S. A White, and J. Mann, *Arrested development and the great escape – The role of cellular senescence in pancreatic cancer.* The International Journal of Biochemistry & Cell Biology, 2014. **57**: p. 142-148.
341. Yuan, Y., et al., *A Small-Molecule Probe of the Histone Methyltransferase G9a Induces Cellular Senescence in Pancreatic Adenocarcinoma.* ACS Chemical Biology, 2012. **7**(7): p. 1152-1157.
342. Neault, M., Frédérick A. Mallette, and S. Richard, *miR-137 Modulates a Tumor Suppressor Network-Inducing Senescence in Pancreatic Cancer Cells.* Cell Reports, 2016. **14**(8): p. 1966-1978.
343. Gradiz, R., et al., *MIA PaCa-2 and PANC-1 – pancreas ductal adenocarcinoma cell lines with neuroendocrine differentiation and somatostatin receptors.* Scientific Reports, 2016. **6**(1): p. 21648.
344. Fares, J., et al., *Molecular principles of metastasis: a hallmark of cancer revisited.* Signal Transduction and Targeted Therapy, 2020. **5**(1): p. 28.
345. Gress, T.M., et al., *Expression and in-situ localization of genes coding for extracellular matrix proteins and extracellular matrix degrading proteases in pancreatic cancer.* International Journal of Cancer, 1995. **62**(4): p. 407-413.

346. Yang, X., et al., *Invasiveness and MMP Expression in Pancreatic Carcinoma.* Journal of Surgical Research, 2001. **98**(1): p. 33-39.
347. Miyoshi, A., et al., *Snail and SIP1 increase cancer invasion by upregulating MMP family in hepatocellular carcinoma cells.* British Journal of Cancer, 2004. **90**(6): p. 1265-1273.
348. Jordà, M., et al., *Upregulation of MMP-9 in MDCK epithelial cell line in response to expression of the Snail transcription factor.* Journal of Cell Science, 2005. **118**(15): p. 3371.
349. Ducreux, M., V. Boige, and D. Malka, *Treatment of advanced pancreatic cancer.* Semin Oncol, 2007. **34**(2 Suppl 1): p. S25-30.
350. Jia, Y. and J. Xie, *Promising molecular mechanisms responsible for gemcitabine resistance in cancer.* Genes & Diseases, 2015. **2**(4): p. 299-306.
351. Rix, U. and G. Superti-Furga, *Target profiling of small molecules by chemical proteomics.* Nature Chemical Biology, 2009. **5**(9): p. 616-624.
352. Yu, J., J. Drisko, and Q. Chen, *Inhibition of pancreatic cancer and potentiation of gemcitabine effects by the extract of Pao Pereira.* Oncol Rep, 2013. **30**(1): p. 149-56.
353. Dong, R., et al., *An RNA-Binding Protein, Hu-antigen R, in Pancreatic Cancer Epithelial to Mesenchymal Transition, Metastasis, and Cancer Stem Cells.* Molecular Cancer Therapeutics, 2020. **19**(11): p. 2267.
354. Ren, B., et al., *Tumor microenvironment participates in metastasis of pancreatic cancer.* Molecular Cancer, 2018. **17**(1): p. 108.
355. Lee, J.W., et al., *Genetically Engineered Mouse Models of Pancreatic Cancer: The KPC Model (LSL-Kras(G12D/+) ;LSL-Trp53(R172H/+) ;Pdx-1-Cre), Its Variants, and Their Application in Immuno-oncology Drug Discovery.* Curr Protoc Pharmacol, 2016. **73**: p. 14.39.1-14.39.20.
356. Torres, M.P., et al., *Novel Pancreatic Cancer Cell Lines Derived from Genetically Engineered Mouse Models of Spontaneous Pancreatic Adenocarcinoma: Applications in Diagnosis and Therapy.* PLOS ONE, 2013. **8**(11): p. e80580.